

NUREG/CR-0226
(ORNL/NUREG/TM-160)

cy. 44

MARTIN MARIETTA ENERGY SYSTEMS LIBRARIES



3 4456 0310736 8

Development of the Capacitor Discharge Vaporization Technique to Produce Aerosols Formed Under Conditions Postulated for Hypothetical Core Disruptive Accidents

M. J. Kelly
G. W. Parker
J. M. Rochelle

Prepared for the U.S. Nuclear Regulatory Commission
Office of Nuclear Regulatory Research
Under Interagency Agreements DOE 40-551-75 and 40-552-75

Oak Ridge National Laboratory
Research Library

4500N, MS-6191

LIBRARY LOAN COPY

DO NOT TRANSFER TO ANOTHER PERSON.
If you wish someone else to see this report, send in
name with report and the library will arrange a loan.

ORNL 11R(10 05)

(3 5-60)

OAK RIDGE NATIONAL LABORATORY
OPERATED BY UNION CARBIDE CORPORATION · FOR THE DEPARTMENT OF ENERGY

Printed in the United States of America. Available from
National Technical Information Service
U.S. Department of Commerce
5285 Port Royal Road, Springfield, Virginia 22161

This report was prepared as an account of work sponsored by the United States Government. Neither the United States nor any of its employees, nor any of its contractors, subcontractors, or their employees, makes any warranty, express or implied, or assumes any legal liability or responsibility for the accuracy, completeness or usefulness of any information, apparatus, product or process disclosed, or represents that its use would not infringe privately owned rights.

NUREG/CR-0226
ORNL/NUREG/TM-160
Dist. Category R7

Contract No. W-7405-eng-26

CHEMICAL TECHNOLOGY DIVISION

DEVELOPMENT OF THE CAPACITOR DISCHARGE VAPORIZATION TECHNIQUE
TO PRODUCE AEROSOLS FORMED UNDER CONDITIONS POSTULATED
FOR HYPOTHETICAL CORE DISRUPTIVE ACCIDENTS

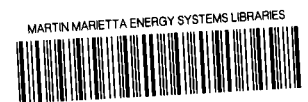
M. J. Kelly
G. W. Parker
J. M. Rochelle*

*Instrumentation and Controls Division

Manuscript Completed: June 22, 1978
Date Published: July 1978

Prepared for
U. S. Nuclear Regulatory Commission
Office of Nuclear Regulatory Research
Washington, D. C. 20555
Under Interagency Agreements DOE 40-551-75 and 40-552-75
NRC FIN No. B0121

Prepared by
OAK RIDGE NATIONAL LABORATORY
Oak Ridge, Tennessee 37830
operated by
UNION CARBIDE CORPORATION
for the
DEPARTMENT OF ENERGY



3 4456 0310736 8

CONTENTS

	Page
ABSTRACT.....	1
SUMMARY.....	1
1. INTRODUCTION.....	4
2. SCOPE.....	5
3. DEFINITION OF PROBLEM.....	6
3.1 Objectives.....	6
3.2 Properties of the System.....	6
4. POTENTIAL APPROACHES.....	8
5. EXPERIMENTAL PROGRAM DEVELOPMENT.....	14
6. CONCURRENT ANALYSIS PROGRAM.....	23
6.1 Computer Calculations for the Preheat Steady- State Phase.....	26
6.2 Effect of Delay Time on Radial Temperature Gradient..	28
6.3 Computer Calculations for the Capacitor Discharge Phase.....	30
7. EXPERIMENTAL RESULTS.....	32
8. COMPUTER MODELING RESULTS.....	48
9. COMPARISONS BETWEEN COMPUTER CALCULATIONS AND EXPERIMENTAL RESULTS.....	59
10. THE ORNL CAPACITOR DISCHARGE VAPORIZATION SYSTEM.....	61
10.1 Introduction.....	61
10.2 The Sample Preconditioning System (the Preheater)...	61
10.2.1 Design features.....	66
10.2.2 Performance.....	69
10.3 The Capacitor Energy Delivery System.....	71
10.3.1 The Energy Storage System.....	71
10.3.2 Charging and Firing System.....	73
10.3.3 Equipment capability.....	75

	Page
10.4 Data Acquisition System.....	77
10.4.1 Equipment used during expansion.....	77
10.4.2 Equipment used after expansion.....	78
10.5 Test Articles.....	83
11. ACKNOWLEDGMENTS.....	83
12. REFERENCES.....	86

DEVELOPMENT OF THE CAPACITOR DISCHARGE VAPORIZATION TECHNIQUE
TO PRODUCE AEROSOLS FORMED UNDER CONDITIONS POSTULATED
FOR HYPOTHETICAL CORE DISRUPTIVE ACCIDENTS

M. J. Kelly
G. W. Parker
J. M. Rochelle

ABSTRACT

This report describes the development of a Capacitor Discharge Vaporization (CDV) method for the out-of-pile creation of energy states in fast breeder reactor fuel (or simulants) that are consistent with those postulated for Hypothetical Core Disruptive Accidents (HCDA).

The results of the development experiments, concurrent planning, test article construction, peripheral equipment design and construction, and computer modeling studies are discussed in relation to their effects on the design of the Oak Ridge National Laboratory's Capacitor Discharge Vaporization (ORNL CDV) System.

The completed ORNL CDV System is described in detail, including all the required subsystems and data acquisition equipment. Operational features, equipment capability, and expected performance are also discussed.

SUMMARY

The assessment of the potential consequences of the very low probability (hypothetical) accidents for fast breeder reactors requires determination of the quantities of biologically hazardous materials released from the fuel and their subsequent interactions and behavior in primary and secondary containment environments.

Laboratory-scale experiments to study their release from fuel, interactions with sodium, conversion to aerosols, and transient behavior in the primary containment appear to require the capability of placing

samples of the fuel (or fuel simulants) into the very high thermodynamic states postulated to exist at the disassembly termination of the prompt-critical stage of a hypothetical core disruptive accident (HCDA) at energy levels up to 3000 J per gram.

The Aerosol Release and Transport (ART) Program at ORNL, sponsored by the Nuclear Regulatory Commission (NRC), has developed an out-of-pile technique for using electrical energy stored in capacitors to achieve high rates of energy deposition ($>10^6$ W per gram) in small Liquid-Metal Fast Breeder Reactor (LMFBR) fuel samples that can then be used in a variety of laboratory safety studies. This report presents the details of the development of this CDV technique, describes the system and equipment, and presents the results of the developmental tests and the accompanying analyses.

The CDV System development was initiated by ORNL through an inter-agency agreement with the Arnold Engineering Development Center (AEDC), where appropriate capacitor storage banks were already available. A series of 40 developmental tests were conducted at AEDC. These tests confirmed the viability of the CDV technique and established the basic design parameters for the ORNL CDV System. This system is now in use in various phases of the ART Program.

The achievement of the appropriate HCDA-like thermal states in the CDV samples was confirmed by energy balance calculations with the measured input electrical energy and by sectioning partially molten samples which has received insufficient energy for disassembly. The measured quantities of UO_2 vapor produced were orders of magnitude greater than those that had been measured during previous attempts to apply this "exploding wire" technique using UO_2 as the electrical energy receptor. However, the vapor yields were still less than what would be expected from adiabatic expansion considerations.

The successful operational procedure developed was to first apply direct electrical energy until the UO_2 sample was almost entirely pre-molten. The lowered electrical resistance of premolten UO_2 compared with that of solid UO_2 makes the sample receptive to the large energy

deposition rates from the capacitive discharge. Consequently, the final CDV system required a specially designed sample holder to contain the premolten UO_2 and a preheating system to premelt the samples.

The UO_2 sample design that evolved from these tests consists of an active (capacitor discharge acceptor) region of UO_2 pellets stacked between spring-loaded tungsten electrodes. These pellets are surrounded by a microsphere region of either UO_2 or ThO_2 , which serves as a thermal barrier to protect a quartz (or sometimes ceramic) tube. This tube provides containment during preheating and during the initial part of the capacitor discharge.

The preheater is a 4000-W system that applies the direct electrical energy, at controlled constant power, over three stages. During the first stage, high voltage (2500 V) is applied until the sample electrical resistance is decreased from an initial value of up to 2,000,000 Ω down to a few hundred ohms, due to the increasing sample temperature. The power is subsequently controlled in two stages -- first from a 440-V supply and then from a 120-V supply -- until the final sample resistance is on the order of 0.2 to 0.5 Ω , a value that would be receptive to the large energy discharge from the capacitors. The preheater power is controlled by the use of modular integrated-circuit analog multipliers coupled with conduction angle control (phase firing) of inverse-parallel silicon control rectifiers (SCRs).

The capacitor energy system itself is of modular design and has six separate modules, each with ten capacitors. Each capacitor is rated at 3 kJ and 2500 V, giving a total stored energy capacity of 180 kJ. Each module uses ignitron switches for firing control and has blocking diodes for internal firing protection. The charging system is capable of delivering up to 500 mA of dc current which will charge the system to full capacity in 4.8 min.

The data acquisition system includes measurements of power, voltage, current, sample temperature (by optical pyrometry), sample expansion (by high-speed motion picture photography), and aerosol sampling for evaluation of the airborne material. The analog data are recorded on a two-channel

storage oscilloscope and a two-channel digital storage oscilloscope. A four-channel magnetic tape recorder provides permanent records.

This CDV System serves as a versatile experimental tool for use in a variety of LMFBR safety-related studies. For example, it is being used in the ART Program to produce small-scale fuel disassemblies under sodium to study the potential thermal attenuation of the fuel source under prototypic fuel-coolant interaction conditions. It is also being used in an auxiliary vessel to produce UO_2 aerosols under "free expansion" conditions in an argon atmosphere. This permits the quantities of airborne fuel to be determined and allows studies to be made of the aerosol characteristics. Although we believe the CDV System is now a viable experimental tool for placing LMFBR fuel (or fuel simulants) into high energy states, additional development is needed for use under sodium in order to fully characterize the distribution of the deposited energy and to understand the lower-than-expected vapor yields as a function of the energy level of the UO_2 samples.

1. INTRODUCTION

Information on the release of biologically hazardous materials from fast reactor cores under various hypothetical accident conditions is required by the NRC for the evaluation of reactor containment and siting. Release of the fission products, plutonium, and other transuranic elements determines the "source term" for further leakage to the containment through postulated primary system failures.

It is important that the fractions of these biologically hazardous materials released from the fuel be known and be related to the accident sequence, energy deposition rates, total energy deposited, fuel burnup, and environmental conditions. In addition, their physical and chemical states after fission termination determine their subsequent interactions with succeeding environments. These states must be established to provide an adequate description of the properties of the aerosol-vapor mixture and its transient behavior as it progresses through the accident pathways to the secondary containment. The transient behavioral properties of this final aerosol must be determined so that its potential hazard can be assessed.

The materials resulting from the HCDAs can be adequately characterized through experiments in which fuel (or simulant) samples are placed in the physical and thermodynamic states expected under postulated conditions. These materials are then allowed to undergo the high-temperature hydrodynamic expansion from this superheated liquid fuel state at the transient chemical potentials provided by fission products, cladding, and coolant.

The CDV technique was developed at ORNL as a practical out-of-pile method for reaching the required high internal energy conditions in fuel disassembly and the resulting release and transport of biologically hazardous materials under conditions representative of postulated accidents. The technique essentially involves the use of massive amounts of electrical energy stored in capacitors to be discharged through preconditioned fuel (or simulant) samples in appropriately controlled quantities and rates.

2. SCOPE

This report covers the initial development of the out-of-pile CDV method of creating energy states in LMFBR fuel that are consistent with postulated HCDA conditions. It covers the planning, analysis, experiments, and design work over the period April 1974 to April 1976, which was an integral part of the ORNL ART Program. The report is presented in chronological order, more or less, so that program development proceeds logically from problem definition up to the present status. Many of the development tests were carried out under an interagency agreement between the Arnold Engineering Development Center (AEDC), a U. S. Air Force facility operated by the Army Research Office, Inc., located at Arnold Air Force Station, Tennessee, and NRC. Planning, test design, test article construction, peripheral equipment design and construction, data analysis, and supporting research were accomplished at ORNL. Forty experiments at AEDC provided the experimental data base for the design and construction of the ORNL CDV System to be used in the ART Program for studying fuel disassembly and the resulting release and transport.

3. DEFINITION OF PROBLEM

3.1 Objectives

Melting and vaporization of fuel have been postulated to occur during two low-probability HCDAs: loss of flow (LOF) and transient overpower (TOP). For each of these accidents, there is an initial "slow" power deposition ramp (pre-disassembly), followed by a "rapid" one (disassembly). The slow ramp preconditions the fuel prior to failure by its effect on sodium and cladding conditions, fuel temperature distribution, energy levels, and melt fractions. The second ramp provides the energy for fuel vaporization and disassembly in a short time (milliseconds). Power levels on the order of 10^6 W per gram of fuel and temperatures of several thousand degrees Kelvin are expected in localized, prompt critical core regions, while other regions remain essentially unperturbed. Diverse failure conditions coexist simultaneously over a wide range of variables.

Large-scale experiments with the system described above appear to be impractical. Therefore, the approach chosen was to design and test an experimental method on which small samples of fuel could be placed into the appropriate ranges of internal energy conditions for subsequent disassembly, with the liquid and vapor expanding into contained systems in the presence of the other chemical species expected in the HCDA. For development experiments, UO_2 was chosen as a simulant for the mixed oxide fuel. Extension of the technique for use with mixed oxide fuel is believed to be practical.

3.2 Properties of the System

With the selection of UO_2 as a simulant for the mixed oxide fuel development purposes, a compilation of electrical, physical, chemical, and thermodynamic data was made and presented in a convenient graphical form. Those relationships most significant for planning experimental test and later test analyses are presented in this section.

The specific electrical conductivity in ohm-cm vs temperature, as determined by Bates et al.,¹ is shown in Fig. 1. A smooth extrapolation

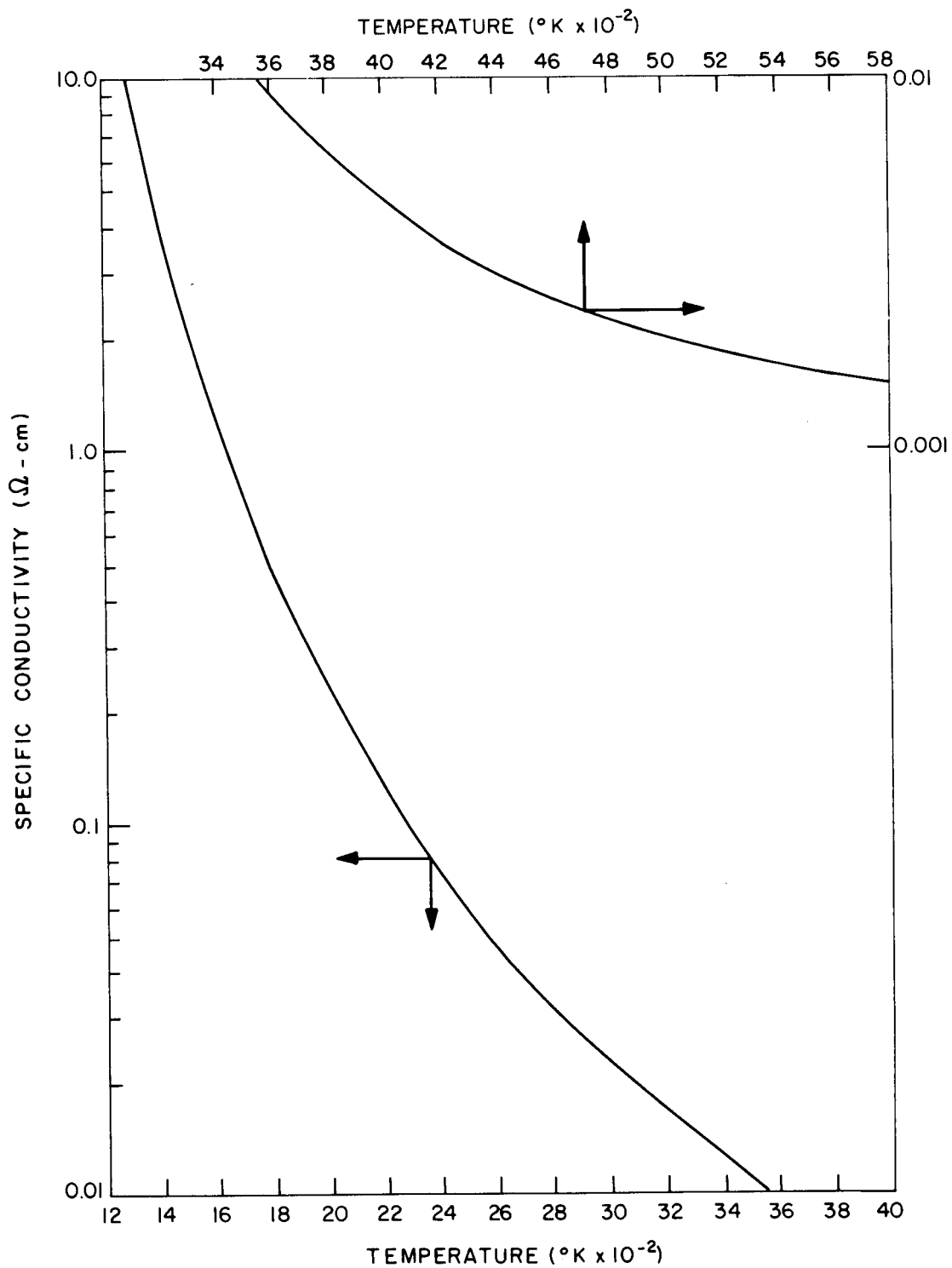


Fig. 1. Variation of the electrical conductivity of UO_2 with temperature (data taken from ref. 1.)

is made above the melting point, although no real data were available. In Fig. 2, the heat capacity data for UO_2 are taken from Leibowitz et al.^{2,3} Figure 3, vapor pressure vs temperature, and Fig. 4, density and specific volume vs temperature, are consistent with the range of values reported for various derived equations of state.⁴⁻⁹ The values shown in Fig. 5, the thermal conductivity of UO_2 vs temperature, are reasonably consistent with the most current literature values. However, these values may only be considered estimates as the temperature increases, and as the critical temperature is approached, they become mere guesses. A continuing survey of current literature is maintained so that justified changes in these properties can be implemented.

4. POTENTIAL APPROACHES

Although various methods of vaporizing the fuel or simulant were available, such as induction heating, plasma torch, various arc techniques, laser methods, and even direct thermal evaporation from heated TaC, the methods that appeared to offer the most promise of actually sustaining the postulated high HCDA thermal states were those that involved direct electrical heating using the fuel itself as the heating element.

Three out-of-pile methods of attempting the electrical power insertion appeared available:

1. a large dc rectifier to supply the necessary power,
2. energy storage in an inductance for later energy transfer to the fuel sample, and
3. energy storage in a capacitor for later energy transfer to the fuel sample.

The difficulty of containing and insulating fuel samples that may exist at HCDA-like states discouraged the use of steady-state power supplies. A steady-state system capacity on the order of 10 MW would be required in order to supply energy at a sufficiently rapid rate to permit containment melting. Consequently, an early decision was made in favor of energy storage in either inductors or capacitors with transient transfer into the samples. This appeared attractive because a 100%

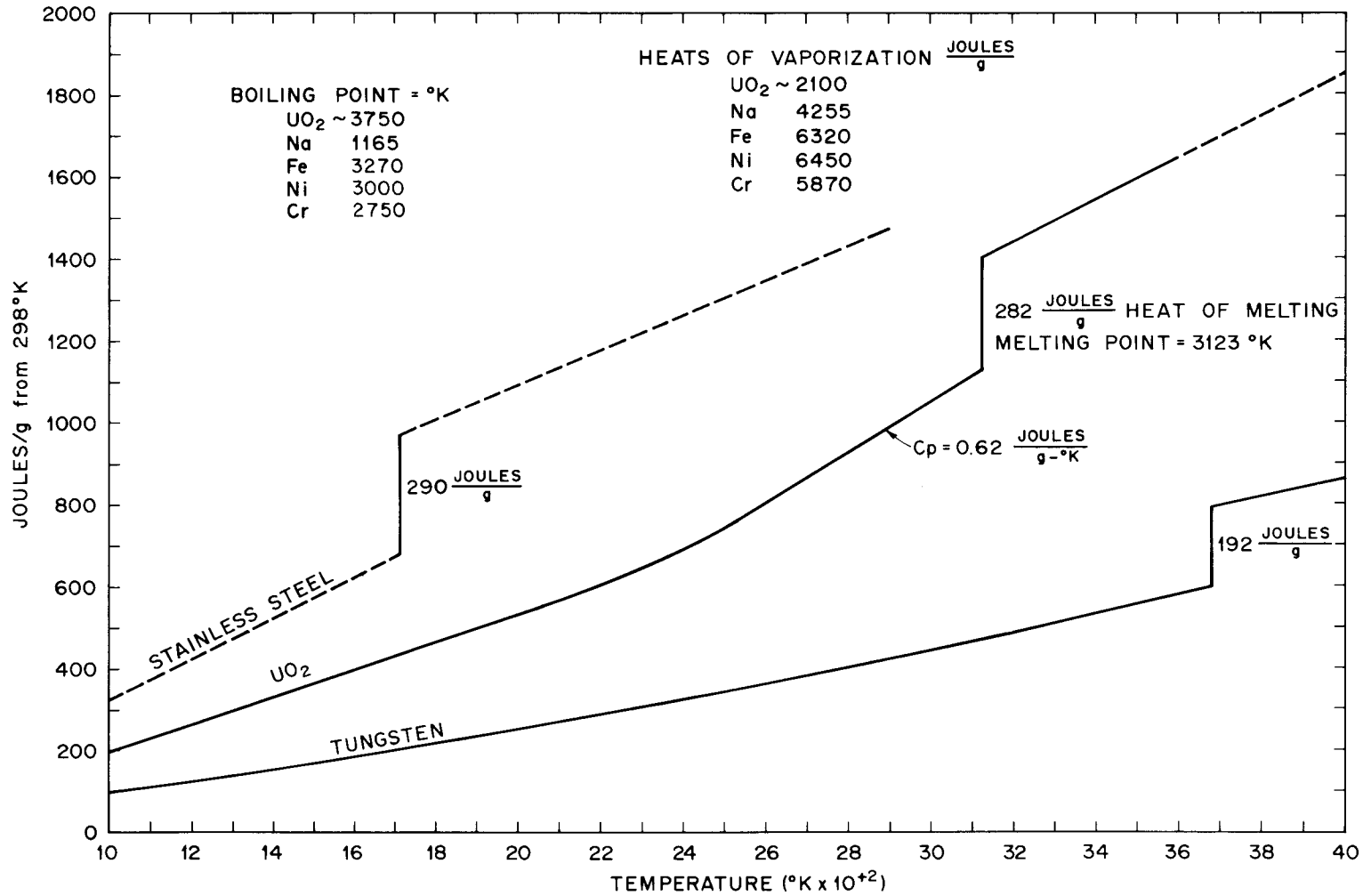


Fig. 2. Heat capacity above 298°K, boiling points, and heats of vaporization for UO_2 and selected other materials (data taken from refs. 2 and 3).

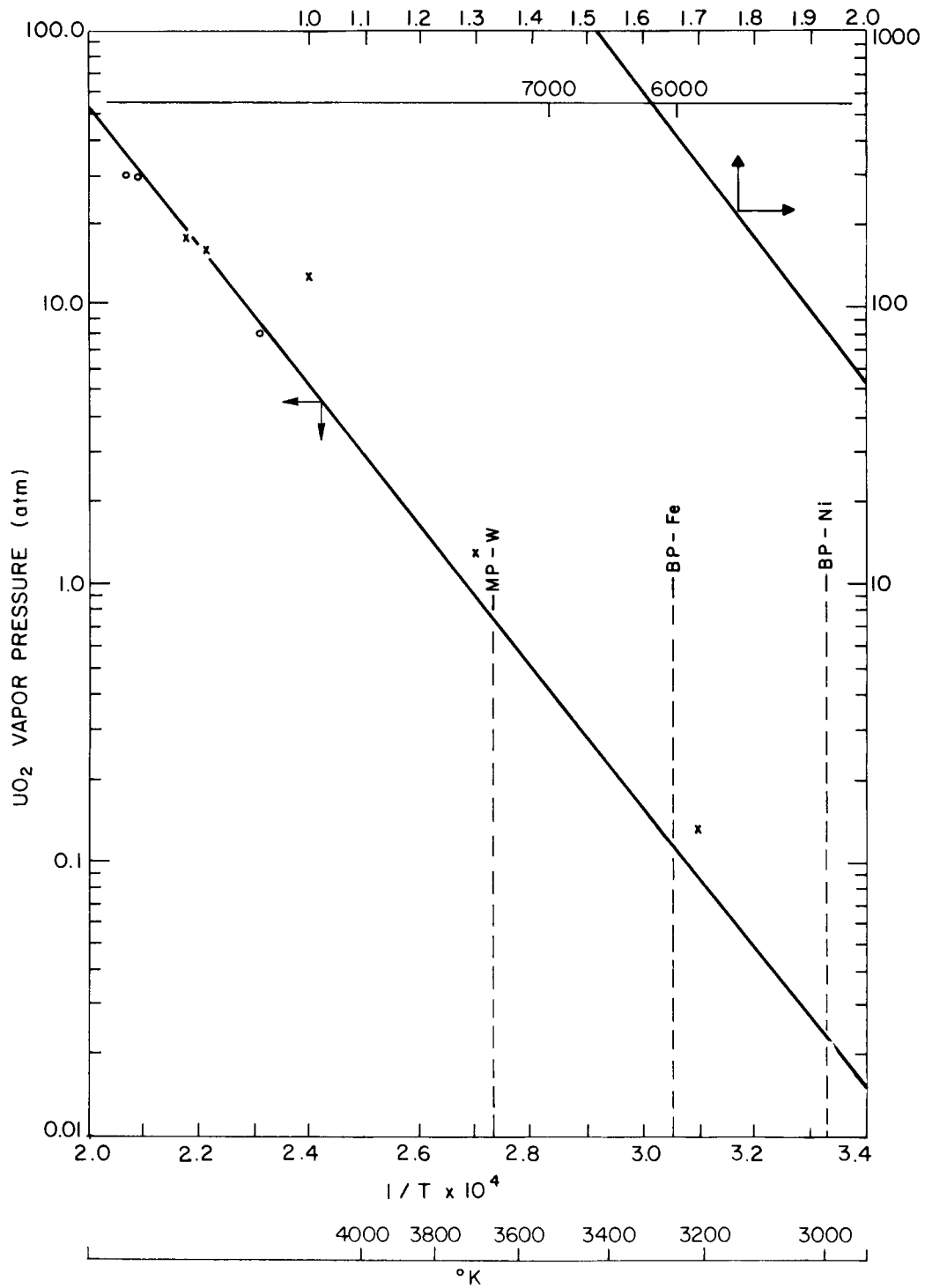


Fig. 3. Vapor pressure of UO_2 versus temperature. (data taken from ref. 10).

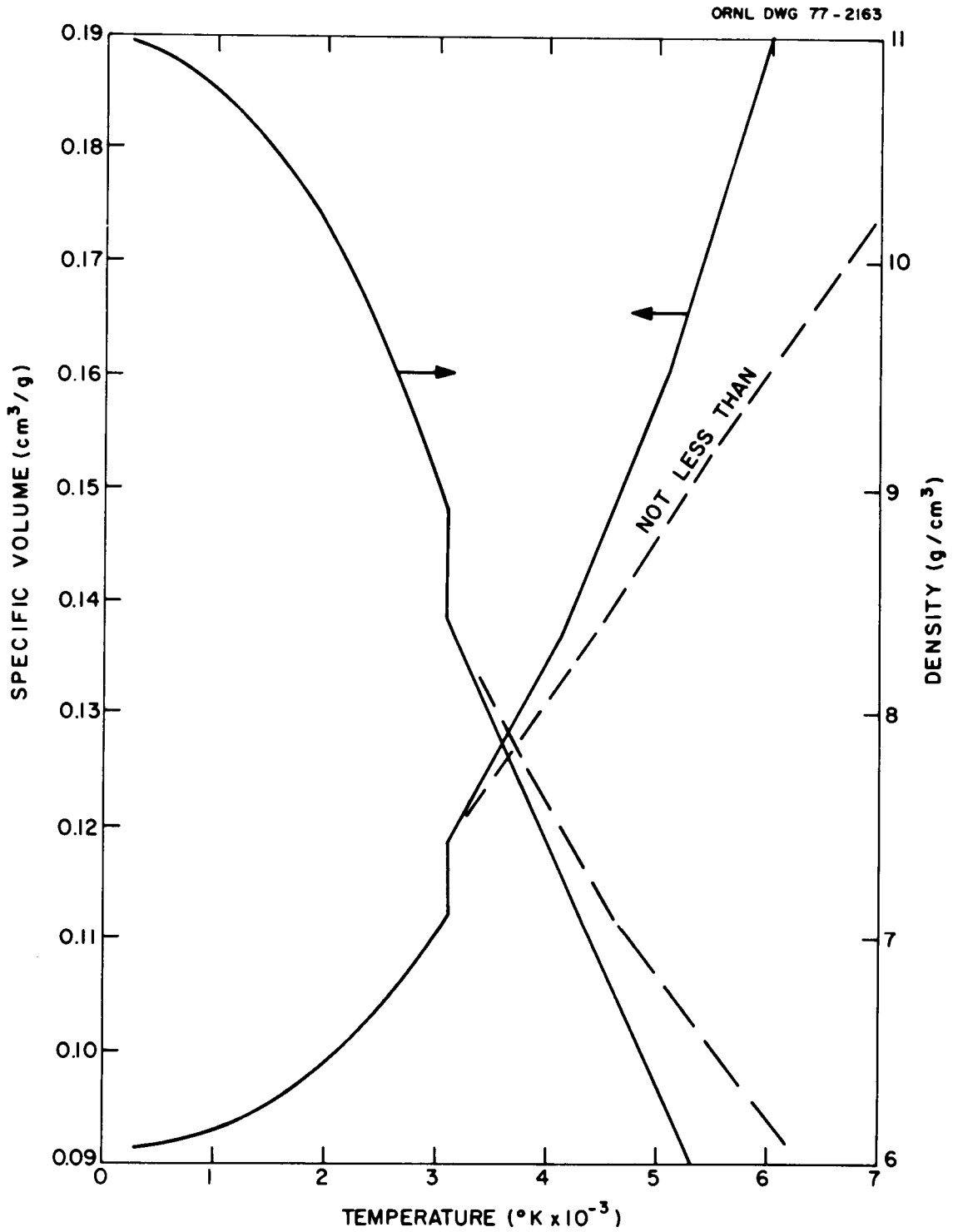


Fig. 4. Density and specific volume of UO₂ versus temperature. (data taken from refs. 4-9).

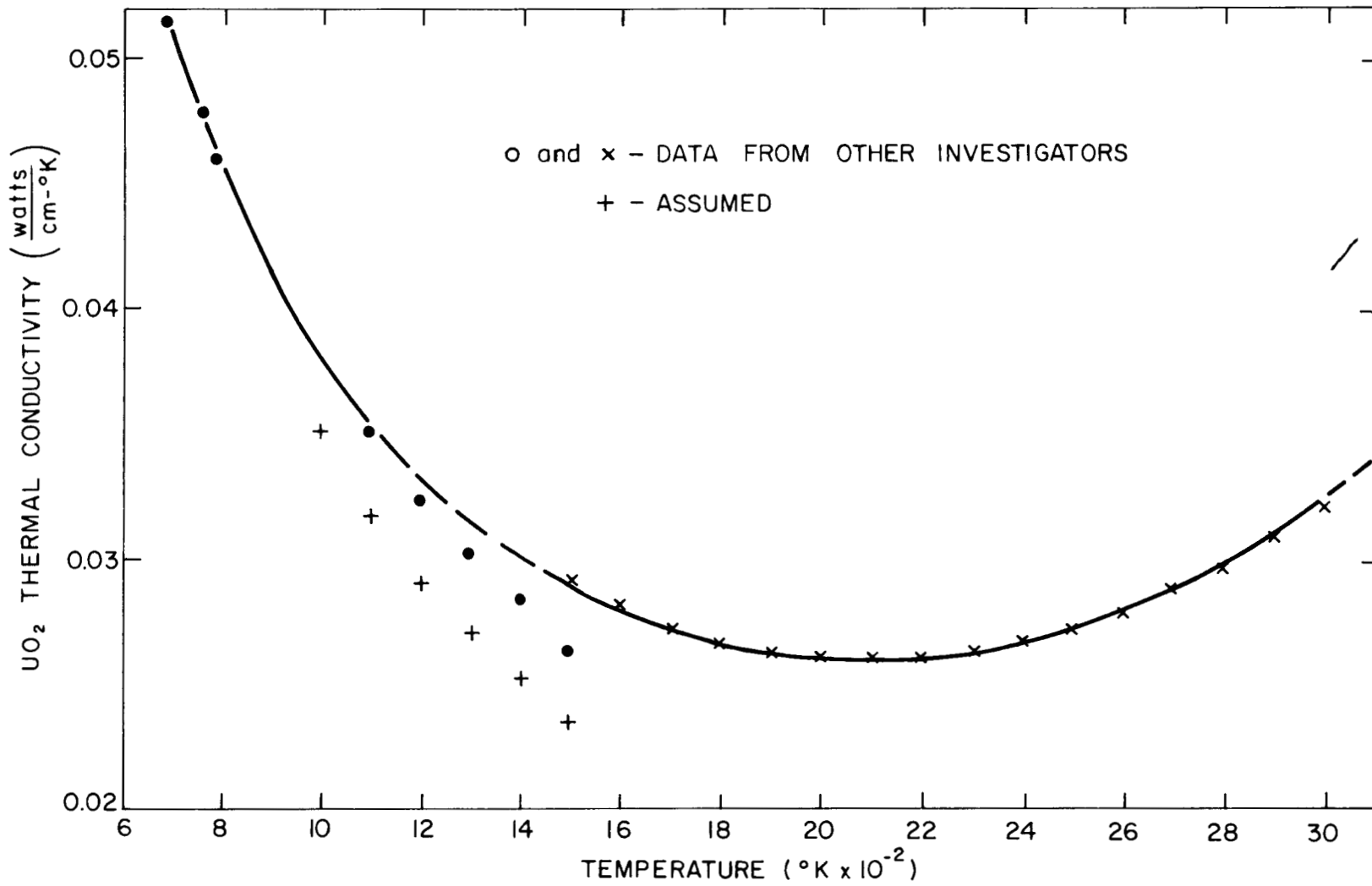


Fig. 5. Variation in the thermal conductivity of UO_2 with temperature.

efficient system would require < 4000 joules to vaporize 1 gram of UO_2 starting from $3000^\circ K$. Only 4 msec would be required for a power level of 1 MW per gram. This "ideal" energy may have to be increased several times for an actual system, but the physical size and cost of such a storage system was estimated to be reasonable.

Many technical facilities were contacted with regard to both the availability of such energy storage devices and their experience in using such equipment. Arnold Engineering Development Center at Tullahoma, Tennessee, was visited in May 1974. A 500-kJ, 175,000-A inductive supply and two capacitor bank storage supplies, one of 394 kJ at 6 kV and the other 280 kJ at 10 kV, were inspected; very productive discussions were held based on their experience with the equipment.

The initial concept of the test fuel sample was to use a segment of the original 5-cm-long fuel rod, complete with ~ 5 grams of cladding. After considering the electrical conductivities of stainless steel and UO_2 , it was apparent that very little energy could be deposited in the fuel until the cladding had been vaporized or otherwise removed. It was believed that the sample could be separated from the surrounding sodium by an insulating structure, probably UO_2 , which would maintain an annular volume between the sample and insulator to allow cladding vapor expansion. To discourage arc discharge through the gas, it was decided that not more than an estimated 500 V per centimeter could be applied and that the annular volume would have to be limited in order to maintain a high gas pressure. The use of inductive storage was discouraged by limiting the applied voltage to 500 V per centimeter, since the energy storage is proportional to LI^2 (L = inductance, I = current). For a 5-cm-long, 0.5-cm-OD UO_2 sample at $3000^\circ K$, 5000 A would require a very large inductance, 0.02 H (the AEDC inductor was about ~ 10 ft high by 10 ft in diameter for an inductance of 16.3 μH). Consequently, it was concluded that the best method for achieving our objectives was to use capacitor bank energy storage.

5. EXPERIMENTAL PROGRAM DEVELOPMENT

An early literature search disclosed numerous references on exploding metal wires by capacitor discharge. However, the literature was not specifically applicable because of the vast differences in the electrical properties of metals and UO_2 or fuel. The most useful reference found was on experiments conducted by Schikarski,¹¹ who attempted to vaporize unclad UO_2 by dumping a 57-kJ, 19-kV capacitor bank into a preheated cylindrical sample. Although the quantities of aerosol produced in these experiments were not explicitly reported, one can estimate from the reported concentrations and chamber volumes that generally <1% of a 7.5-g sample was vaporized. Schikarski's best results were obtained when the energy deposition rate was slowed by the use of a series circuit inductance; this suggested that greater success might be obtained with a lower voltage-higher capacitance storage bank. Calculations using the system properties shown in Sect. 3.2 and several sample configurations supported this assumption. They also indicated that the preliminary radial temperature gradient and the ability of the system to accommodate early expansion without incurring severe, internal, mechanical stresses would be important in aerosol yield. These supporting calculations were developed into a computer simulation model used in an analysis program which was conducted in parallel with the experimental program. The development of and results obtained from this analysis program are included in subsequent sections of this report.

The early studies resulted in the first conceptual sample shown in Fig. 6. which was then believed to provide an appropriate geometry for achieving significant vaporization before loss of electrical continuity. This coaxial energy input system allows a symmetrical current to flow down the center conductor and through a tungsten electrode into the sample to be vaporized. A lower tungsten electrode takes the current from the sample to the outer stainless steel pipe and tubing - the coaxial current return path. This test sample design appeared sufficiently flexible to allow easy variation in the physical details and materials used. The actual sample configuration and design now in use has undergone considerable evolutionary changes.

ORNL DWG 74-10160R2

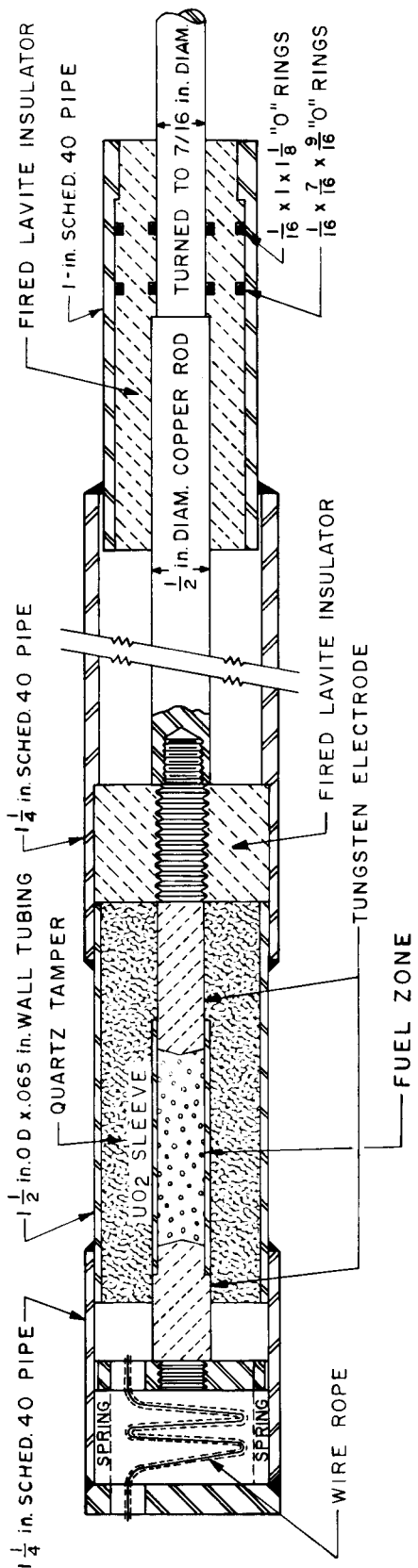


Fig. 6. Conceptual coaxial design for fuel vaporization by capacitor discharge.

To establish the feasibility of the concept and sample design, a proposal was made to conduct some early experiments using the capacitor banks of the AEDC-Von Karman Facility (VKF), Tunnel J, located at AEDC. The Tunnel J facility had seven identical banks of 56 kJ (6 kV) each, two identical banks of 112 kJ (10 kV) each, and one bank of 42 kJ (10 kV). The AEDC-VKF banks appeared particularly useful for exploratory experiments, requiring low (<5-kV) initial bank voltages. At 2 kV, the 6-kV AEDC banks store 44 kJ.

Acceptance of our test proposal by AEDC in September 1974, a pretest planning conference, and a formal test proposal submission in October 1974, resulted in an interagency agreement between the AEC (now NRC) and the Department of the Air Force to conduct a limited series of feasibility tests early in 1975. This program was later expanded to provide additional CDV testing in support of the design and construction of an ORNL CDV facility.

During this same period, an early version of a sample preheater was designed and constructed at ORNL. This preheater was necessary in order to bring the UO_2 or fuel sample into an electrical conductivity state suitable for accepting power from the capacitor bank on the order of 10^6 W per gram. A standard power supply appeared unsuitable for the preheater because the electrical resistivity of UO_2 (and PuO_2) has a large negative temperature coefficient, which results in a sample resistance change of about six orders of magnitude when heating a specimen from room temperature to vaporization conditions. The change is about two orders of magnitude over the temperature range 2000 to 5000°K. The sample must be preheated to some selected temperature to obtain sample resistance values that would allow rapid energy transfer from the capacitor storage banks at acceptable potentials between the high-voltage electrode and the containment, as well as to minimize the power rate variation during discharge. A constant power mode was selected for this preheating in order to maintain stable operation with a given sample configuration. Operation, while in this mode, was unaffected by changes in resistance (within about two orders of magnitude), changes in sample packing, and any unavoidable sintering changes.

The device developed to regulate the supply of energy to the fuel sample at a constant power is pictured in Fig. 7. The basic power control elements for this device are ac phase-fired silicon-controlled rectifiers. The fast response and infinite resolution of this control technique allowed the system to be designed with a response time of less than one-tenth of a second.

Sample power is established by measuring the voltage across and the current through the sample and then electronically multiplying them to give a signal proportional to power input. This signal provides feedback to the energizing circuitry to maintain power at the selected value when the sample resistance changes.

Sample heatup is begun by applying high voltage (2500-V ac maximum which is manually decreased with a variac) as the sample resistance decreases. When the resistance is sufficiently lowered (typically to 500 Ω), the load is transferred to the two-stage constant power regulator (Fig. 7). Initial tests indicate that <1 min is required to reach the 500- Ω range from an initial sample resistance of 50,000 to 70,000 Ω . Successful operation of the controller was demonstrated with UO₂ samples contained in alumina and silica sleeves. These preliminary experiments were conducted with power inputs from 100 to 1000 W and load resistances varying down to 0.2 Ω during preheating.

Continuing investigation of the requirements for the test sample to be used in the initial AEDC experiments appeared to eliminate any possibility of using a section of a fuel pin with the supplied cladding. The design of a containment system that would remain intact in the presence of the metal vapor while the fuel reached vaporization temperatures (2 to 3 msec at 500 V per centimeter of fuel length) appeared to be unlikely, even if electrical continuity through the fuel could be maintained after cladding vaporization.

Because the cladding had to be removed, the fuel itself had to be physically self-supporting until an acceptable amount of energy could be deposited. An additional requirement was that arcing through the sample or to the containment walls should not be permitted. Argon, the initial

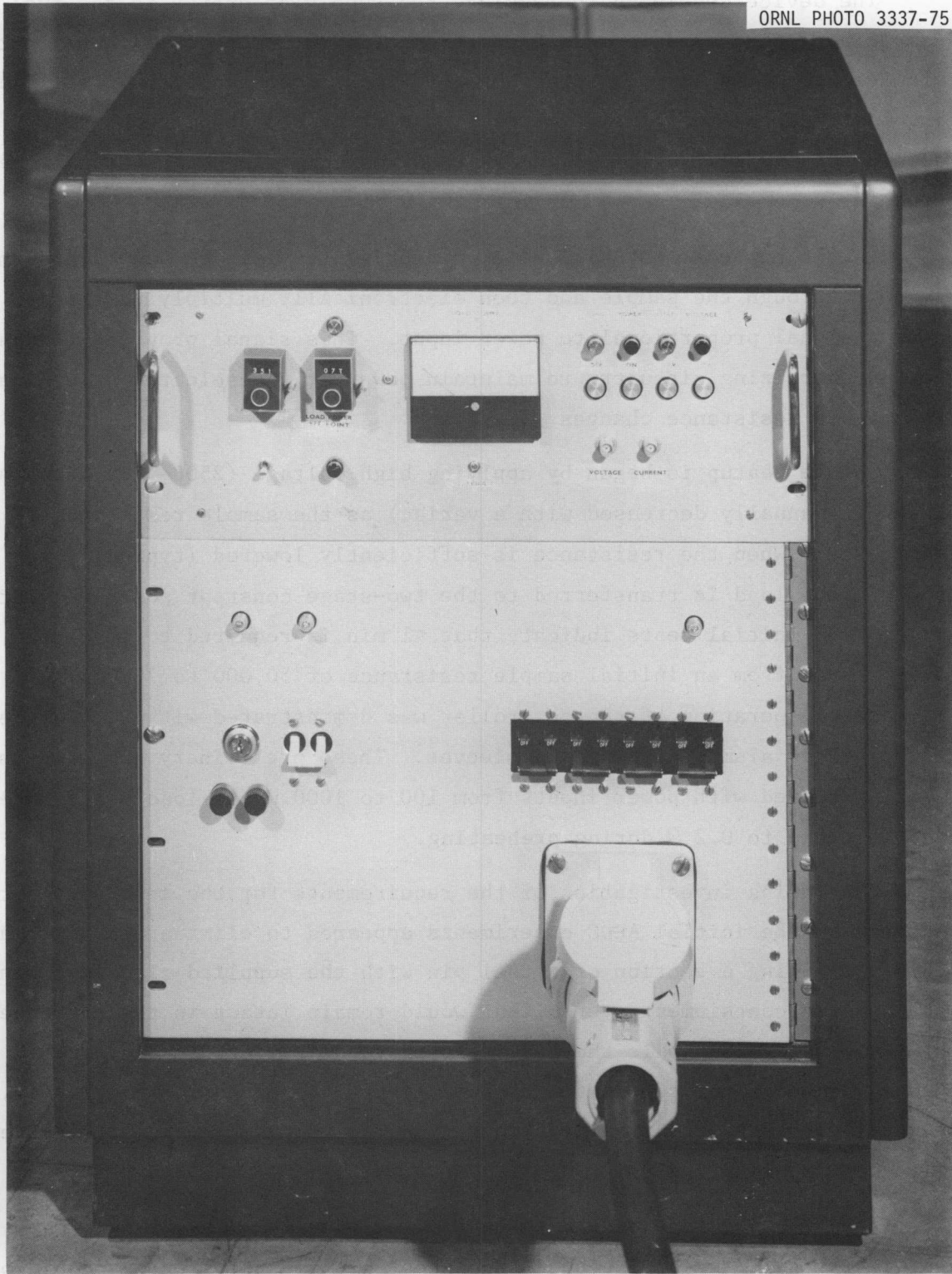


Fig. 7. Prototype Constant-Power Energy Supply Regulator.

gas phase, will support a corona discharge at a potential gradient of ~ 7500 volts per centimeter. However, if a sufficient number of free electrons are present in the high-temperature vapor, arc discharge can be supported at lower potentials. For example, cesium vapor at high temperature, which is very available in high burnup fuel, can be a source of free electrons. To minimize arcing possibilities in anticipation of using irradiated fuel, we limited the potential gradient at any point in the interior of the test sample to 500 V per centimeter. It also appeared necessary to provide a significant void region in the sample to compensate for the expansion of the fuel during the preheat stage. The lack of such a void region may explain the low aerosol yields that had been obtained by investigators who had previously attempted to use rigidly mounted solid fuel pellets.

To meet the above requirements, the prototype fuel-simulant sample assemblies used initially at AEDC with the CDV System consisted of a stack of simulated LMFBR fuel pellets (UO_2) contained between spring-loaded tungsten electrodes and surrounded by loose UO_2 packing, all contained by an outer quartz (or sometimes Al_2O_3) sheath mounted in a flanged, open-structure stainless steel housing. The spring loading compensated for the expansion during the preheat cycle, and the quartz provided electrical insulation as well as structural containment. The UO_2 packing served as thermal insulation which prevented quartz melting and helped minimize stresses from the thermal expansion.

Figure 8, an X-radiograph of an actual assembly, clearly shows the pellet stack between the electrodes. The compression spring is between the caplet top and the electrode holder. Figure 9 is a closeup of the quartz outer sheath, with UO_2 microsphere packing evident between the sheath and the pellet stack. Figure 10 shows the complete assembly ready to insert in the test vessel. The quartz sheath containing the microspheres and pellet stack is visible at the index finger of the holder, and the compression spring is visible in the second opening. Another assembly, mounted and ready for CDV firing, can be seen in the background through the test vessel viewing port.

ORNL PHOTO 1198-75

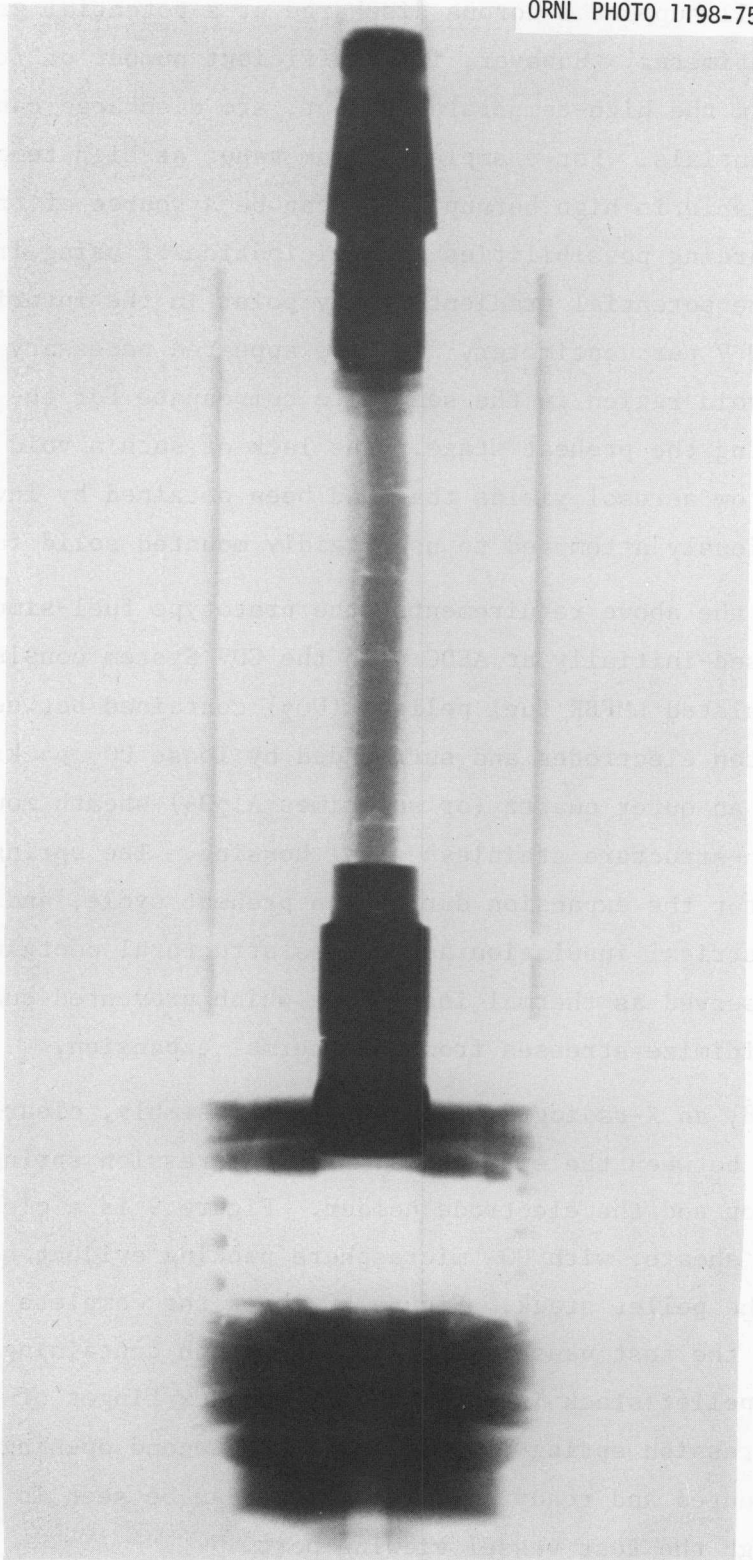


Fig. 8. X-radiograph of a fuel-simulant sample assembly loaded axially with pellets surrounded by microspheres.

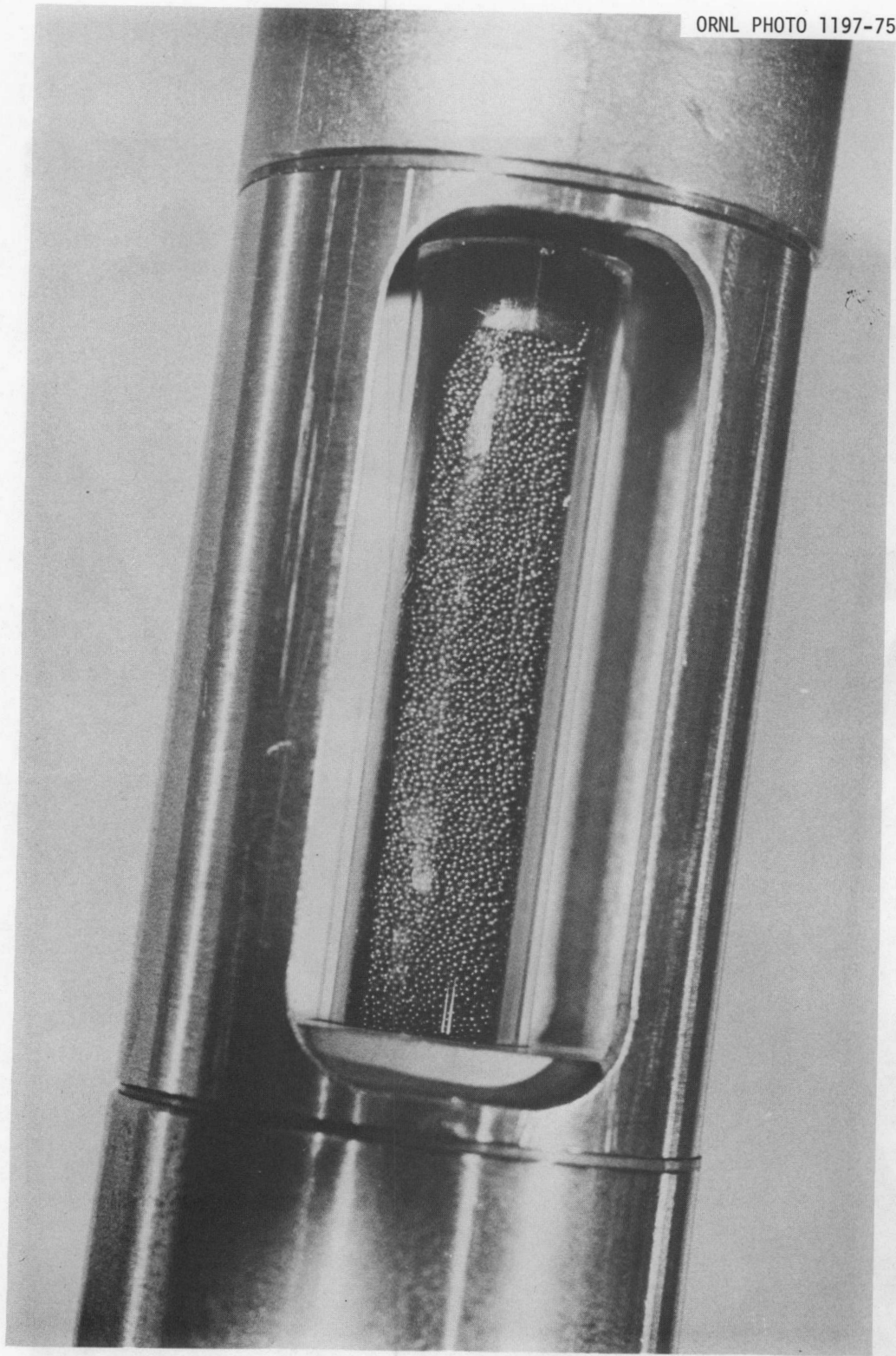


Fig. 9. Closeup of fuel-simulant test sample showing packing microspheres within quartz containment.



Fig. 10. Typical fuel-simulant sample assembly used in the capacitor discharge vaporization test.

Three assemblies for the first test series were completed in February 1975. At that time, four groups of three experiments each were planned, extending through April 1975, for the purpose of demonstrating the feasibility of the CDV technique. Operating voltages between 2 and 5 kV, short-circuit currents from 26 to 47kA, and discharge times of 1.0 to 3.3 msec were observed. A visible, persistent aerosol in the 0.4 m³ test vessel was not produced until test No. 6. The succeeding series of five tests during April 1975, all gave measurable quantities of aerosol, including one test in which stainless steel filings were added to the micro-sphere packing as a cladding simulant.

We believed that the feasibility of the CDV technique had thus been demonstrated, but many unanswered questions still remained. Our working relationship with AEDC personnel had been very good, and the arrangement appeared to be cost-effective. Therefore, it was proposed by ORNL and accepted by NRC that we should continue the program in an exploratory and parametric manner in order to resolve some of the remaining questions and attempt to optimize the CDV design.

A particular objective was to improve the aerosol yield by attempting to optimize fuel-sample design, bank voltage, bank discharge rate, and preheater time and power input. Information of direct use in the design and construction of the ORNL CDV System could thereby be acquired. It was felt worthwhile to also include attempts to vaporize samples with the cladding still intact, since this condition would be more prototypical of the postulated HCDA conditions.

A total of 40 experiments were conducted by the end of the development program in April 1976. The most pertinent results are presented in Sect. 7, Experimental Results.

6. CONCURRENT ANALYSIS PROGRAM

In addition to the preliminary analytical design studies by the staff during the early phases of the program, we developed a "design" computer program to model the power input and resulting heat flows and temperature

distribution in the CDV test article, as then conceived. In summary, equations for heat transfer with simultaneous electric power dissipation through five concentric cylindrical annuli were formulated for temperature variation in the radial direction only. The equations were originally developed to simulate an experimental system that would use powdered UO_2 in the center annulus. The effects of varying the power inputs, containment sleeve material, void fraction (VF) in the powder, and external coolant were studied using a numerical solution for the temperature profile. Significant decreases in the centerline temperature were calculated for a UO_2 containment sleeve in comparison with those of an alumina sleeve. No significant differences were calculated for the temperature profiles of a system externally cooled by air at room temperature as compared with one cooled by liquid sodium at $840^\circ K$.

The original system model configuration is shown in Fig. 11. This was similar to the configuration used for AEDC testing, except that the stainless outer sheath in the model was continuous and no central pellet stack was included. In addition, the model contains no provision for phase changes and was intended only for the preheat cycle; however, because of the apparent usefulness of this approach, we extended the finite-difference computer simulation to include the capacitor discharge phase.

Complete analytical modeling of the CDV tests required consideration of three different phases: a low-power preheat period which brings the test sample to the desired steady-state thermal distribution, a zero-power waiting period which allows the temperature gradient across the UO_2 (or fuel) pellet stack to decrease and flatten, and the capacitor discharge period up to sample disassembly.

The final computer simulation then treats a representative cylindrical geometry of fuel sample within a quartz containment tube. The cross section is subdivided into concentric finite-element rings (up to 50) and a forward marching-in-time procedure is used. The computer program is pragmatic in the sense that it was developed as an experimental design tool to describe the effects of various design and experimental parameter changes so that value judgements could be made concerning their effects on

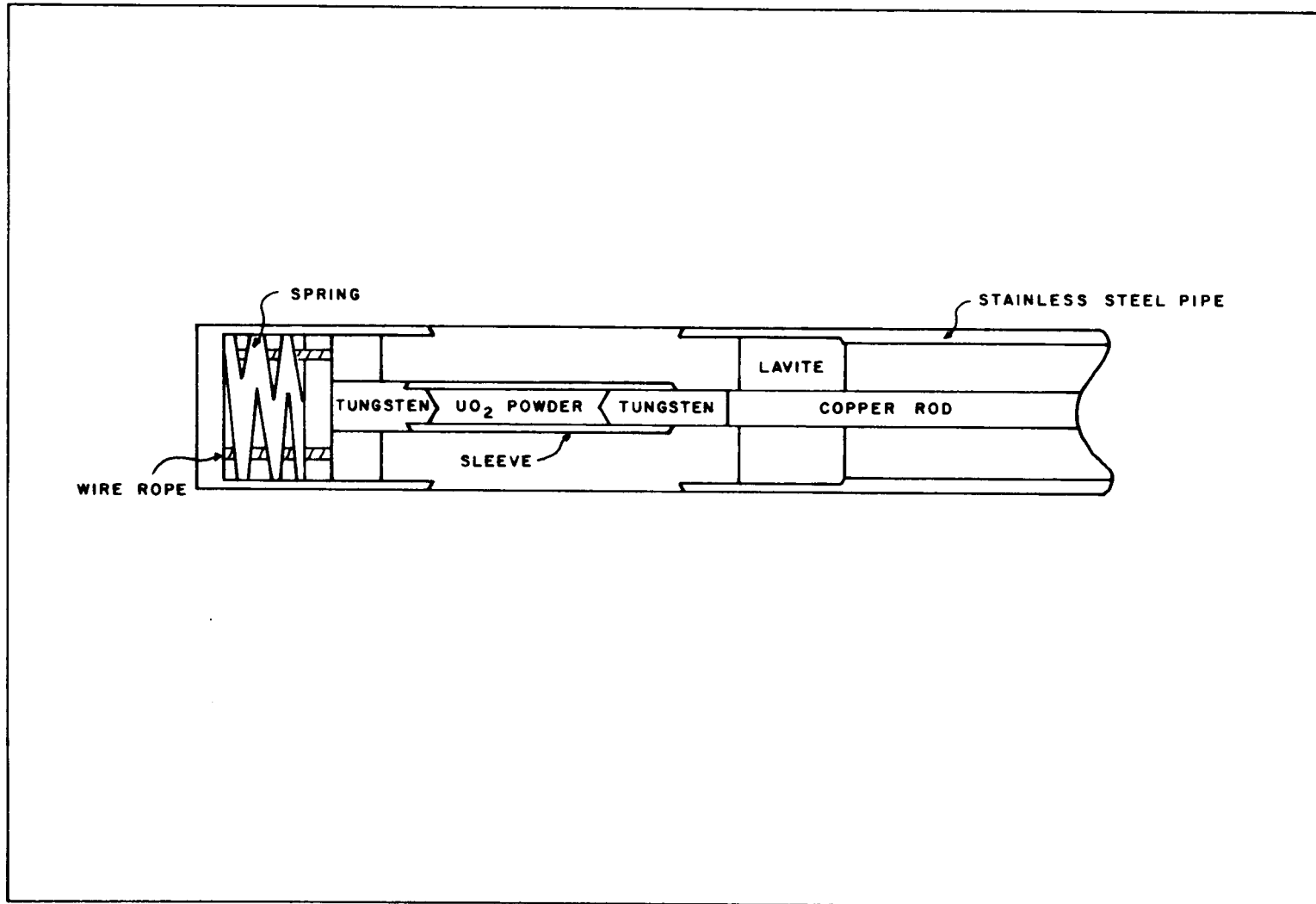


Fig. 11. Detailed sketch of the initially modeled system.

the potential aerosol yield. Some details and results of the design computer model are discussed below.

6.1 Computer Calculations for the Preheat Steady-State Phase

The preheat period is treated as a steady-state conduction problem in cylindrical geometry with variable material properties and nonuniform internal electrical heat generation with surface losses due to radiation only.

Finite element ring thickness and sample length, both variable, are normally chosen as 0.015 cm and 4 cm respectively; hence, 1.5 cm is the maximum sample diameter that can be analyzed. The central pellet stack normally occupies the interior 18 rings (0.54 cm), although assessments have also been made for all-powder or all-microsphere systems. The void fraction in the outer pack between the pellet stack and quartz containment is input which must be consistent with the particular type of packing used (powder or microspheres). The physical constants originally used in the calculations are as follows:

$$\text{Electrical conductivity} = 5.38 \times 10^{15} T^{-5} \Omega\text{-cm};$$

$$\text{Thermal conductivity} = 3 \times 10^{-2} \text{ W/cm-}^\circ\text{K};$$

$$\text{Melting point} = 3100^\circ\text{K};$$

$$\text{Heat of fusion} = 282 \text{ J/g};$$

$$\text{Specific heat} = 0.62 \text{ J/g-}^\circ\text{K};$$

$$\text{Thermal radiation} = 5.75 \times 10^{-12} T^4 \times \epsilon \text{ W/cm}^2,$$

where

$$\begin{aligned} \epsilon &= \text{emissivity of the } \text{UO}_2 \text{ outer surface,} \\ &\text{usually taken as 0.8;} \end{aligned}$$

$$\text{Density vs temperature} = \text{Algebraic fit.}$$

Good approximations of electrical and thermal conductivities may be obtained in the range of 1800 to 3000°K and around the melting point respectively. It is assumed that since UO₂ powder or microspheres are placed in the region between the outer containment and the pellet stack the thermal and electrical properties in this region have local values calculated as (1-E) times the theoretical value. The void fraction, E, varies from 0.4 to 0.6. This assumption, however, cannot be completely justified on theoretical grounds.

The preheat program proceeds by computing the specific electrical conductivity, RHO, for the center ring at a trial temperature using either

$$RHO = 5.38 \times 10^{15} T^{-5},$$

or

$$RHO = \frac{1}{58833.62 \frac{14.697 \times 10^3}{T} + 0.77e \frac{1.846 \times 10^8}{T}}.$$

Both functions give good fits to literature values ranging from 2000°K to the melting point of UO₂. The validity of extending these empirical fits to much higher temperatures has not been demonstrated. Ring power is then calculated as:

$$\nabla P = \frac{E^2}{R} = \frac{E^2 \times A}{RHO \times TALL},$$

where

VP = ring power,

E = applied voltage,

R = ohms,

A = $\pi(r_n^2 - r_{n-1}^2)$ = ring cross-sectional area, and

TALL = ring length.

The temperature difference, ∇T , established to transfer the steady power to the next ring; is then calculated using

$$\nabla T = \frac{VP \times \nabla R}{THCD \times SX(VDFR)},$$

where

∇R = ring thickness, cm;

THCD = thermal conductivity (W/cm-°K) = 0.03, or

$8.088 \times 10^{-2} - 5.305 \times 10^{-5} \times T + 1.245 \times 10^{-8} T^2$ when calculated using best fit to reported literature values;

S = $4.443 \times TALL \times \sqrt{r_n^2 + r_{n-1}^2}$ = average ring surface;

X = surface area, cm²; and

VFDR = void fraction.

The ∇T value is subtracted from the initial temperature to obtain the temperature for the next ring. The calculations are repeated, with successive ∇T s determined by the sum of the ∇P s, since all generated heat is assumed to be transferred symmetrically in the radial directions. This computation scheme continues for the chosen number of rings and results in a final steady-state surface power and temperature.

Convection losses are assumed to be negligible, and the radiation surface heat loss, Q_0 , is calculated to be:

$$Q_0 = 5.75 \times 10^{-12} \times \text{EMIS} \times 2\pi \text{ LX} \times \text{No. of rings} \times \text{DR} \times T_s^4,$$

where

EMIS = surface emissivity chosen (usually 0.8);

LX = sample length, cm;

DR = sample radius, cm; and

T_s = surface temperature of outside ring.

The program iterates on applied voltage until the total power, $\Sigma \nabla P$, is equal to Q_0 .

As a subroutine within the main preheat program, the mass of UO_2 above the melting point within each ring is calculated, using volume and density vs ring temperature, as:

$$\text{WT} = 12.6755 - T \times 1.204 \times 10^{-3} (1-\text{EMP}) \text{ g/cm}^3,$$

where EMP is the void fraction assigned for packed rings.

When steady-state equilibrium has been calculated for the imposed conditions, the information is printed in the format shown in Table 1.

6.2 Effect of Delay Time on Radial Temperature Gradient

At the end of the preheat cycle, a significant temperature difference (gradient) existed between the center and edge of the pellet stack. It was believed that a reduction in this difference would result in more stable operation and an increase in aerosol yield. A short time delay between preheat and capacitor bank discharge was thought to be the simplest method of achieving this reduction in the temperature gradient. Efforts to arrive at an optimum delay time using a transient version of our computer model were unsuccessful. Therefore, the optimum range of

Table 1. An example of computed steady-state high preheat conditions^a

No.	Temperature (°K)	Ring Mass (g)	End Area	Fraction Filled	Fraction Melted
1	3400.0000	2.3396E-02	7.0686E-04	1.0000E 00	1.0000E 00
2	3396.5886	7.0233E-02	2.1206E-03	1.0000E 00	1.0000E 00
3	3390.4910	1.1719E-01	3.5343E-03	1.0000E 00	1.0000E 00
4	3381.9873	1.6433E-01	4.9480E-03	1.0000E 00	1.0000E 00
5	3371.0901	2.1172E-01	6.3617E-03	1.0000E 00	1.0000E 00
6	3357.7976	2.5943E-01	7.7754E-03	1.0000E 00	1.0000E 00
7	3342.1064	3.0751E-01	9.1891E-03	1.0000E 00	1.0000E 00
8	3324.0132	3.5603E-01	1.0603E-02	1.0000E 00	1.0000E 00
9	3303.5144	4.0506E-01	1.2017E-02	1.0000E 00	1.0000E 00
10	3280.6069	4.5466E-01	1.3430E-02	1.0000E 00	1.0000E 00
11	3255.2883	5.0490E-01	1.4844E-02	1.0000E 00	1.0000E 00
12	3227.5571	5.5583E-01	1.6258E-02	1.0000E 00	1.0000E 00
13	3197.4136	6.0753E-01	1.7671E-02	1.0000E 00	1.0000E 00
14	3164.8604	6.6007E-01	1.9085E-02	1.0000E 00	1.0000E 00
15	3129.9036	7.1349E-01	2.0499E-02	1.0000E 00	1.0000E 00
16	3092.5542	7.7481E-01	2.1913E-02	1.0000E 00	0.0
17	3052.8293	8.2939E-01	2.3326E-02	1.0000E 00	0.0
18	3010.7544	8.8482E-01	2.4740E-02	1.0000E 00	0.0
19	2966.3647	5.6469E-01	2.6154E-02	6.0000E-01	0.0
20	2890.9106	6.0140E-01	2.7567E-02	6.0000E-01	0.0
21	2812.7336	6.3899E-01	2.8981E-02	6.0000E-01	0.0
22	2732.0037	6.7746E-01	3.0395E-02	6.0000E-01	0.0
23	2648.9829	7.1683E-01	3.1809E-02	6.0000E-01	0.0
24	2564.0391	7.5709E-01	3.3222E-02	6.0000E-01	0.0
25	2477.6521	7.9822E-01	3.4636E-02	6.0000E-01	0.0
26	2390.4106	8.4016E-01	3.6050E-02	6.0000E-01	0.0
27	2302.9932	8.8286E-01	3.7463E-02	6.0000E-01	0.0
28	2216.1326	9.2622E-01	3.8877E-02	6.0000E-01	0.0
29	2130.5679	9.7016E-01	4.0291E-02	6.0000E-01	0.0
30	2046.9897	1.0146E 00	4.1704E-02	6.0000E-01	0.0
31	1965.9919	1.0594E 00	4.3118E-02	6.0000E-01	0.0
32	1888.0374	1.1044E 00	4.4532E-02	6.0000E-01	0.0
33	1813.4441	1.1497E 00	4.5946E-02	6.0000E-01	0.0
34	1742.3904	1.1951E 00	4.7359E-02	6.0000E-01	0.0
35	1674.9329	1.2406E 00	4.8773E-02	6.0000E-01	0.0

^aCenter temperature = 3400°K; sample length = 4 cm; delta radius = 0.0150 cm; emissivity = 0.8000; estimated voltage = 15; void fraction = 0.40000; small loops = 35; large loop = 100; printing frequency = 10; starting voltage = 15; total preheat power = 8.962E 02; optimum voltage = 1.400E 01.

delay time at 100% pellet melt was estimated to be between 1 and 4 sec by manual calculational methods.

6.3 Computer Calculations for the Capacitor Discharge Phase

The capacitor discharge phase deposits energy so rapidly that internal heat transfer between regions can be neglected and each finite-difference element can be treated as a separate element in an array.

A fixed total power in the entire sample (usually 15 MW) is applied over a small time increment (10^{-5} sec). The power distribution among elements is determined by the conditions for each element at the start of the time increment.

That is,

$$\text{Joules per ring} = \text{initial ring conductances} \times E^2 \times 10^{-5} \text{ sec,}$$

where

$$E = \frac{\text{Desired power rate}}{\text{Total sample conductance}}.$$

Using the energy input into the given ring mass, a new ring temperature is calculated, which included the effect of the heat of melting. This sequence is continued until a fixed total power input is calculated.

Table 2, calculated for 12 kJ of energy insertion from the conditions shown in Fig. 2, is representative of the calculated conditions within a sample near disassembly. The total amount vaporized, assuming adiabatic expansion to 1 atm, is the sum of the calculated vapor quality resulting above the boiling point of UO_2 from each ring.

For each individual ring,

$$\text{Grams yield as vapor} = \text{mass} \times \left[(T \text{ ring} - 3750) 0.62/2100 \right]$$

where

$$\text{UO}_2 \text{ boiling point} = 3750^\circ\text{K,}$$

$$\text{heat capacity} = 0.62 \text{ J/g-}^\circ\text{K, and}$$

$$\text{heat of vaporization} = 2100 \text{ J/g.}$$

This calculation can be superceded by the use of a more precise equation of state and constant internal energy expansion.

Many parametric studies have been made using this computer simulation model. The calculated results are descriptively adequate and are

Table 2. An example of calculated conditions during capacitor discharge close to disassembly^a

No.	Temperature (°K)	Ring Mass (g)	Ring (Joules)	Fraction Melted	Fraction Filled
1	6162.50781	1.10470E-02	2.85663E-01	1.00000E 00	1.00000E 00
2	6151.98438	3.32828E-02	8.56133E-01	1.00000E 00	1.00000E 00
3	6136.48438	5.58211E-02	1.42478E 00	1.00000E 00	1.00000E 00
4	6116.60547	7.87781E-02	1.99086E 00	1.00000E 00	9.99999E 00
5	6092.26172	1.02277E-01	2.55363E 00	1.00000E 00	9.99999E 00
6	6063.39063	1.26442E-01	3.11229E 00	1.00000E 00	1.00000E 00
7	6029.99219	1.51395E-01	3.66600E 00	1.00000E 00	1.00000E 00
8	5991.92969	1.77270E-01	4.21387E 00	1.00000E 00	1.00000E 00
9	5949.16406	2.04195E-01	4.75498E 00	1.00000E 00	1.00000E 00
10	5901.57031	2.32309E-01	5.28831E 00	1.00000E 00	1.00000E 00
11	5849.01563	2.61753E-01	5.81273E 00	1.00000E 00	1.00000E 00
12	5791.32031	2.92683E-01	6.32700E 00	1.00000E 00	1.00000E 00
13	5728.26953	3.25258E-01	6.82974E 00	1.00000E 00	1.00000E 00
14	5659.57813	3.59660E-01	7.81932E 00	1.00000E 00	1.00000E 00
15	5584.84766	3.96093E-01	7.79381E 00	1.00000E 00	1.00000E 00
16	5484.48438	4.37690E-01	8.28013E 00	1.00000E 00	1.00000E 00
17	5315.71094	4.91810E-01	8.57007E 00	1.00000E 00	1.00000E 00
18	5050.02734	5.64579E-01	8.74897E 00	1.00000E 00	1.00000E 00
19	4710.07031	6.54110E-01	8.74173E 00	1.00000E 00	1.00000E 00
20	4352.11328	7.52057E-01	8.66982E 00	1.00000E 00	1.00000E 00
21	4020.85010	8.50822E-01	8.26349E 00	1.00000E 00	1.00000E 00
22	3726.07422	9.48304E-01	7.80041E 00	1.00000E 00	1.00000E 00
23	3449.72949	1.04762E 00	7.01782E 00	1.00000E 00	1.00000E 00
24	3174.57202	1.15188E 00	5.33228E 00	1.00000E 00	9.99999E-01
25	3100.00000	1.22342E 00	4.98582E 00	5.62660E-01	9.99999E-01
26	3049.84351	1.28576E 00	4.61676E 00	0.0	9.99999E-01
27	2778.29663	1.38710E 00	2.98501E 00	0.0	9.99999E-01
28	2519.43726	1.48901E 00	1.80956E 00	0.0	9.99999E-01
29	2285.99121	1.59064E 00	6.85861E-01	0.0	7.42877E-01
30	2128.08887	1.67419E 00	4.35810E-01	0.0	6.05968E-01
31	2025.18530	1.75296E 00	3.22476E-01	0.0	6.04290E-01
32	1931.21069	1.83119E 00	2.39498E-01	0.0	6.03084E-01
33	1844.99341	1.90898E 00	1.78819E-01	0.0	6.02220E-01
34	1765.55518	1.98638E 00	1.34510E-01	0.0	6.01605E-01
35	1692.07764	2.06346E 00	1.02207E-01	0.0	6.01169E-01

^aTotal amount vaporized = 0.278E 01 g, sample resistance = 7.476E-02Ω. Voltage = 1.059E 03, accumulated time = 8.000E-04 sec.

reasonably consistent with the experimental observations. Since many unknown factors are assumed in the calculations and large uncertainties exist in the physical and electrical properties, the results are not considered to be rigorous. However, apparent trends are being used as engineering guides.

7. EXPERIMENTAL RESULTS

Forty experiments were conducted during the ORNL CDV Development Testing Program at AEDC. The purpose of each experiment and detailed test results have been reported in quarterly progress reports.¹²⁻¹⁷ This section summarizes the results of these tests with emphasis on their application to the development of the ORNL CDV System.

The tests fell into three categories, although a definite distinction could not be made in every case. The most important tests involved variation in preheat cycle and capacitor bank voltage (or bank energy) using test samples with a pellet-microsphere-containment configuration. These were expected to confirm the viability of the CDV technique and to establish the basic design parameters to be used for design of the ORNL CDV System.

A supplementary series of 11 tests was made to observe the effect of varying the test sample geometry and loading on the proven design. These variations included increasing the packing fraction thickness, changing the quartz containment wall thickness, and loading test samples with UO₂ microspheres only. These tests demonstrated that such variations did not offer substantial improvement over the basic design.

The remaining 16 experiments were exploratory in nature and included considerable departures from the standard configurations. Stainless steel containment, massive quartz containment, high-argon cover gas pressure, and other items were tested to explore their effects.

Of the 13 "standard configuration" tests containing a pellet stack surrounded by UO₂ microsphere packing within a nominal 10-mm-ID quartz containment tube, four did not produce measurable amounts of aerosol. Three of these were among the first four tests conducted at AEDC and

failed because of early design deficiencies. The fourth, test 29, had quartz containment failure during the preheat cycle, and energy transfer was low during capacitor bank firing. During the second AEDC test, aerosol was formed but the equipment for measuring the concentration had not yet been installed. The results from the remaining standard experiments (tests 6, 7, 14, 24, 30, 31, 37, and 39) are shown on Figs. 12, 13, and 14, together with pertinent results from selected category 2 and 3 tests. Figure 12 is a plot of the initial grams of aerosol per cubic meter vs the observed disappearance time of one-half the initial concentration. This demonstrates good correlation between initial concentration and the disappearance rates of standard tests and implies the reproducibility of the aerosol properties.

Test 25, the highest yield AEDC experiment, was an attempt to use the CDV System in a different mode which might produce large amounts of UO_2 vapor directly from the outer surface of the UO_2 pellets. This, and a similar, earlier test (test 18), used a configuration consisting of UO_2 pellets surrounded by a stainless steel tube. The steel tube was then surrounded by UO_2 microsphere packing (test 18) or ThO_2 powder (test 25). The tube was intended to be the power acceptor during the preheat cycle, thus serving as an external heater for the UO_2 pellet stack and creating a more uniform temperature distribution with a higher temperature on the pellet surface. Upon discharge of the capacitor bank, the stainless steel tube would vaporize first, thereby adding more heat and further increasing the outer surface temperature of the UO_2 pellets. This would lower the electrical resistance of the outer surface, as compared with that of the interior regions. After the steel tube had been vaporized, it was felt that the electrical current would be preferentially deposited in the outer, hotter portion of the pellets, with surface melting and vaporization of the UO_2 progressing inwardly. In test 18, there was a large energy deposition of ~ 30 kJ, but only a very small yield of aerosol resulted. Based upon posttest examination, it was postulated that the vaporized (and possibly recondensed) stainless steel served as a continuous-phase shunt for dissipation of the discharge current to ground.

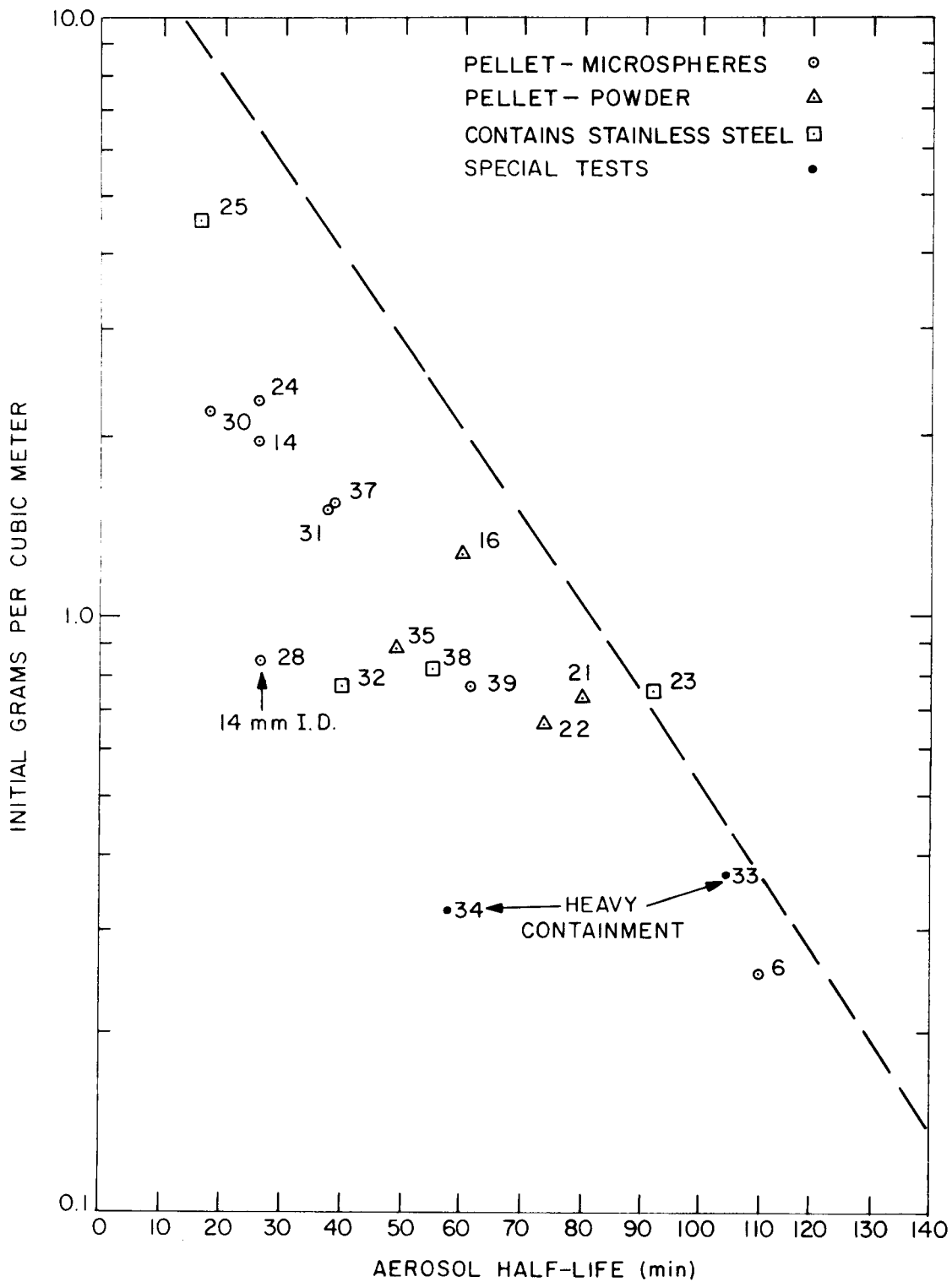


Fig. 12. Variation of deposition half-time with maximum concentration.

ORNL DWG 77-2166R

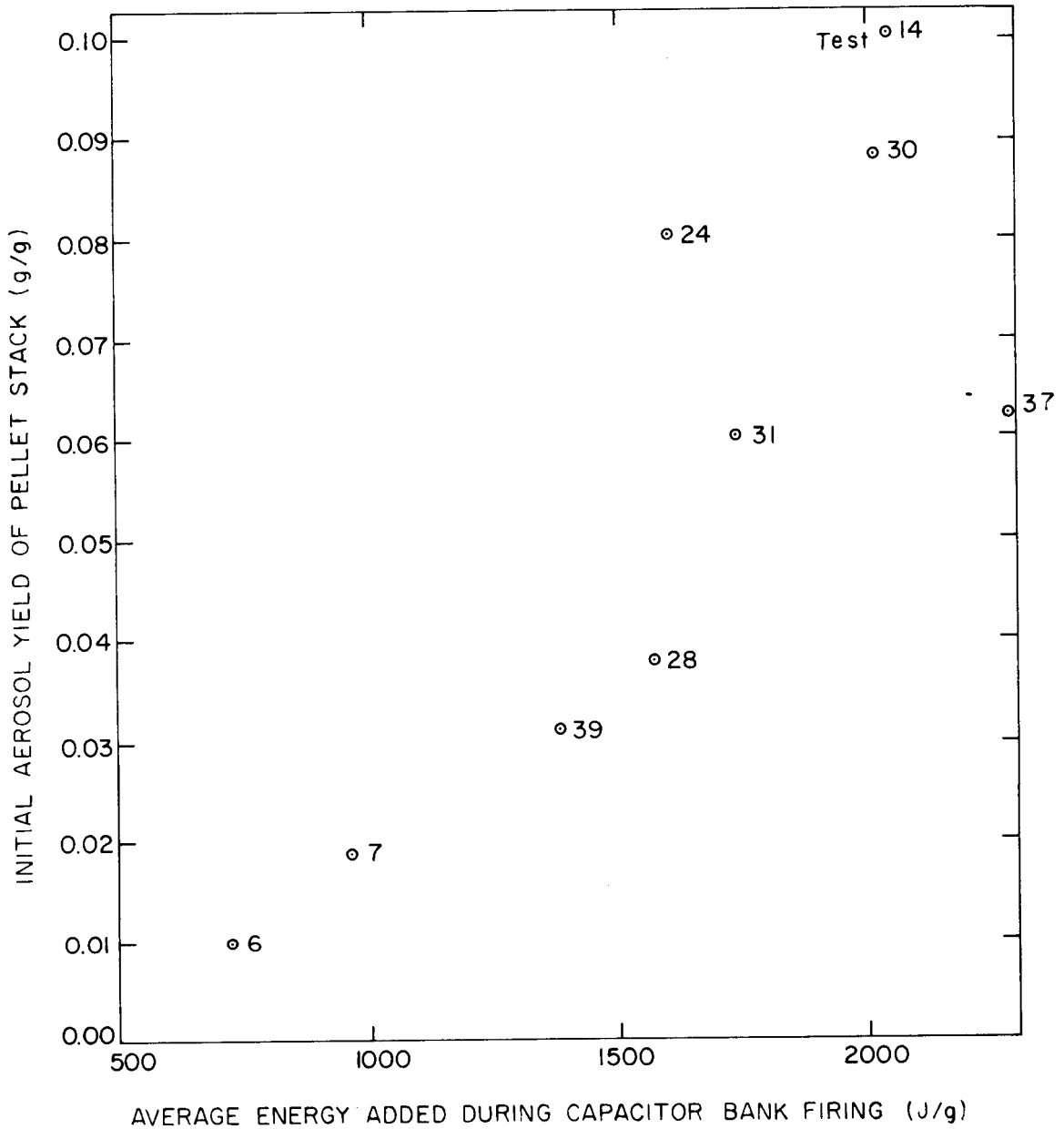


Fig. 13. Variation of aerosol yield with energy input.

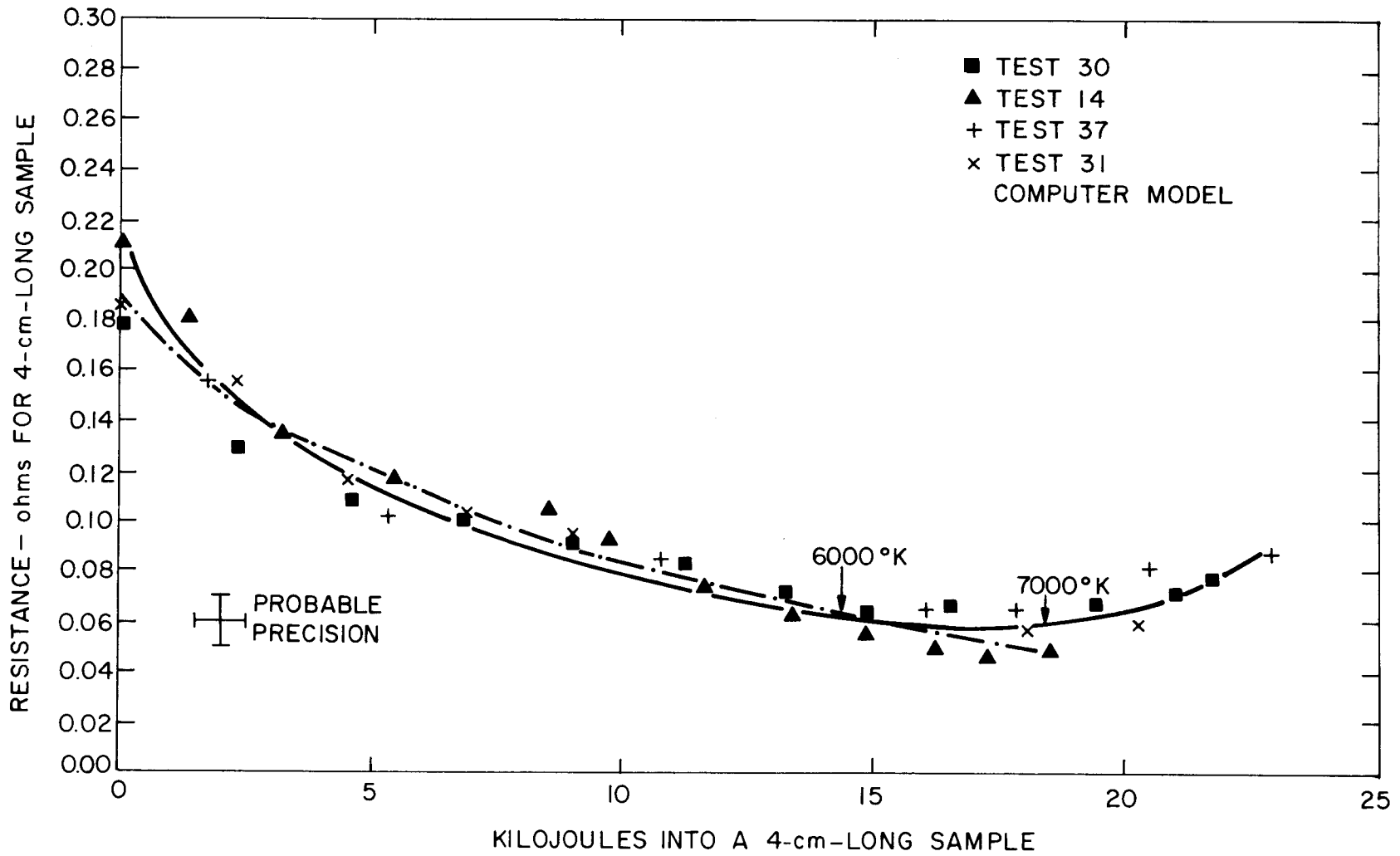


Fig. 14. Variation of sample resistance with input energy.

The test assembly for test 25 consisted of UO_2 pellets surrounded by a stainless steel tube, which in turn was surrounded by ThO_2 powder. A powder packing was used (rather than microspheres as in test 18) in an effort to prevent the stainless steel vapor from permeating the packing and to provide postulated electrically conducting pathways to ground. The powder used for this test was ThO_2 , rather than UO_2 , because the ThO_2 is a poorer electrical conductor and has a higher melting point. Using a different material for the packing also affords a means of differentiating the quantity of aerosol originating from the pellets and that from the packing.

During preheat, the power level was lowered to ~ 200 W in order to avoid premelting of the stainless steel tube. The capacitor-bank-firing sequence was normal, but the electrical data during the firing phase indicated a higher-than-normal electrical resistance and an extended time of energy deposition. The aerosol yield was quite large.

The test assembly was also contained in a longer-than-normal metal holder (as was test 24); posttest examination of the test assembly and the films showed prompt expulsion of the lower electrode, venting of the vapor, and no disassembly of the quartz containment tube. Significant erosion of the tungsten electrode by the venting vapors was also noted.

Two independent aerosol yield measurements (weight measurement and chemical analysis of the deposits contained on filter samples) were inconsistent. A yield of 4.6 g per cubic meter (287×10^{-6} lb per cubic foot) was determined by weight; the combined yield from UO_2 , ThO_2 , and stainless steel oxides was determined to be 2.1 g per cubic meter (131×10^{-6} lb per cubic foot) by chemical analysis. Tungsten was not detected in the aerosol samples. Two similar experiments (32 and 38) gave low aerosol yields, so the concept was abandoned.

Tests 16, 21A, 22, and 35 were similar to the standard tests except that powder was used as the packing fraction instead of the microspheres. The powder should have provided a better thermal barrier than microspheres which would allow a greater preheat energy input. However, higher aerosol yields were not obtained. Test 21A used ThO_2 powder, and from the

analysis of the aerosol it was determined that over 85% of the yield was from the pellet stack.

Tests 33 and 34 are examples of the results obtained when using relatively massive quartz containment (13.5 mm thick). Low aerosol yields appeared characteristic, so this concept was also abandoned. Good aerosol yields were not obtained in any large diameter test samples. Since 10- to 11-mm-ID containment provided suitable thermal protection to the quartz containment during the preheat cycle and capacitor discharge energy losses were increased by the electrically conducting packing fraction which shunted the pellet stack, the effect of using thicker packing was not studied in depth.

In Fig. 13, a plot of energy deposition in test samples from the capacitor bank vs aerosol yield, the individual test results have been normalized on the following basis. Total aerosol yield is the extrapolated initial aerosol concentration at t_0 , zero time, multiplied by the volume of the AEDC test vessel (0.4 m^3). The active pellet mass is taken as 2 g per centimeter multiplied by the spacing between the electrodes. This automatically corrects for the unmelted and inactive pellet mass inserted into the recesses in each electrode to ease assembly problems. Eighty percent of the measured energy deposited in the sample from the capacitor bank is assumed to be deposited in the pellet stack, with the remainder deposited in the microsphere region. This ratio was determined through the computer modeling results and preheat test results using UO_2 (conductive) and ThO_2 (nonconductive) in microsphere packing. Figure 13 does not include the significant amount of energy already added to the test samples at the start of capacitor discharge which was supplied by the initial high preheat cycle. The amount of energy that can be inserted before sample disassembly (during bank discharge) appears to depend on the mechanical strength of the containment and the physical forces imposed by the energy insertion. Ideally, the increasing vapor pressure of the sample will be the primary cause of containment fracture. The larger the fraction of melted pellet, the greater the probable energy insertion must be before local high-energy regions (in theory, the centerline of the pellet stack) can provide sufficient pressure for disassembly to occur.

Tests 6 and 7 were performed prior to test experience and computer simulation calculations which would have predicted minimal pellet melting under the preheat conditions used. All other tests were conducted under preheat conditions which should have provided full pellet stack melting prior to CDV discharge.

Test 37 is an unusual case in that the electrode clearance was sufficient to allow molten UO_2 to be ejected through the annulus between the electrodes and the quartz containment. As UO_2 vapor formed within the containment, an arc developed between the electrodes, but the sample pressure remained below that required for containment failure. The ejected UO_2 touched many heat transfer locations not seen in a normal disassembly, which may account for the apparent low aerosol yield. Test 37 did confirm that flashing of the superheated liquid was a primary source of aerosol formation.

Figure 14 shows the variation of test sample resistance with energy deposition. It is a composite from four experiments normalized to a length of 4 cm. Also shown is the expected resistance, as calculated by our computer model. The temperatures shown are sample centerline values and are also calculated by the model. To deliver power at a level of 1 MW per gram at the minimum resistance requires $\sim 13,000$ A at ~ 195 volts per cm across the sample.

These data were also used to establish our original design criteria for the ORNL Capacitor Energy Delivery System, which included a 2500-V nominal capacitor voltage (3000-V peak) and a 30-kJ bank section storage (43.2-kJ peak). Based on a 5-cm-long sample, these should provide ~ 1.0 g of aerosol using 25 kV of bank energy. The remaining 40% of stored energy in the capacitor bank at peak charge was reserved for system losses. The final design of the capacitor energy delivery system is reported in Sect. 10.3.

Development of the sample preconditioning system (the preheater) proceeded concurrently with the AEDC experiments. As a part of the sample preconditioning optimization process, a series of specific tests to measure the thermal end losses from the UO_2 pellet stack during the

preheat cycle were completed. To determine the thermal end losses, experimental measurements were obtained for the axial voltage drop along a UO_2 test assembly. Tungsten wires were inserted into the test assembly through the quartz containment tube at measured axial locations. A typical preheat cycle was initiated, and voltage measurements were made at these locations. The voltage profile was found to be uniform along the UO_2 pellet stack; however, marked discontinuities were detected at the two electrode-pellet interfaces. It was assumed that the end losses were proportional to the electrical resistance changes at the interfaces. A typical voltage profile and calculated end losses are shown in Fig. 15.

Figure 16 shows the condition of the UO_2 pellets and the UO_2 powder or microsphere packing following two preheating tests. In each case, the length of the pellet stack was 5.4 cm, and total power input was ~ 120 W per cm. The UO_2 pellet- UO_2 microsphere sample on the right did not exhibit complete pellet melting, although the center of the pellets had been molten during the preheat cycle. In order to achieve full pellet melting, the 1000-W preheater capability was increased to 4000 W (100-A maximum). Another sample was then preheated under conditions for which our computer simulation code predicted full pellet melting. The sample contained 13.14 g of an axial pellet stack surrounded by 26.7 g of 30- to 50-mesh microspheres contained within a quartz cylinder having a 11-mm ID and a 17.5-mm OD. The length between the spring-loaded tungsten electrodes was 50 mm. The sample was preheated to 200 W in argon at a pressure of 1 atm, our normal procedure, and then was given a nominal high preheat of 1400 W for 30 sec. After cooling, it was disassembled and the microsphere-pellet combination was removed from the quartz containment. Most of the microspheres had sintered together and to the pellet stack. Without the loose microspheres, the diameter of the sample ranged from 9 to 9.5 mm. The 50-mm-long sample was then sectioned at the midplane. The section of the UO_2 pellet stack that had been melted could be easily identified. Microscopic examination revealed a central axial void.

For metallographic examination, the pieces were cast in resin and sectioned axially, but not exactly at the midline. About half of the pellet-microsphere stack showed uniform melting in the pellet region.

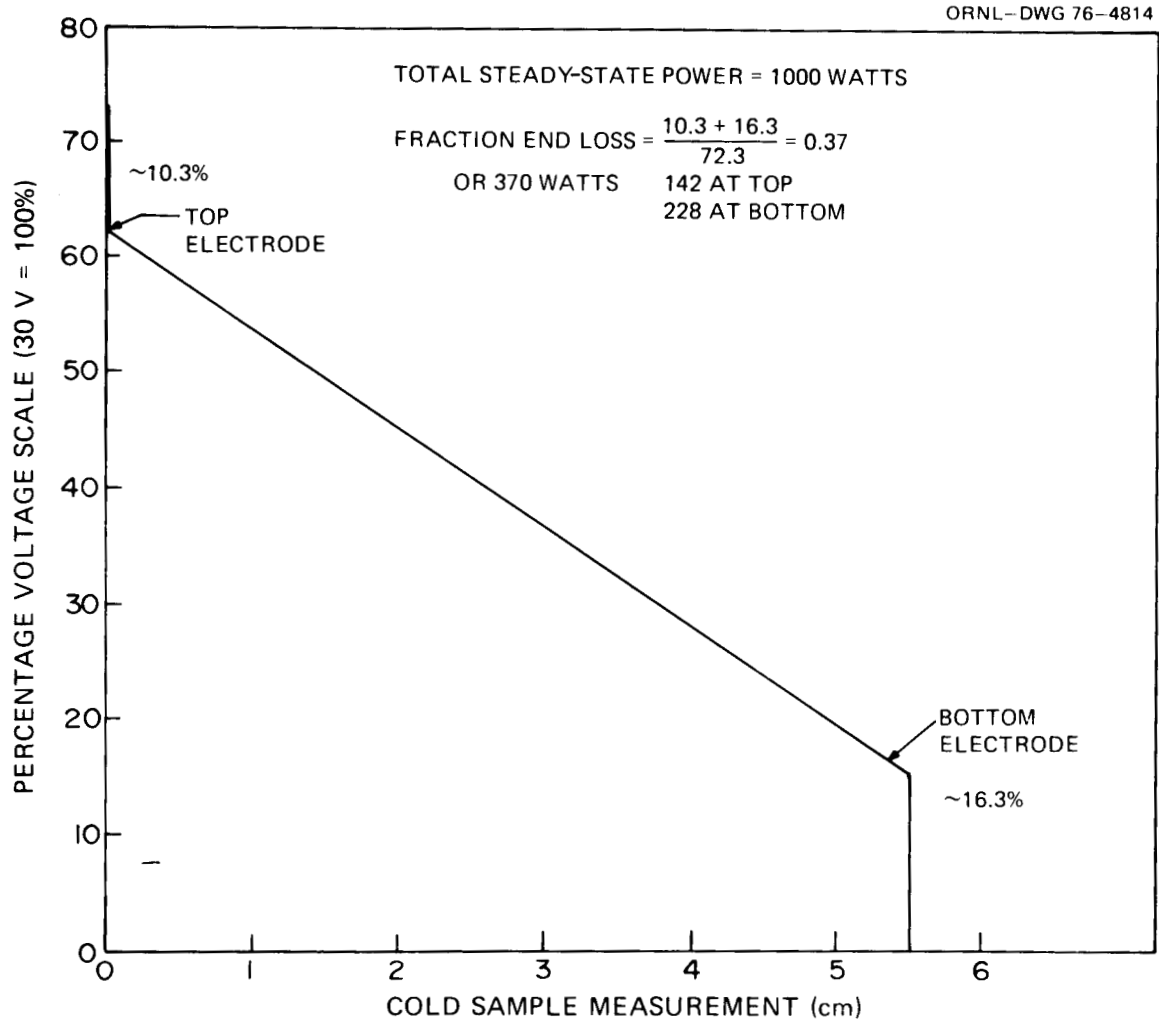


Fig. 15. Data and results from an experiment to determine preheater power lost through the electrodes.

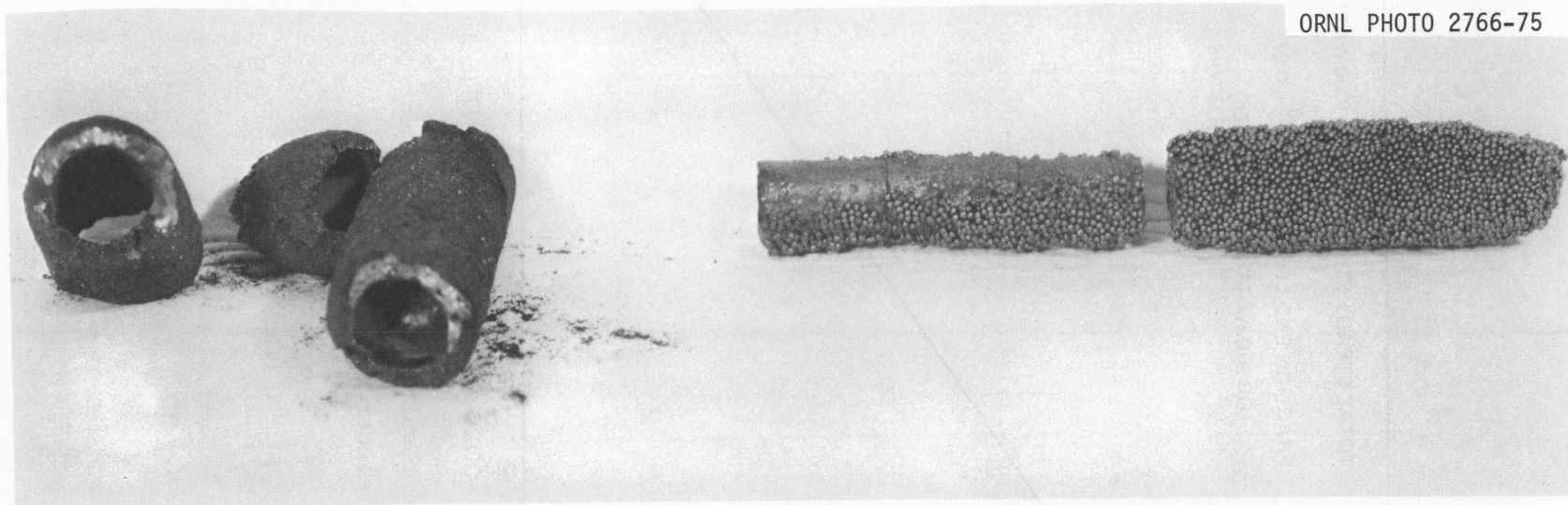


Fig. 16. Condition of posttest samples from preheater experiments.

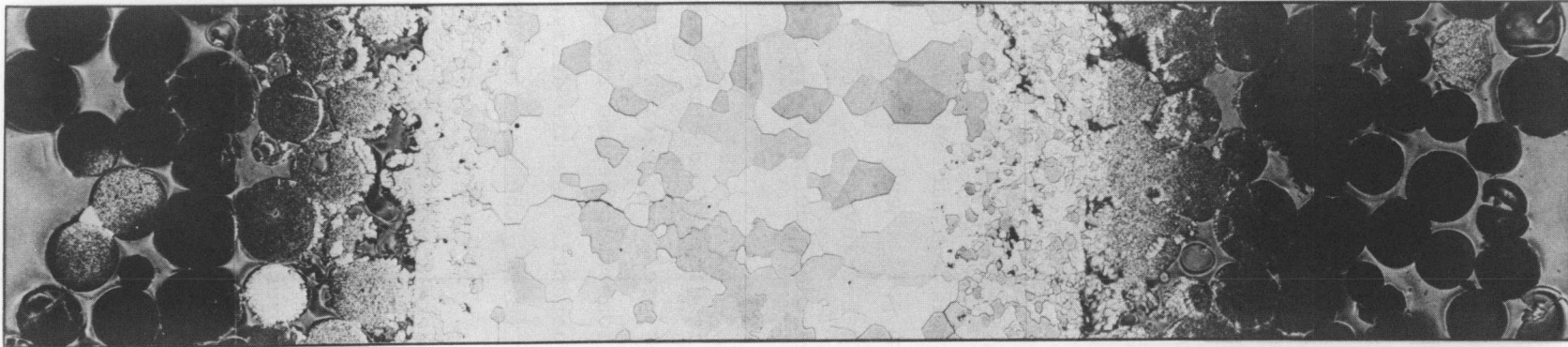
Deformation and fractional melting were apparent in the microspheres adjacent to the pellet stack. Figure 17, an enlarged etched section, shows clearly that most of the pellet stack had melted, as demonstrated by the large grain growth structure.

Fig. 18 shows definite channeling of the melted fraction. On the right of the picture, the pellet does not appear to have melted. On the left, the melted zone appears to have intruded into the microsphere region. The large shrinkage holes, which probably formed as solidification of the melt occurred, lead one to assume that this melted region was hotter than that shown in Fig. 16.

Figs. 17 and 18 indicate that the preheat calculations and assumptions used to determine the fraction of pellet melting under uniform conditions were reasonably correct. The hot channeling away from the midline of the pellet stack shown in Fig. 18 was unexpected. We postulate that the cause was either initial, nonuniform pellet-end contact or, perhaps, stratification of the temperature with the inverse of the resistance-temperature coefficient of UO_2 which compounded the nonuniformity of the energy deposition.

When the capacitor bank is discharged into a sample in this condition, both the temperature and vapor pressure rise much faster in the hot channel regions. The hot channel regions then become the controlling factor for sample disassembly. Several potential sample design changes could possibly minimize this effect (e.g., the use of a UO_2 rod rather than pellets as the fuel simulant). Typical voltage and current recordings during the high preheat cycle are exemplified in Fig. 19.

During the development tests, a few collections of aerosol plateout on electron photomicrograph grids were made. Counting the primary particles from high-magnification transmission electron-microscope pictures enabled us to determine the primary particle-size distribution on a number basis. Table 3 and Fig. 20 show the results. Only plate 34 from Test 14 represents aerosol at a high initial energy density.

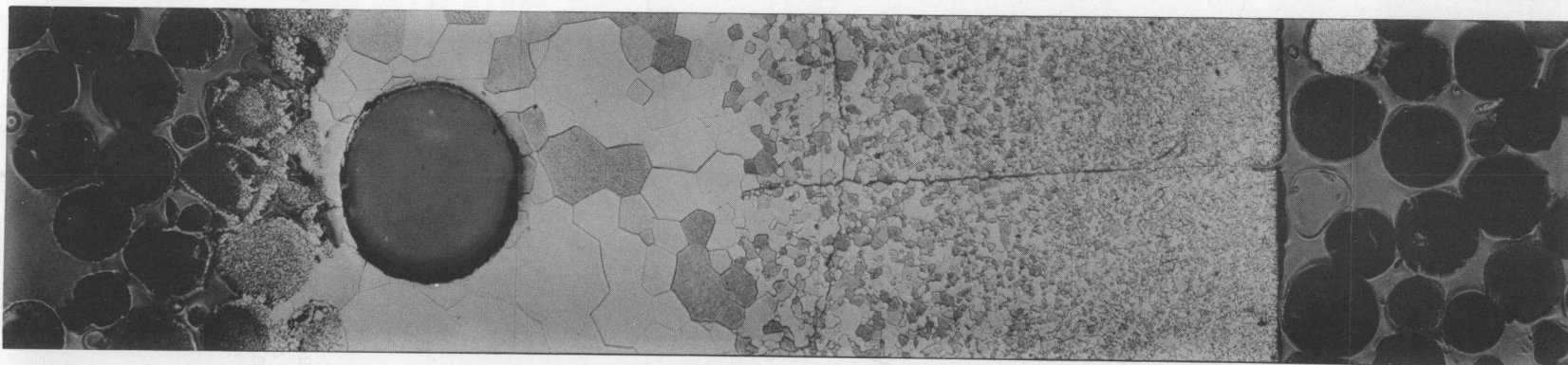


84081 #1

50 X

Fig. 17. Enlarged etched section of the uniform melt region.

Y 138777



84080 #2

50 X

Fig. 18. Enlarged etched section showing unmelted pellet fraction and narrow microsphere-pellet melted region.

ORNL-DWG 75-16883

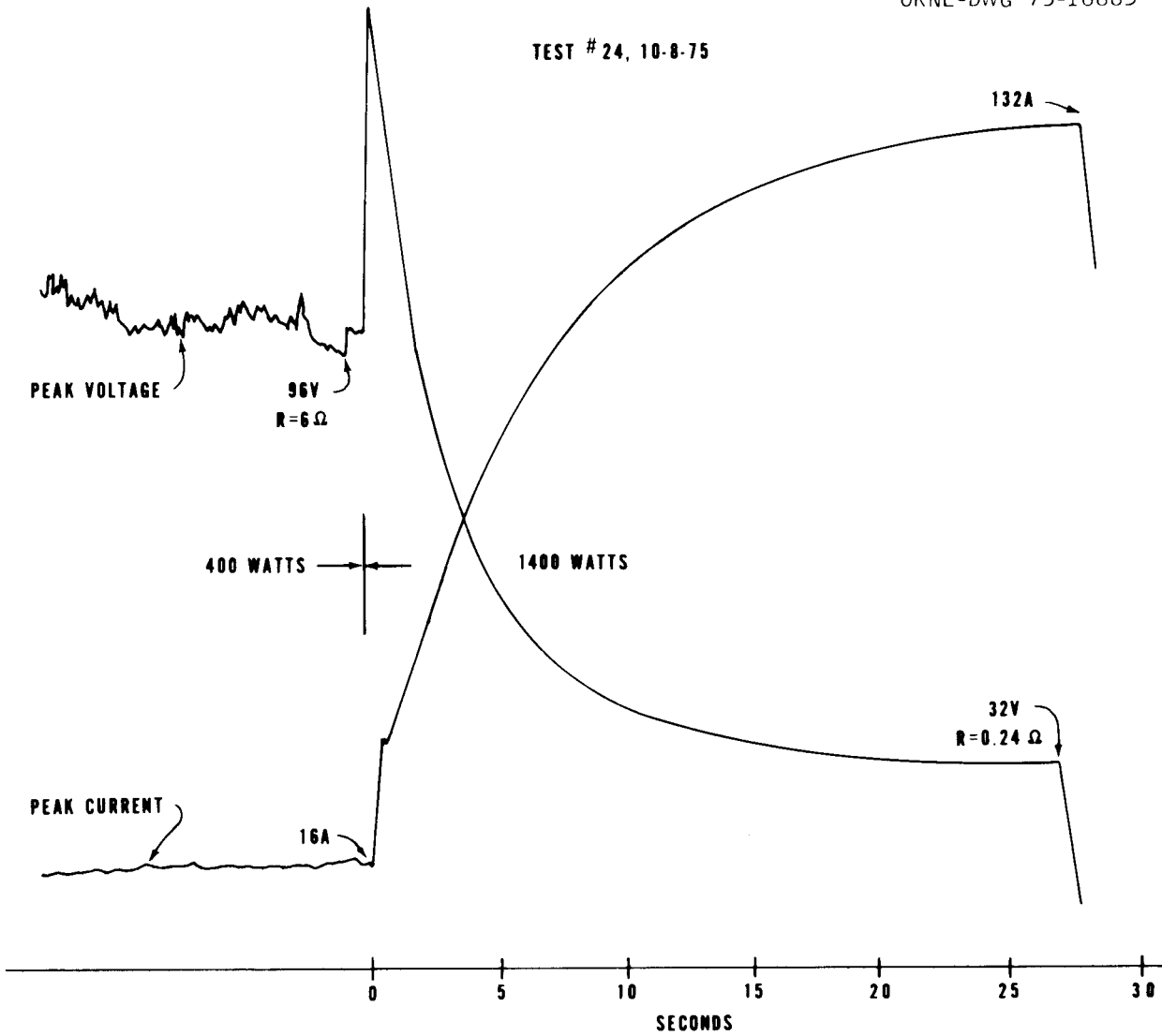


Fig. 19. Typical preheat voltage and current recordings from Arnold Engineering Development Center.

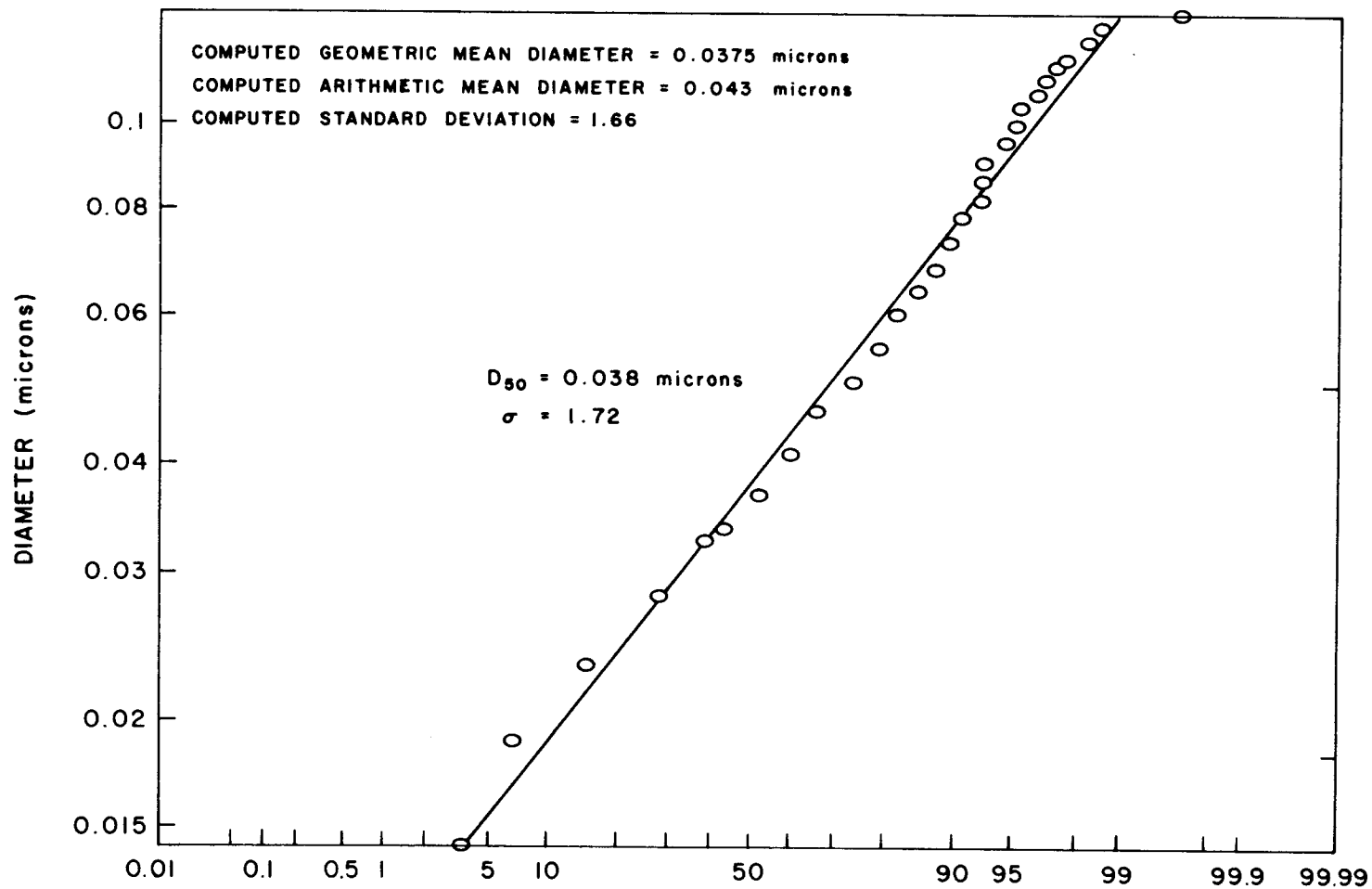


Fig. 20. UO₂ primary particle size distribution in Capacitor Discharge Vaporization aerosol from test 9.

Table 3. Nominal primary particle sizes for AEDC tests

Test and Plate No.	Magnification	D_G^a	D_A^b	σ^c
9 - 35	213,000	0.022	0.030	1.56
10 - 35	165,000	0.025	0.044	1.80
10 - 34	165,000	0.032	0.042	2.15
10 - 34	213,000	0.022	0.032	2.01
14 - 34	213,000	0.016	0.017	1.55

D_G^a = geometric mean,

D_A^b = arithmetic mean, and

σ^c = standard deviation (size in microns).

8. COMPUTER MODELING RESULTS

The computer simulation modeling program discussed in Sect. 6 was used to provide insight into the probable effects of test-article design changes. The model was not expected to reproduce experimental results, but rather to serve as a tool with which parametric studies could be made quickly in order to minimize faculty logic mistakes in designing the physical experiments.

Figure 21 is representative of early calculations used to estimate the radial temperature distribution at a steady-state power input for the preheat cycle. Figure 22 is representative of the preliminary temperature results expected from capacitor-bank power insertion starting with two arbitrary, initial radial temperature gradients (one low and one high). The solid lines represent an initial temperature distribution that varies within the melt region from 3141°K at the melt boundary to 3471°K at the center of the sample. The dashed lines are the results for a temperature in the range of 3141°K to 3158°K (essentially uniform) in the melt region. Assuming that disassembly (containment fracture) occurs at the same peak UO_2 temperature in each case, approximately twice the total energy input can be expected for the uniform temperature case.

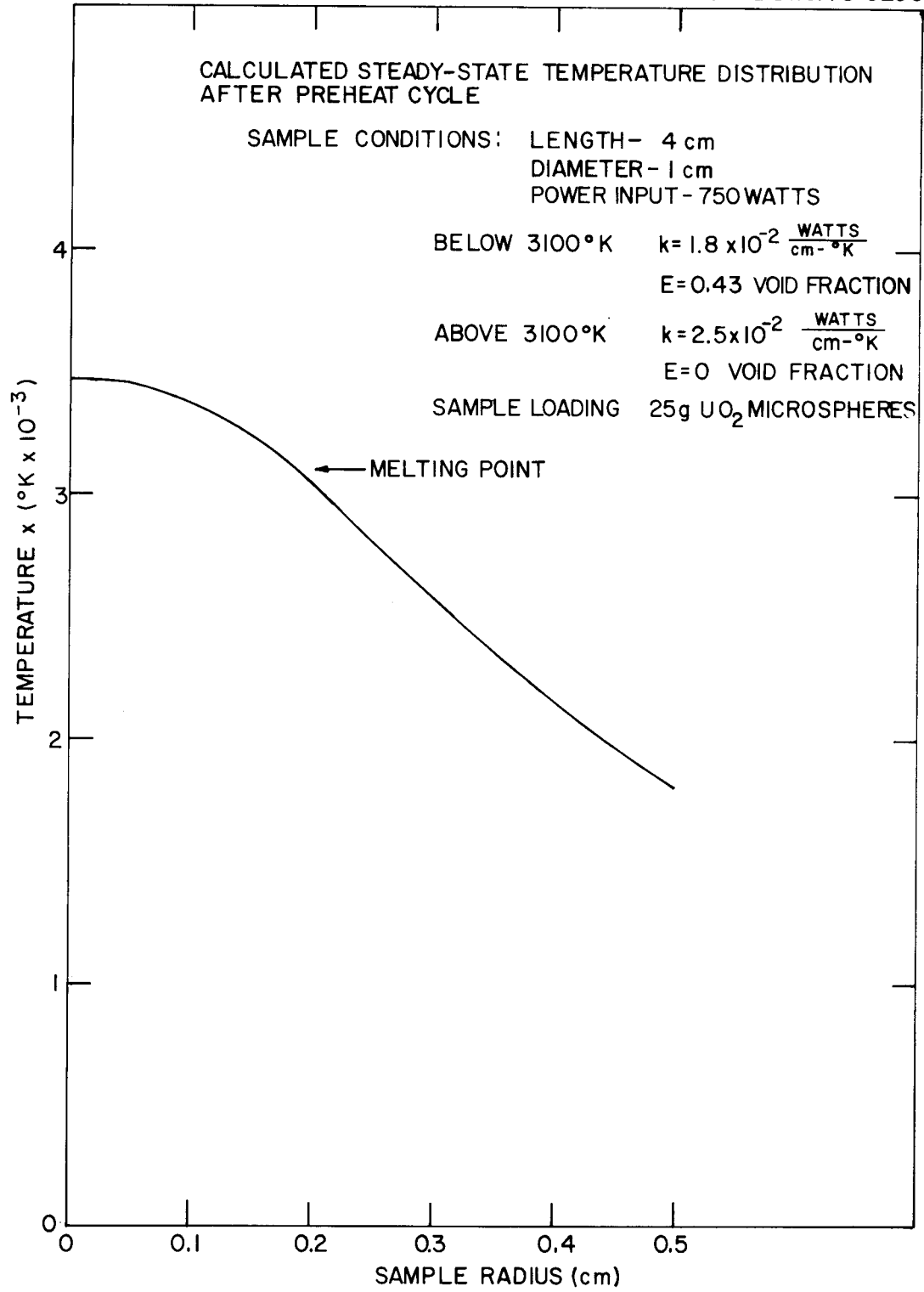


Fig. 21. Calculated steady-state temperature distribution after preheat cycle.

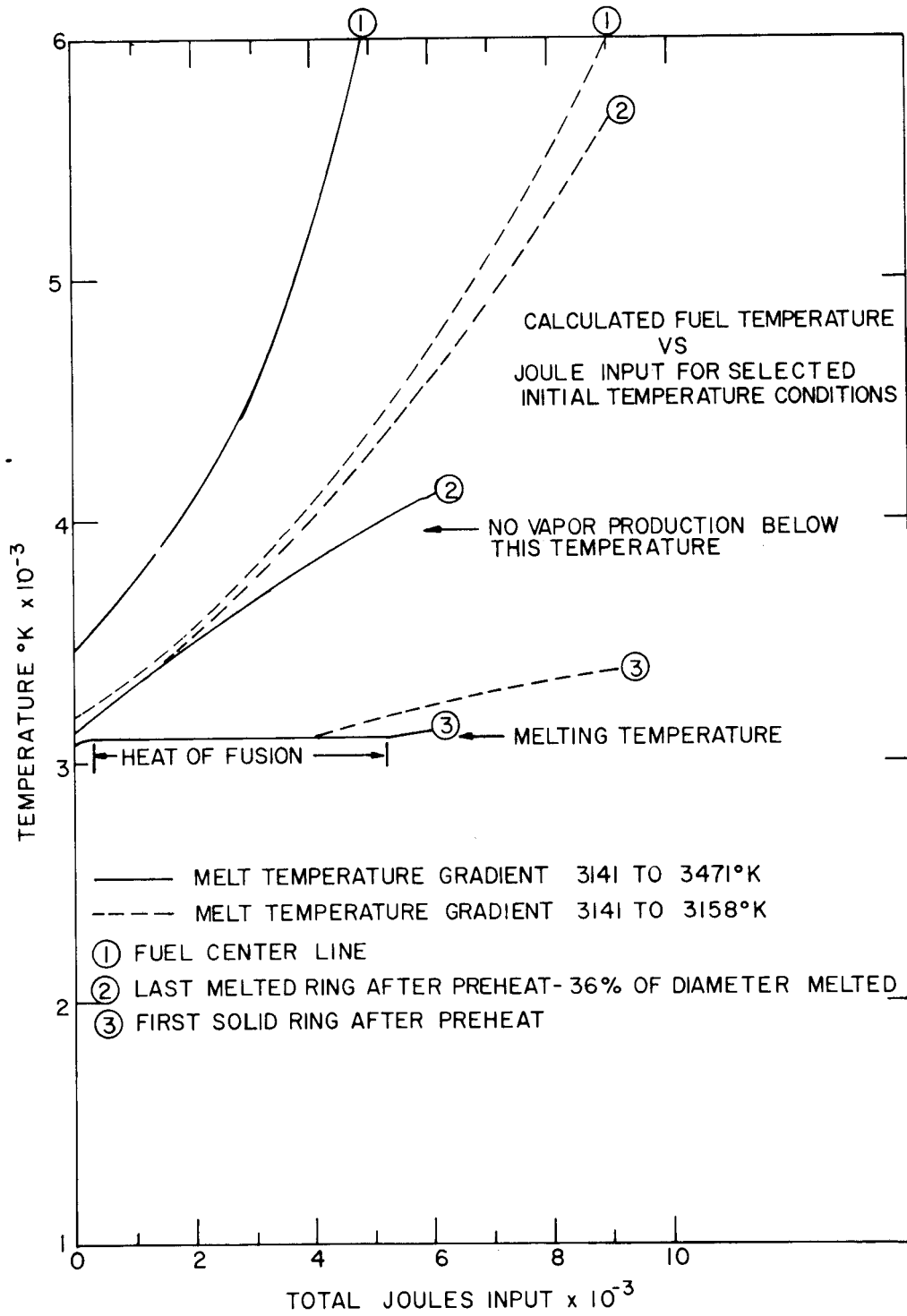


Fig. 22. Calculated transient temperatures during capacitor discharge.

The other important conclusion from these calculations is that practically all of the potential aerosol is produced from material that is melted during the preheat stage.

Figure 23 is a graphical representation of the theoretical aerosol yields for various pellet-melt fractions, as calculated from the computer model before various model refinements. All yields shown are based on adiabatic expansion to 1 atm. The internal pressure was taken as the vapor pressure of UO_2 at the calculated temperature of the pellet centerline (representative centerline temperatures are given at top). It is assumed that energy deposition ceases at a given stress on the quartz; consequently, these yields are not calculated on an equivalent energy insertion basis. These computed curves in Fig. 23 indicate that three factors are involved in maximizing the energy input.

1. As large a pellet fraction as possible should be molten before capacitor bank discharge.
2. The fracture pressure of the containment tube should be >5000 psi.
3. Only a small yield increase is obtained with large increases in containment strength >5000 psi.

Using the same model parameters, the effect of varying the packing void fraction (essentially changing the electrical and thermal conductivity of the packing) on the fraction of the pellet stack melted during preheat vs preheat power is shown in Fig. 24. Values >1 indicate that melting extends into the packing region. The void fraction could be changed by using finely powdered UO_2 (~ 0.6 VF) or microspheres (~ 0.4 VF), or an intermediate combination. There appeared to be potential advantages to using the UO_2 powder (~ 0.6 VF) and lower preheat power with a smaller gradient across the melted pellet stack. However, experiments performed under these conditions did not result in greater energy deposition before disassembly.

As our computer model parameters were refined and the use of microsphere packing became standard, parametric studies were made to determine the minimum containment inside diameter (ID) required to achieve full pellet melting without weakening (softening) the quartz outer containment.

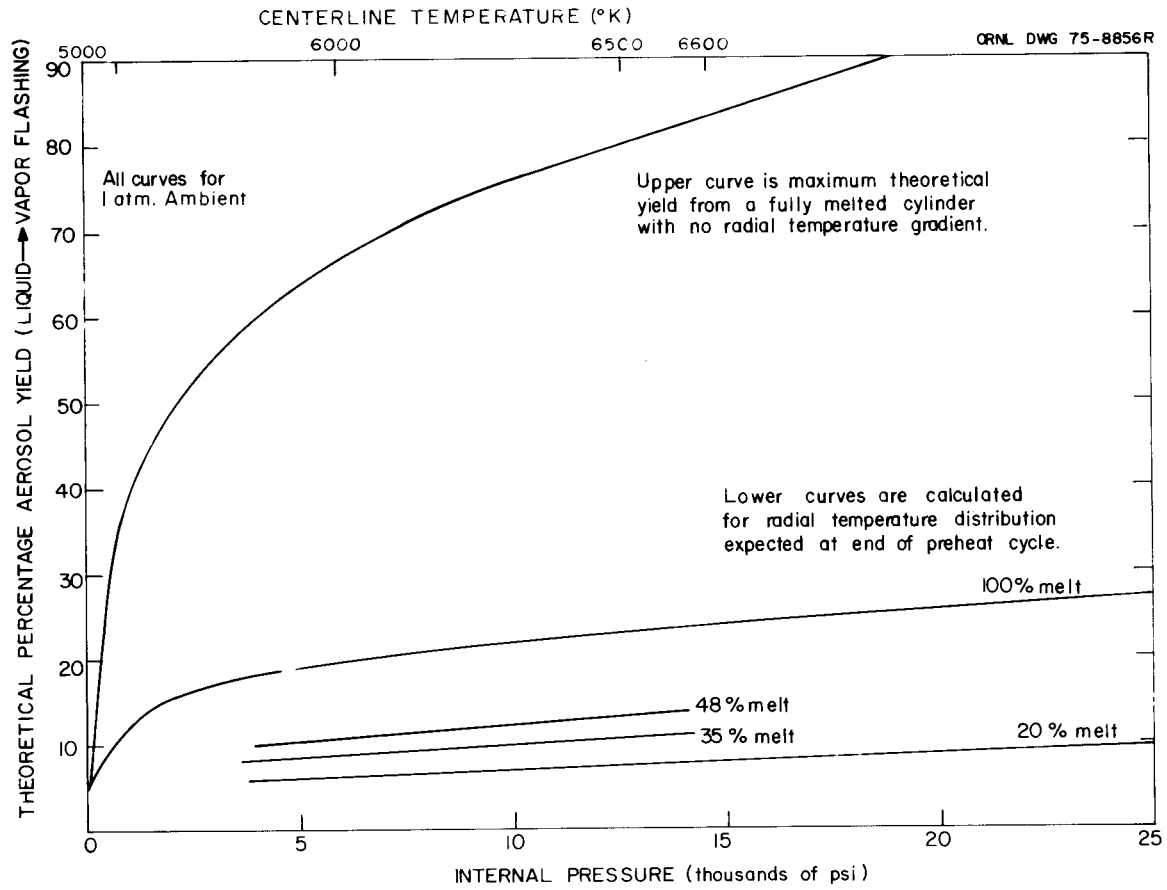


Fig. 23. Aerosol yields calculated by the finite-element Capacitor Discharge Vaporization simulation code at various pellet-melt fractions compared with maximum theoretical aerosol yield.

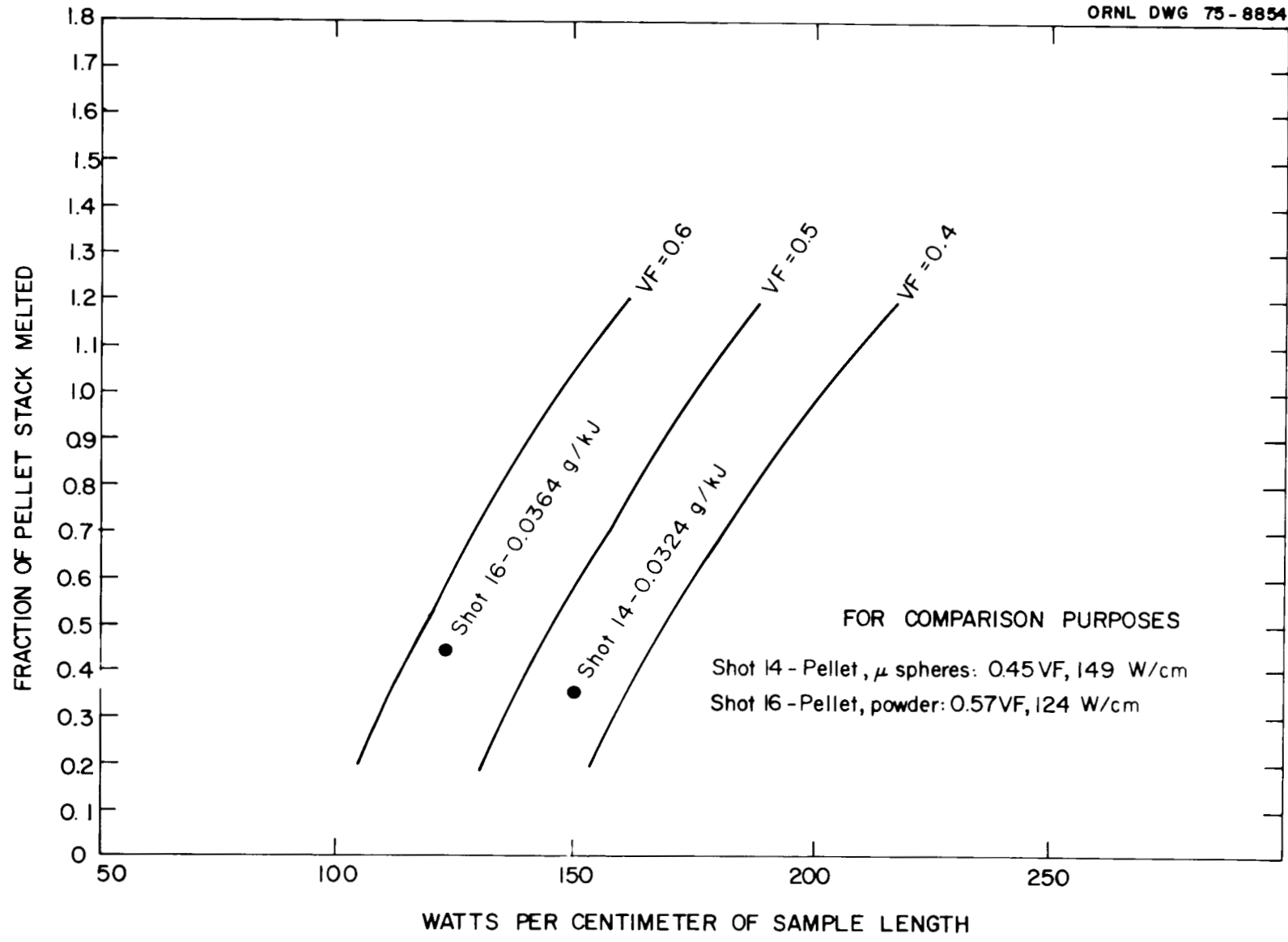


Fig. 24. Effect of varying void fraction on power required for pellet melting.

These results are shown in Fig. 25. To maintain quartz strength, the quartz-packing interface should not exceed 1940°K. For full pellet melting, the pellet outer surface should reach 3123°K. The parametric cross-plot of the containment ID vs centerline temperature indicate a required containment ID of 11 mm or greater. This ID has proven to be adequate.

Figure 26 shows the fractional aerosol yield calculated from adiabatic expansion vs centerline temperature after capacitor energy is added to the test sample, with the initial centerline temperature as a parameter. Energy inputs per centimeter are crossplotted at several discrete energy levels. The model sample was 4 cm long, with a 5.4-mm-diam pellet stack packed with microspheres. The effective theoretical density (VF of 0.4) between the pellet stack and the 10.5-mm ID of the quartz containment (wall thickness of 4.8 mm) was 0.6. An emissivity of 0.8 was assumed for the steady-state preheat energy balance.

These calculations were made after all model refinements had been added to the computer program. Sample disassembly would be expected at a centerline temperature of ~6000°K. The calculated yield is strongly affected by the centerline temperature (directly related to the fraction of sample melted) prior to capacitor-bank discharge. Based on the assumptions used in Fig. 26, 3500°K corresponds to 100% pellet melt.

Figure 27 shows the calculated radial temperature distribution for a test sample after preheat and at two energy deposition levels during simulated capacitor bank firing. The steady-state preheat conditions of the current (as measured in ohms per centimeter and watts per centimeter) were matched to the results from a successful test by selecting the model parameters. The effect of the heat of melting of the UO₂ during simulated firing is clearly shown. The given values (joules per grams) are calculated for the pellet stack. Sample disassembly would be expected as the centerline temperature approaches 6000°K.

Figure 28 shows the calculated yield from the pellet stack vs power (joules per gram) from the capacitor bank, starting with an initial centerline temperature of 3500°K and 100% pellet melt. Increasing the pressure into which adiabatic expansion occurs, of course, decreases the yield.

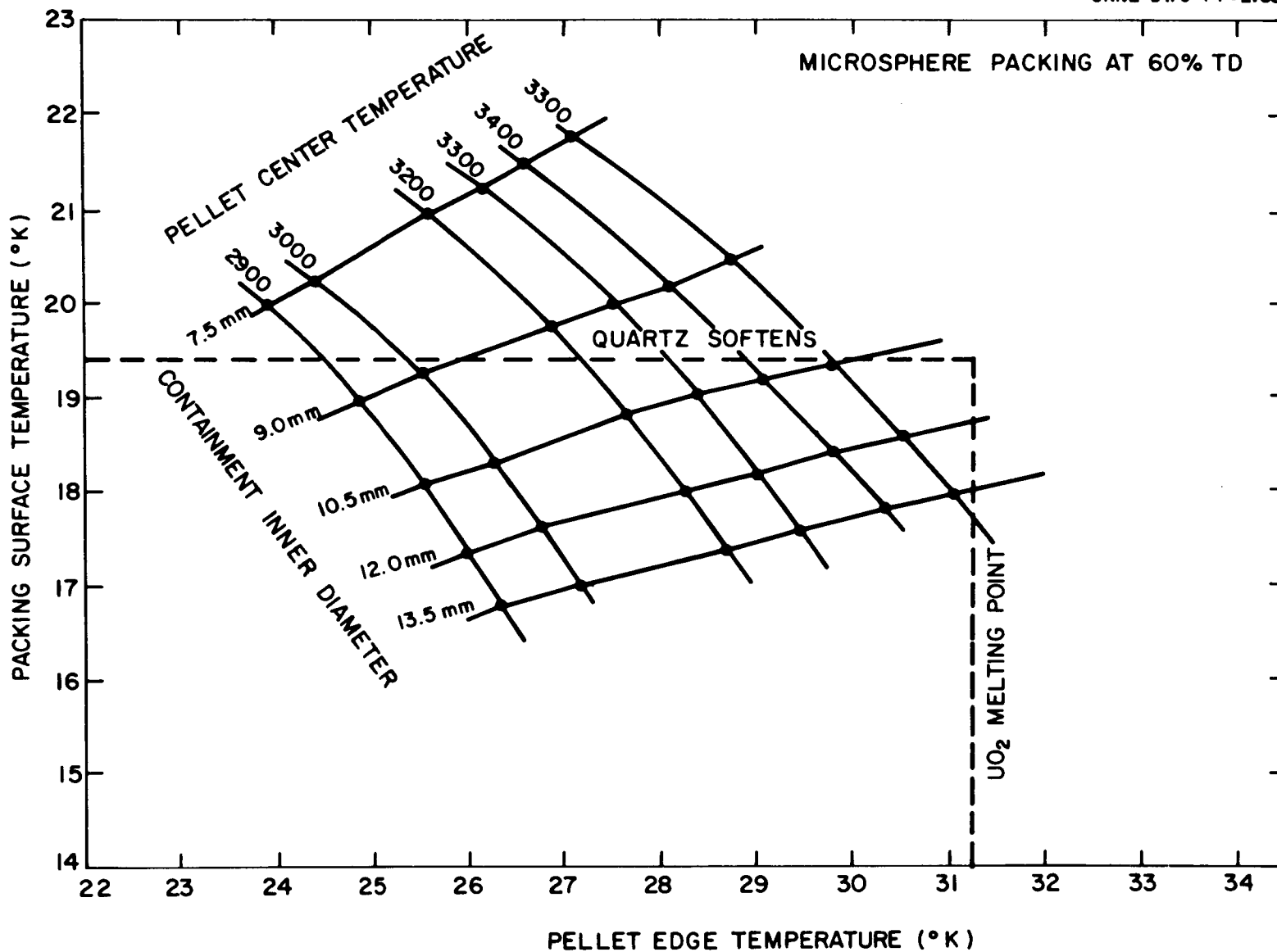


Fig. 25. Parametric plot of packing surface temperature versus pellet edge temperature, varying containment inner diameter, and pellet centerline temperature.

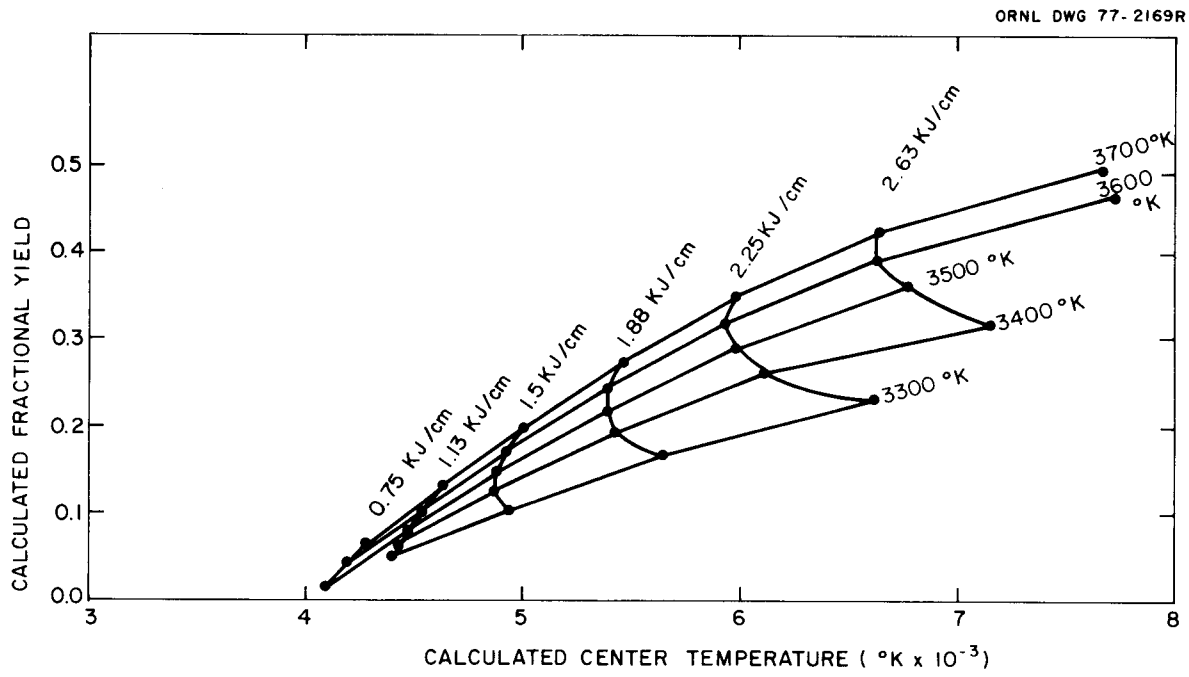


Fig. 26. Fractional yield versus centerline temperature.

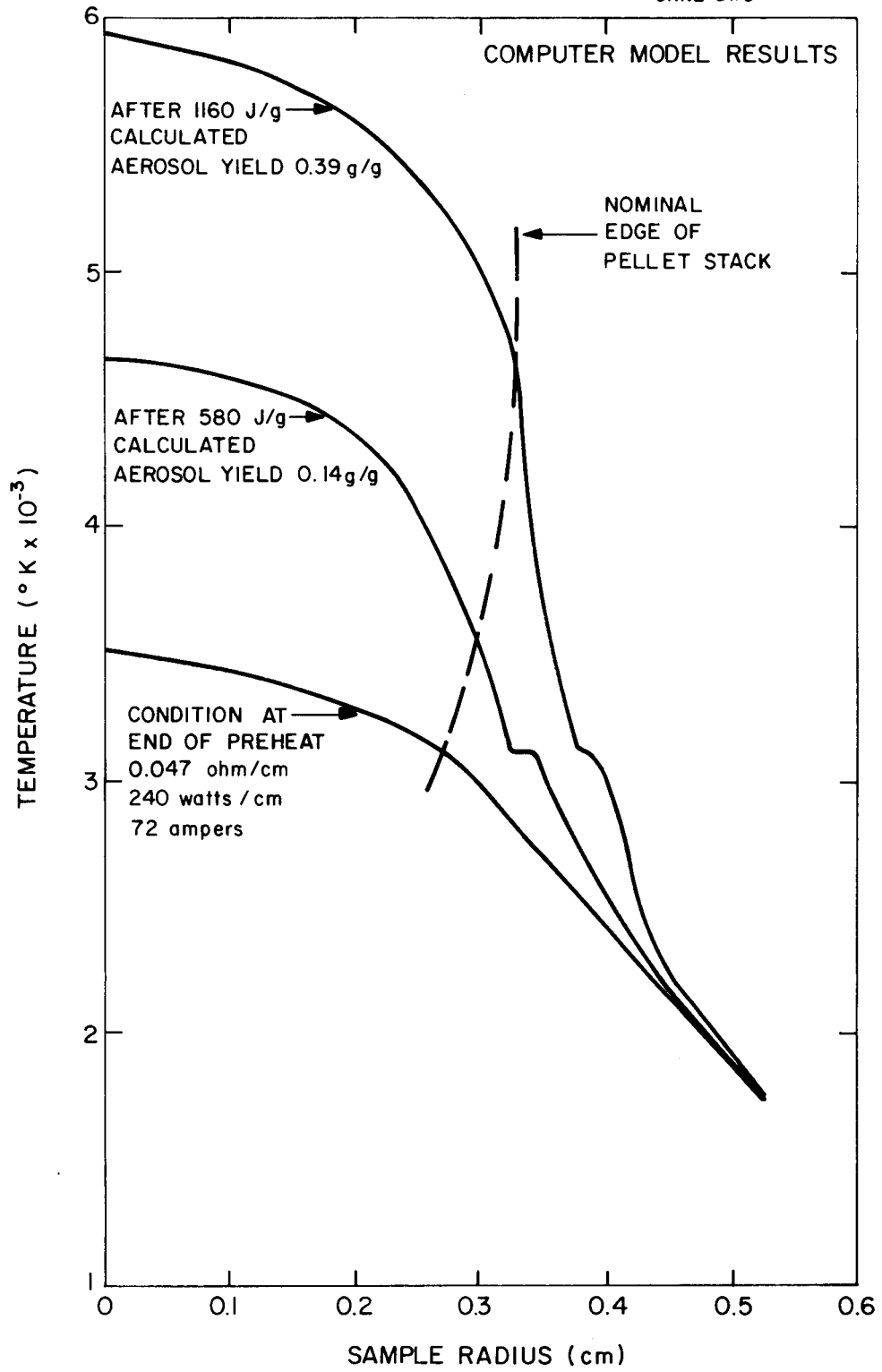


Fig. 27. Computer model results.

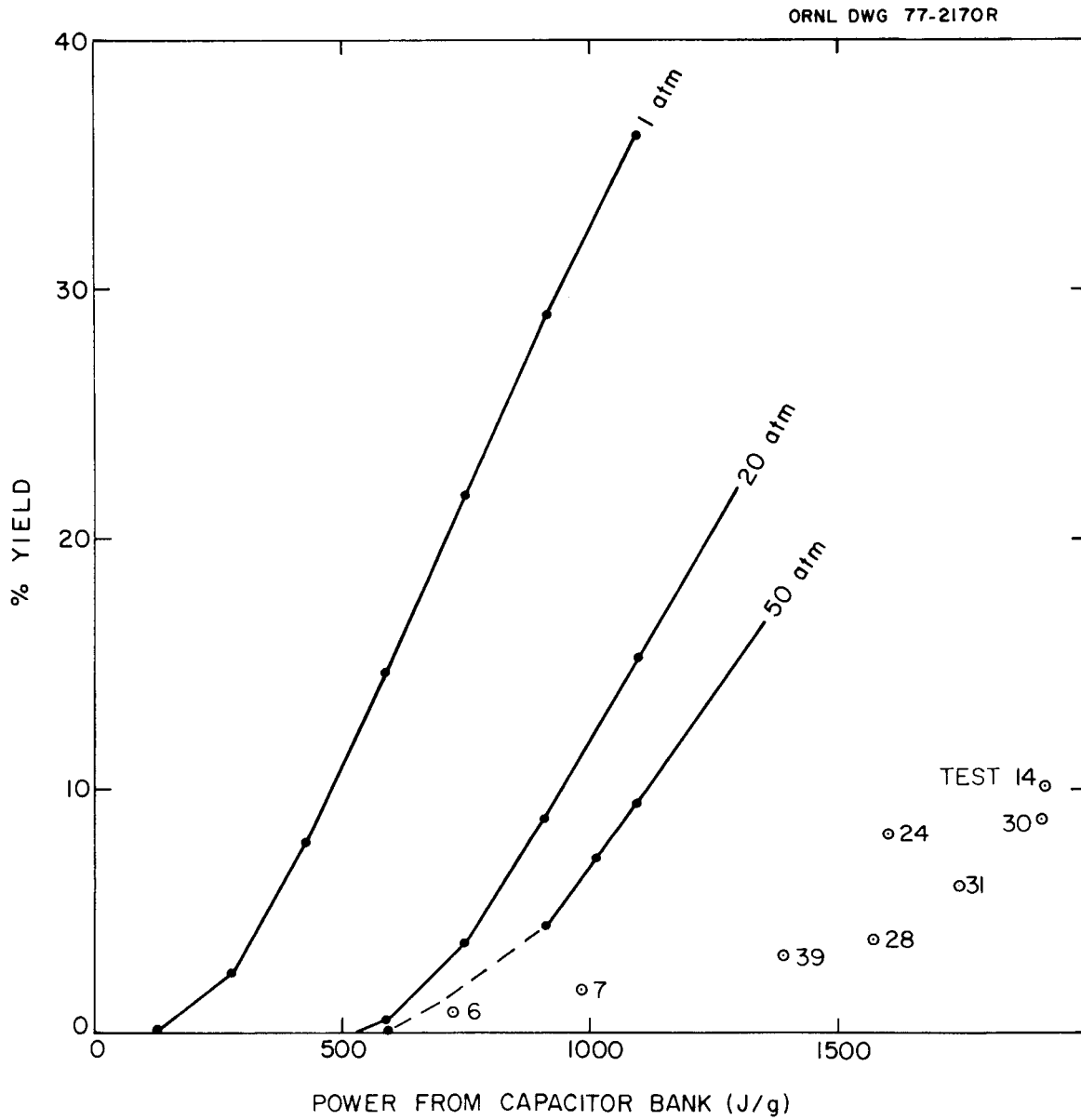


Fig. 28. Calculated yield versus power from capacitor bank.

Many other studies were made using our computer model, but the above examples demonstrate the more useful parametric studies conducted during the development of the ORNL CDV System.

9. COMPARISONS BETWEEN COMPUTER CALCULATIONS AND EXPERIMENTAL RESULTS

After adjustments of some of the parameters in the computer model (e.g., in the electrical conductivity-temperature function above the melting point of UO_2) were made, the calculated results conformed closely to preheat results and to posttest sample examination used to determine the fraction of pellet melting. This is not considered to be a validation of the computer model for calculating steady-state preheat conditions, especially if the sample designs and geometry are significantly different from those used during the experimental program. There is a lack of data on three important parameters used in the model, namely, the variation of temperature with (1) the thermal conductivity of the packing fraction, (2) the electrical conductivity of the packing fraction, and (3) the electrical conductivity of molten UO_2 .

The use of the computer model with adiabatic expansion to forecast aerosol yield results has not as yet been successful. Figure 28 shows the theoretical adiabatic yield at various energy levels compared with actual yields from the AEDC tests.

The short (4- to 5.6-cm) samples tested at AEDC could be expected to show a loss in the potential aerosol production as a result of capture of the expanding UO_2 on the end caps of the test assembly and the current-return members (see Fig. 29). However, it is unlikely that >50% of potential aerosol production could be lost by this mechanism. It was demonstrated by experimentation that a significant quantity (~35%) of the preheat power is lost from the test sample through the electrodes. The "cold" UO_2 at these electrodes could absorb some of the bank energy unproductively, but it is unlikely that this would be a significant fraction of the total energy deposited during a test. Cursory calculations of possible radiation energy losses during bank discharge indicate that <10% of the inserted energy could be dissipated by this mechanism.

ORNL PHOTO 6792-76



Fig. 29. Small-housing-diameter Arnold Engineering Development Center test article.

10. THE ORNL CAPACITOR DISCHARGE VAPORIZATION SYSTEM

10.1 Introduction

Previous sections have described the basic CDV System requirements. The pertinent design details and performance capabilities of the ORNL System, as constructed, are discussed in this section. It should be remembered that the CDV technique is still under development and that one of our prime objectives was to maintain flexibility so that subsequent design and test improvements could be implemented by modification of the existing hardware rather than the replacement of equipment.

The system presently consists of a test aerosol vessel, a vessel heating system, a CDV installation and associated controls, sampling, and data acquisition instrumentation. The test aerosol vessel is a 42-in.-diam chamber, ~35 in. high, connected to a lower chamber, which is flanged to accept CDV test assemblies and equipped with optical ports for pyrometric and photographic data acquisition. The upper chamber is flanged for insertion of plateout and concentration samplers. The vessel is code-certified up to 140 psig at 1000°F. It was designed for eventual hot-cell installation, which dictated its relatively small size. A small vessel is advantageous when trying to produce aerosols at high concentrations. However, it is still large enough to permit sufficient time for making the various aerosol property measurements.

The CDV portion of the installation is shown schematically in Fig. 30, including its relationship to the aerosol test vessel. The CDV facility may be considered to have three separate but interacting parts: the pre-heat power supply, the capacitor energy delivery system with associated charging and discharge control circuitry, and the data acquisition instrumentation.

10.2 The Sample Preconditioning System (the Preheater)¹⁸

The resistivity of UO_2 (and PuO_2) decreases almost five decades between room temperature and the onset of melting.¹⁹ Therefore, test samples may vary in resistance from over $10^6 \Omega$ down to less than

ORNL DWG 77-2135R

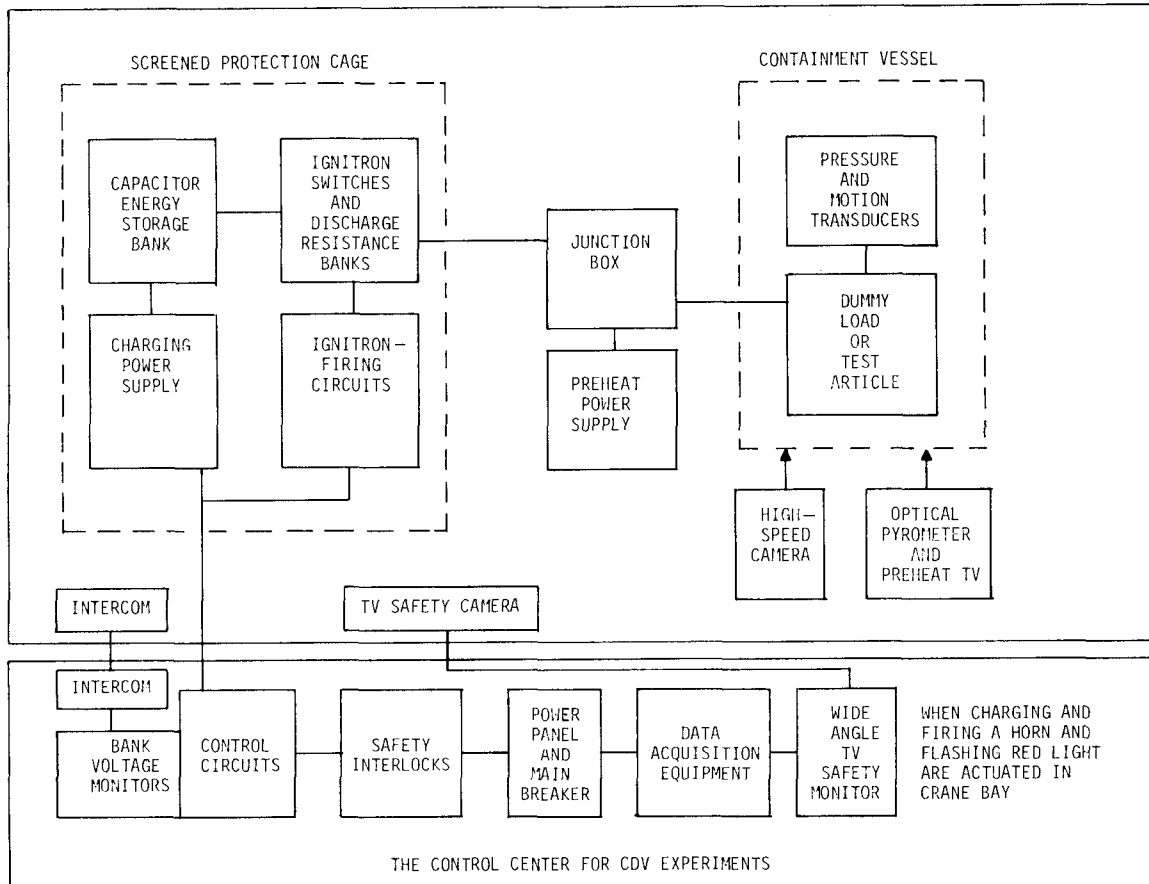


Fig. 30. Block Diagram of CDV-CRI-III System.

1 Ω when brought to preaccident energy conditions. Three preheater power supply stages are required to cover this broad range. The first stage is a high-voltage source (2500 V), initially supplying <5 W to the sample. As the sample temperature increases, the sample resistance rapidly decreases with the increasing current which is limited by a series resistance in the high-voltage transformer primary circuit. Steady-state conditions are reached when heat losses from the test sample equal the available power input. At that time, the resistance generally will have decreased to only a few hundred ohms. Subsequently, a controlled power supply operating at 440 V is used to increase the sample temperature until the resistance reaches the power output capability of a final 120-V power controller. This 120-V input stage is employed over the test regime when the total load resistance typically is between 75 and 0.2 Ω . The operation of both controlled power stages is similar; subsequent discussions will apply to each, except for the total power capability at specific load resistances.

Direct electrical heating of material with a negative temperature coefficient is possible with a power supply having controlled-current or controlled-power output. Actual power control and regulation was preferred for the CDV ORNL experiments because power density is an explicit thermodynamic parameter, whereas current density is not. In the past, the implementation of power regulators has been discouraged by the unavailability of electronic multipliers which perform acceptably at a reasonable cost. This situation has recently been changed by the appearance of a number of modular and monolithic integrated-circuit analog multipliers which are quite suitable for ac- or dc-power controllers. Using these devices for power computation, a regulated power system need be no more elaborate or expensive than a regulated voltage- or current-regulated system of comparable size.

The preheater power regulator is designed to deliver a full-range load power (average) of 4 kW from a single-phase, 120-V, 60-Hz source using conduction angle control (phase firing) of inverse-parallel SCRs. This configuration enhances the flexibility and improves the performance of the power circuit components at a cheaper cost than that for a dc output system.

The potential for polarization phenomena is also eliminated. Transient response approaches one or two cycles, and the output can be transformer-coupled if the load requirements do not match the available feeder-circuit capabilities.

Whether one employs ac or dc, the regulation of power in loads having an inverse resistivity-temperature characteristic can present special closed-loop stability problems. With this type of load, the small signal gain of a power-control loop can increase from a relatively low value when power is first applied to a very high value after the load reaches temperature. Instability can occur at either extreme.

For a simple controller with a fixed-source voltage and no series element other than the SCRs and resistive load, a low load resistance means a high loop gain, which can lead to instability because of shrinking phase margin and violation of the Nyquist criterion. This type of high-gain instability can occur in many types of ac controllers which incorporate conduction angle control and has been the subject of several investigations using various circuit models and analysis techniques.²⁰⁻²⁶ Generally, such a system becomes unstable if the closed-loop damping time constant is less than one-half the sampling period.

At the other extreme, when the load is cooler, its resistance range may be large and the loop gain will be low if the source voltage is fixed. At low gains, another type of instability can occur as a direct result of the inverse temperature resistance and other thermodynamic properties of the load. Oscillating frequencies associated with this low-gain instability will generally be low (~ 1 Hz) and inversely related to the effective thermal time constant of the load.

In order to cover the broadest possible load resistance range and maintain loop stability, we added series inductance to the power circuit, as illustrated in Fig. 31. This simple expedient effectively limits the loop gain when the load resistance is low and provides crest factor reduction of the load current waveform. High crest factors can be particularly troublesome in constant power controllers because the root mean square (rms) load current must increase when the rms load voltage

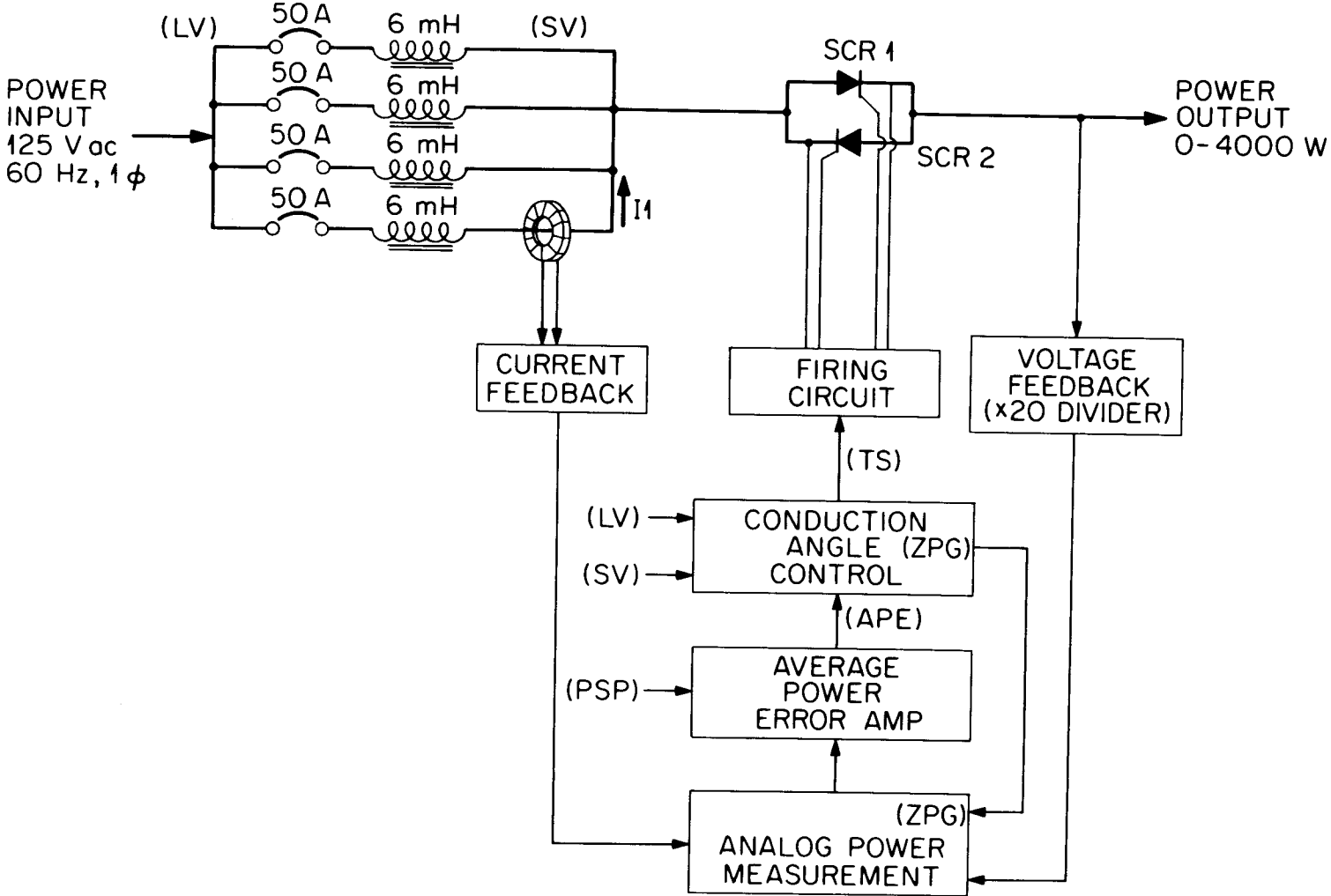


Fig. 31. Preheater Power Supply block diagram.

decreases. With conduction angle control and a purely resistance power circuit impedance, constant power to a decreasing load resistance requires a decrease of the conduction angle, even when the rms current must increase. This situation leads to high peak currents and crest factors, which in turn impose undue dynamic range requirements on the feedback and measurement circuitry, especially the analog multiplier.

The addition of inductance in series with the load circuit provides a simple but effective remedy. With the inductance values shown, the power circuit in Fig. 31 behaves like a voltage source when the load resistance is high and a current source when the load resistance is low.

10.2.1 Design features

The power circuit is given in Fig. 31, along with a block diagram of measurement and control functions. For source power, we connect a single phase and the neutral of a 100-A (or larger) 120-V feeder system. The input current is supplied by four parallel branches, with the current feedback signal for power computation and control derived only from one branch. This arrangement permits the full-scale power calibration to be easily changed by simply closing the appropriate number of circuit breakers. Calibrations are 1, 2, 3, and 4 kW (full scale) for one, two, three, or four circuits respectively. This current splitting also minimizes flux in the current transformer core, which permits the use of smaller cores. Equal splitting of the total load current among the active input circuits is maintained by a 6-mH inductor located in each branch.

Maximum conduction angles for the SCRs and load current are limited to $\sim 135^\circ$. This feature also aids in holding the SCRs "on" if the load resistance is high. Maximum power circuit voltage (total across load and inductance) with a 135° conduction is $\sim 95\%$ of the input source voltage.

A current transformer is used to develop the load current feedback signal because this method permits earth grounding at the source and/or load points. A total current reduction of 5000 is provided by cascaded transformer stages. This two-stage arrangement is especially suitable for experimental and development work because the current ratio can be easily altered by adjusting the second-stage primary turns.

Low frequency components of the phase-fired load waveform which are attenuated by the current transformers are partially restored by a simple pole-zero active filter. This technique extends the overall low-frequency response to $<1\text{Hz}$, which is sufficient for good reproduction of the 60-Hz phase-fired waveform.

Load-voltage and load-current feedback signals are fed to an integrated circuit analog multiplier which produces the time-domain power signal. The dc component of this signal is directly proportional to the time-averaged real load power, in accordance with chosen scale factors. The multiplier is inverting; that is, real load power gives a negative multiplier output.

The maximum multiplier inputs referred to the load are 800 V (peak) and 200 A (peak) if all input branch circuits are used. The high voltage rating was required to accommodate the 440-V controlled stage without requiring scale-factor switching when changing from the 440-vac source to the 120-vac source shown in Fig. 31.

A zero-power interval of at least 45° always follows the turn-off of each SCR. These periodic zero-power intervals are unique to phase-fired ac controllers and represent a distinct advantage because they permit the employment of automatic zero correction techniques for stabilizing key stages, such as the multiplier used here. Using this technique, the ac regulator performance can equal or exceed a comparable dc unit in terms of steady-state accuracy of averaged output.

With no external stabilization, the multiplier dc output drift is typically 0.7 mV per degree centigrade (for the 4-kW full-scale range), which is inconsistent with our overall accuracy requirement of $\pm 1\%$ full scale. Using automatic zero correction, the multiplier drift stability is improved to an accuracy better than 0.04% per degree centigrade.

The time-domain power signal generated by the analog multiplier is compared with a dc level representing setpoint power by converting each signal to a current and integrating the difference with a common op-amp. Polarities are such that the integrator output becomes positive when measured power exceeds setpoint power. During normal operation,

the signal ranges between 0- and +10-V dc, with the latter corresponding to zero SCR conduction. Proper conduction angles for the power SCRs are generated by a logic control circuit, which produces a trigger signal for the SCR firing circuits. The main output of this conduction angle control circuit is a 60-Hz square wave, which ultimately triggers SCR 1 (see Fig. 31) on its positive transition and SCR 2 on its negative transition. The phase of this trigger signal defines the phase of the load current and always lags that of the source voltage, with more lag producing less conduction (and, therefore, less power) for a given load condition. This phase lag of the SCR trigger signal, relative to the source voltage, is commonly designated as the firing angle, α , in the literature.²⁷

The two most popular firing schemes are the inverse cosine scheme and the constant $-\alpha$ scheme.²¹ We have used the latter primarily for ease of implementation and because the inverse cosine approach has no particular merit unless load voltage is the controlled parameter. When the power supply is regulating, the firing angle will change proportionately from 180° to 0° and the conduction angle will increase from 0° to 135° maximum as the average power error signal decreases from +10 V to 0 V. This is implemented by a comparator, which makes a positive transition each time a sawtooth time base crosses the input level.

If the error amplifier (integrator) output is +10 V, no firing pulses are generated (i.e., no power flows to the load). This condition prevails after the control electronics is energized but before the logic input (PSP) is lowered to initiate power flow (firing). The input is forced low to initiate firing, thus allowing the integrator output signal to decrease from the +15-V clamp position at a rate which is dependent on the setpoint power. As this output passes below +10 V, SCR firing commences and the conduction angle increases from zero until the measured and setpoint powers balance. This arrangement ensures a smooth buildup of load power and is often called "soft starting." The maximum conduction angle for each SCR is limited by a pulse which clamps the flip-flop clock for a period of 2.1 msec immediately after each SCR turns off. These 2.1-msec pulses also serve as gating pulses for the automatic-multiplier zero circuit.

Firing pulses for the main SCRs (SCR 1 and SCR 2 in Fig. 31) are generated by half-wave rectifier circuits. Energy to fire SCR 1 during positive line voltage is supplied by a capacitor which was charged to ~ 170 -V dc during the preceding negative half cycle of line voltage. Similarly, SCR 2, which conducts on negative line voltage, is fired with energy stored on another capacitor that was charged during the preceding positive half cycle. With this arrangement, adequate firing energy for SCR 1 is being stored while SCR 2 is conducting and vice versa. These capacitors are discharged by alternate firing of smaller SCRs (type 2N4172), which are triggered by a differentiated version of the trigger signal via a pulse transformer. Control of the 120-vac firing circuit power provides a convenient and reliable method of interlocking the regulator for safety purposes.

10.2.2 Performance

When operated within the calibrated power range,* the output power error is $< \pm 1\%$ of full scale at any power setpoint and $< \pm 2\%$ of reading for setpoints between 10 and 100% of full scale. This accuracy is maintained over a reasonable temperature range (15 to 35°C) by automatic zero correction of the multiplier output offset.

To use zero-correction techniques, we have restricted the conduction angle to 135°, which obviously required some sacrifice in maximum power output and load rangeability, especially on the low resistance end. As illustrated by the curves in Fig. 32, the load resistance to which full power (4 kW) can be delivered ranges from ~ 0.45 to 2.5 Ω with the 135° limit, whereas the range would be 0.1 to 3.5 Ω with full 180° conduction. Another curve in Fig. 32 illustrates how the current for 135° conduction is inherently limited to slightly < 100 -A rms, which is well within the SCR capabilities.

* Only one of the four possible power ranges can be accurately calibrated. Accuracy of the other three depends on inductor matching, which is typically $\pm 10\%$.

ORNL-DWG 77-14060

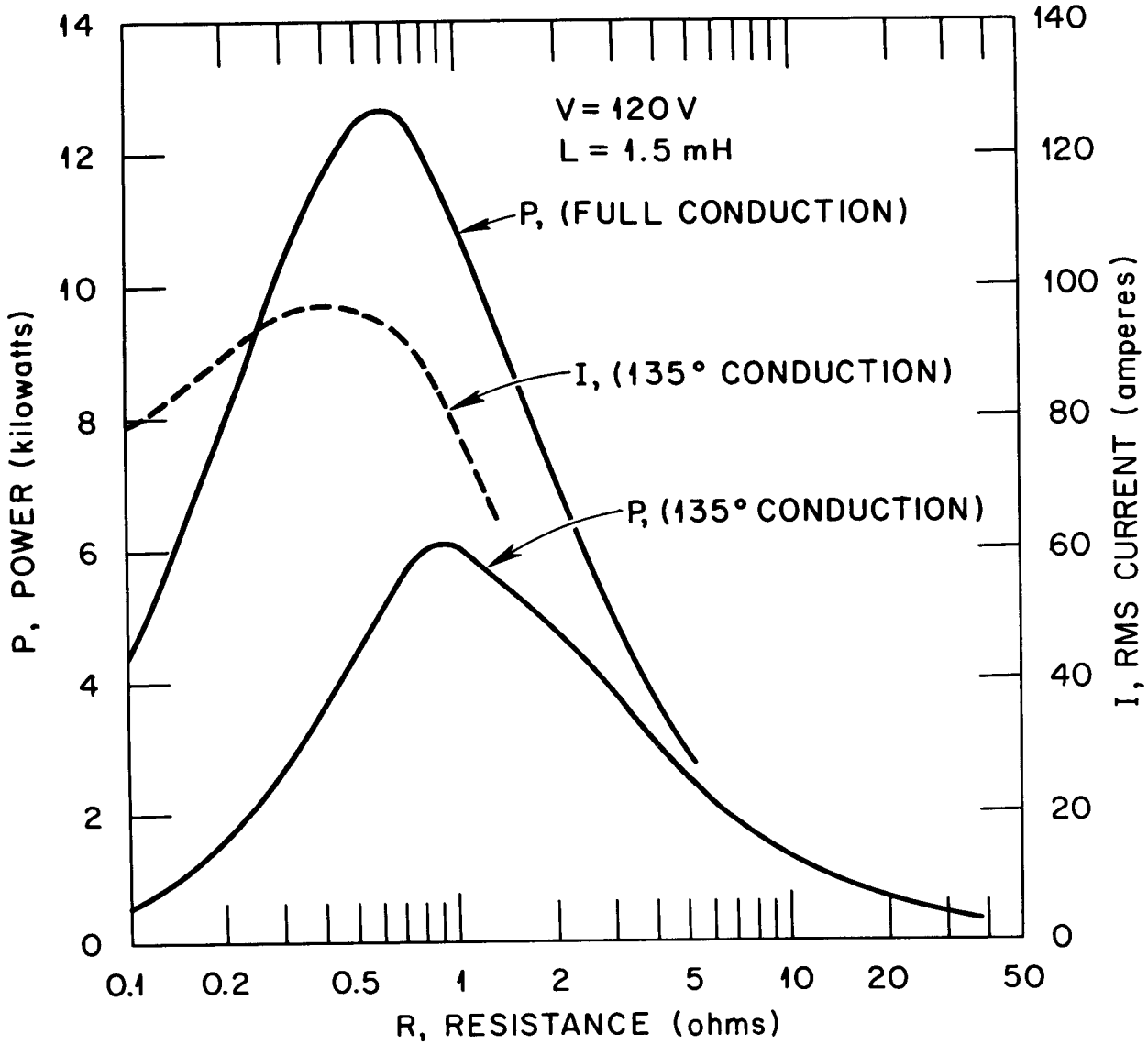


Fig. 32. Power regulator output capability as a function of load resistance.

When the load resistance is relatively high, we have observed two types of unstable behavior. By far the more common of the two is for the load to completely "drop-out" simply because its power --- resistance characteristic falls beyond the maximum power curve (135°) given in Fig. 32 (i.e., the heat power loss for a particular temperature) --- resistance state exceeds the maximum regulator output). This condition may exist when the regulator is first energized (the load temperature being previously elevated by other equipment), or it may be triggered by load restructuring or a shift in heat transfer properties.

On a few occasions when operating at high resistance ($R > 25 \Omega$) and low power, we have observed low-amplitude limit cycle behavior. Under these conditions, the loop gain is very low and the closed-loop response time is several seconds long. We suspect this unstable mode is precipitated when loop response and load thermal response time are comparable in magnitude. Although unwanted, this unstable mode is not destructive because any excursion toward higher temperature is self-limiting; that is, the unstable condition only applies when the gain is critically low.

The preheater system is inherently flexible, and any range of voltage and power input requirements can be accommodated without major control changes. A three-unit version is under construction, in order to meet multiple test requirements, but the basic design concepts remain the same.

10.3 The Capacitor Energy Delivery System

10.3.1 The Energy Storage System

The Capacitor Energy Storage System is shown installed in its protective cage in the left portion of Fig. 33. Capacitors have been purchased for installation in the vacant lower section. This will provide a nominal energy storage capacity of 180 kJ. Construction is modular in order to maintain operational flexibility. Each module has ten capacitors rated 3 kJ at 2500 V connected in parallel. A $0.1\text{-}\Omega$ resistance wire is in series with each capacitor to limit the surge current if an internal short circuit should occur in any capacitor while the module is energized. The capacitor purchase specifications were written so that even when the

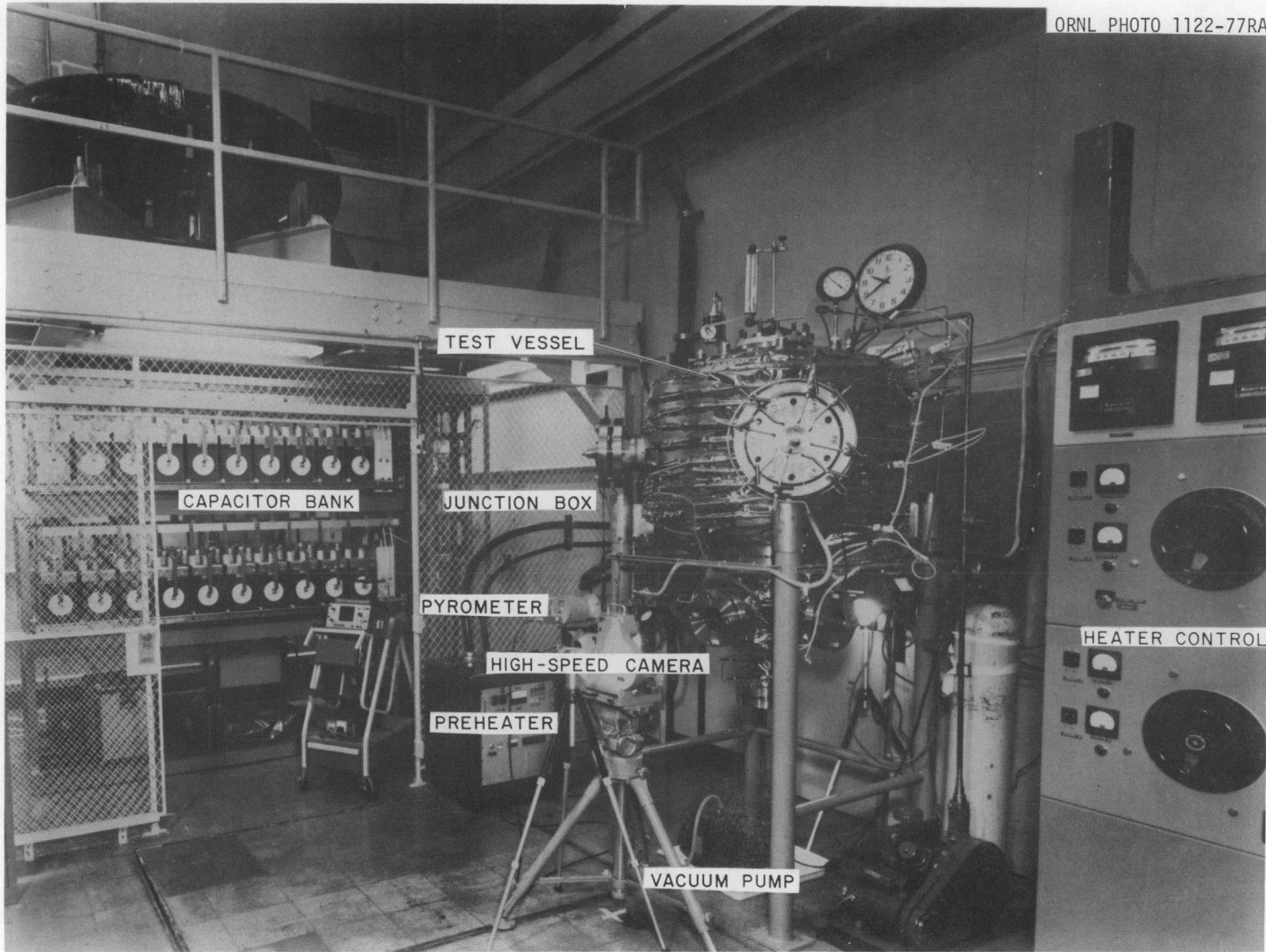


Fig. 33. Overall view of the operational area where ORNL Capacitor Discharge Vaporization experiments are conducted.

module is fully charged no case rupture would occur if all of the module stored energy is deposited in a failed unit. Each capacitor has been tested by charging to 3000 V and can be used up to this voltage level, which increases the ultimate energy storage capacity to 144% of the nominal rating given above.

An internal resistance bank, relay operated, can be used to dissipate the stored energy safely without discharge to the sample under test if experimental difficulties occur.

Each module has an ignitron for firing control and blocking diodes which effectively isolate each module from interaction with others.

A high-voltage manual disconnect (hotstick-pole-type) shorts the capacitors in each module, except during experimental operations as a safety precaution.

10.3.2 Charging and Firing Systems

In order to operate the Charging and Firing Systems, electrical door interlocks must be engaged which prevent access between the operational area and the control station. The control panel, shown in the upper right section of Fig. 34, then controls all sequencing.

Prior to energizing the interlocks, the manual disconnects are opened and all switches on the charging and bank-firing equipment are switched on. This equipment is contained in a single cabinet within the capacitor-bank protective enclosure. The circuit components can only be operated from the control panel.

The charging system is capable of delivering up to 500 mA of dc current (36 kJ per minute) into the capacitor bank and has an automatic safety cutoff at 3000 V which requires no operator action. The firing circuits are by charged capacitors that supply a shaped current pulse of proper amplitude and width to the ignitron ignitors which initiates mercury ionization and subsequent ignitron conduction. The charge voltage on each capacitor module appears on both electronic meters on the control panel and mechanical meters mounted on the protection cage. Each bank module is separately controlled.

ORNL PHOTO 1124-77RA

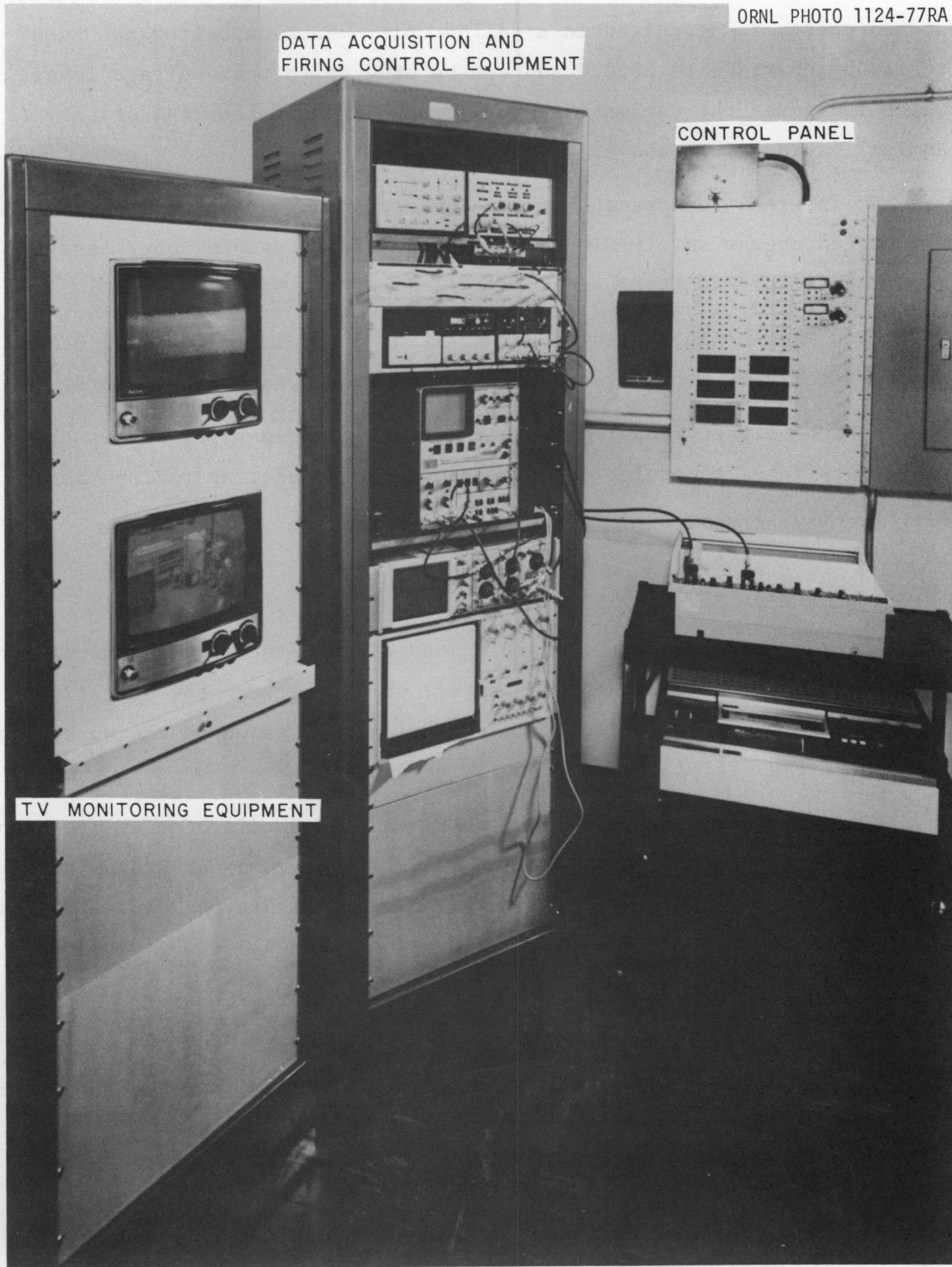


Fig. 34. Experimental control and data acquisition area.

The operating sequence is as follows:

1. select number of bank modules to be used,
2. set chosen capacitor final voltage (energy per module),
3. open discharge relays on modules used,
4. close charging relays on modules used,
5. energize ignitor circuits on modules used,
6. energize charger and wait for capacitors to charge,
7. open charging relays on modules used.

The capacitor energy system is then ready to be discharged into the test article. The internal resistance of the charged capacitors results in a slow energy loss (~ 1 V per second) while the high preheat phase is in progress. This loss is not significant since test-article preconditioning (pellet melting) normally is completed in 30 sec.

After high preheat and equipment disconnection, which is accomplished automatically on a preset time cycle, the stored capacitor energy is discharged into the test sample. Any combination of modules can be used, and module firing can be simultaneous or sequential with preprogrammed delays.

10.3.3 Equipment capability

Each capacitor module is connected to a transition junction box by five coaxial cables. Single coaxial cables then lead to each test assembly. After completion of the three-unit preheater, three test assemblies can be simultaneously disassembled.

Capacitor modules have been calibrated individually and in parallel. The design objective was an effective resistance of $< 0.05 \Omega$ per module, including all connecting cables. The measured value per module during testing was $0.041 \pm 0.002 \Omega$. For the worst case (single module), circuit losses are $< 20\%$ of the bank stored energy released before sample disassembly. As modules are added, this loss fraction decreases rapidly since the module resistance are parallel.

The load-voltage and current-signal conditioners reproduce the transient waveforms with a precision of $\pm 2\%$ with a response time of $\sim 30 \mu$ sec.

The commercial current shunts initially used deteriorated rapidly when currents exceeded 50,000 A. An ORNL-designed coaxial shunt with a thick Inconel tube as the active element has eliminated this problem.

Original design criteria proposed the addition of a variable inductance in series with the capacitor modules to control the energy discharge rate into the test samples. This was proposed so that any potential effects on aerosol yield caused by the energy deposition rate could be determined. Later calculations using the known thermal properties of UO_2 demonstrated that, over the expected time periods for energy deposition (0.1 to 10 msec), little radial or axial energy transfer could be expected from thermal gradients developed during energy deposition. In addition, for a fixed test-sample configuration with six bank modules available, a power rate rangeability of ~ 6 to 1 could be achieved. This is best shown using a constant sample resistance (in actual experiments, the sample resistance varies less than a factor of 3 during bank discharge) and the exponential decay properties of a resistor-capacitor (RC) network. For a constant 0.15- Ω load, 75% of the bank energy will be delivered from one bank module in 1.44 msec. For six bank modules in parallel, 75% of the energy will be delivered in 8.64 msec. Intermediate times are achieved by other combinations between these limits.

In actual experiments using four capacitor modules in various combinations, we have calculated energy deposition rates from observed electrical data ranging from 1.2 to 0.4 MW per grams (differing by factor of 3 compared with the theoretical factor of 4). There is no evidence that this variation in rate has any effect on aerosol yield or properties. As experiments are conducted using five- and six -bank modules, we expect to approach a variation factor of 6 in the energy deposition rate.

We have concluded that a variable inductance to control the energy discharge rate is no longer required, and the concept has been abandoned.

The present energy delivery system is capable of delivering energy to test samples at rates of 0.2 to 1.2 MW per gram sample, with sufficient energy storage to promote ~ 50 g of UO_2 from the melting point to the critical point. Sample containment during energy insertion limits the thermodynamic energy state which can actually be reached. Present data

indicate an upper limit for aerosol production using three test samples, simultaneously energized, of ~10 g when disassembly occurs as free expansion in 1 atm of argon.

10.4 Data Acquisition System

The purpose of the ORNL CDV System is to place simulant (UO_2) or fuel samples into energy states that cover the range of thermodynamic states postulated for core disruptive accidents and permit analysis of the properties of the aerosols formed by hydrodynamic expansion for this condition.

The information needed to accomplish this assignment requires highly specialized data acquisition equipment as shown in Figs. 33 and 34. The instrumentation and sampling devices for this program can be separated into two groups: (1) the equipment concerned with the energy input phase and sample expansion and (2) the equipment used to determine the properties of the aerosol formed during expansion.

10.4.1 Equipment used during expansion

Both electrical and visual records are needed for the three time periods of interest: the high preheat phase, where pellet melting occurs; the capacitor discharge phase in which the sample is brought to core disruptive thermal energy; and the sample expansion phase.

For the high preheat phase (seconds), the sample containment is visually monitored by a television camera to ensure uniformity of heating and containment integrity. A permanent video tape record is also acquired. The applied voltage, current through, and power into the sample are recorded on a four-channel strip chart recorder. The fourth channel is used for other measurements of interest, such as sample surface temperature or linear expansion rates.

During the entire capacitor discharge phase (milliseconds), the sample is visually monitored by a 16-mm color camera operating at a rate of 10,000 frames per second. A high-speed, self-powered radiation pyrometer is focused on the sample. The transient voltage across and current through the sample are converted to suitable amplitudes by dividers,

shunts, and signal conditioners and are recorded. Special purpose data may be acquired, such as transient pressure within the test vessel.

All of these measurements are operative during containment failure and subsequent expansion (microseconds) with aerosol formation. Measurement-device and signal-conditioner response times are such that their transient response is compatible with event rapidity, except for camera coverage.

To record this data, we have a two-channel storage oscilloscope from which permanent photographic records are made plus a two-channel digital storage oscilloscope that digitizes analog input data as rapidly as 0.5 μ sec per point. This second oscilloscope has a 4096 (12-bit)-word main-frame memory and a triggering feature that allows data to be stored on each side of a triggering event, as well as a dc plotting output from memory so that direct plots on an X-Y recorders can be made. It is a very versatile data storage device.

In addition, a four-channel tape recorder with a nominal 15,000-Hz frequency response is paralleled with the storage oscilloscopes and provides another permanent record. Each of these channels can be triggered into the digital storage scope at a later time; the X-Y plotting feature can be utilized to provide a graphical record. The transient response of this tape recorder results in poorer data reproduction than that from the storage oscilloscopes; hence, the recorder is used primarily as a backup unit.

10.4.2 Equipment used after expansion

During hydrodynamic expansion, the vapor-liquid system fractionates into the argon with turbulent mixing and quenching of the vapor followed by liquid and the remaining solids. Sampling does not commence until after the larger particulates ($>4\mu$) have precipitated (~ 2 to 3 min). The properties of the remaining aerosol system are then determined over an extended time period using the sampling apparatus described below.

Two primary sampling devices are installed in the test vessel. Both have sampling surfaces essentially flush with the vessel wall at the tank midline.

Figure 35 is an assembled view of the sampler used for plateout collection. The sampler used for concentration determination is similar except for flexible tubes leading to each sampling point and a valved manifold. The front cover plate can be indexed to any of eight sample positions.

Figure 36 shows the plateout sampler with the coverplate removed and collection coupons and electron photomicrograph grids in place. Chemical analysis and time of exposure are used to determine the plateout (diffusion) rate. Transmission electron microscopy is used to determine particle size and agglomeration state.

Figure 37 shows a front view of the aerosol concentration sampler after use (coverplate removed). A stainless screen supports each filter. The normal sample volume is 5 liters. Larger samples may be taken if the aerosol is very dilute. Both collected mass and chemical analysis are used, together with aliquot sample size, to determine aerosol concentration variation with time.

Six and eight-stage Andersen impactors are used to determine the mass distribution of aerodynamic sizes in the agglomerated aerosol. Chemical analysis of each stage collection plate is made and these results, together with impactor calibration data, are used to determine the aerosol aerodynamic size distribution.

An electrostatic sampler is used to collect samples on electron photomicrograph grids for later determination of primary particles by sizing and counting particles from high-magnification electron microscope photographs.

Particle number density is determined by a condensation nuclei counter. This device has an upper limit of 10^7 particles per cubic centimeter. Normally in a good CDV test, 10 to 15 min elapse before particle number densities decrease to this value.

All of the above measurements and collections are taken at times and time periods which have been selected on the basis of previous experience.

ORNL PHOTO 6420-76

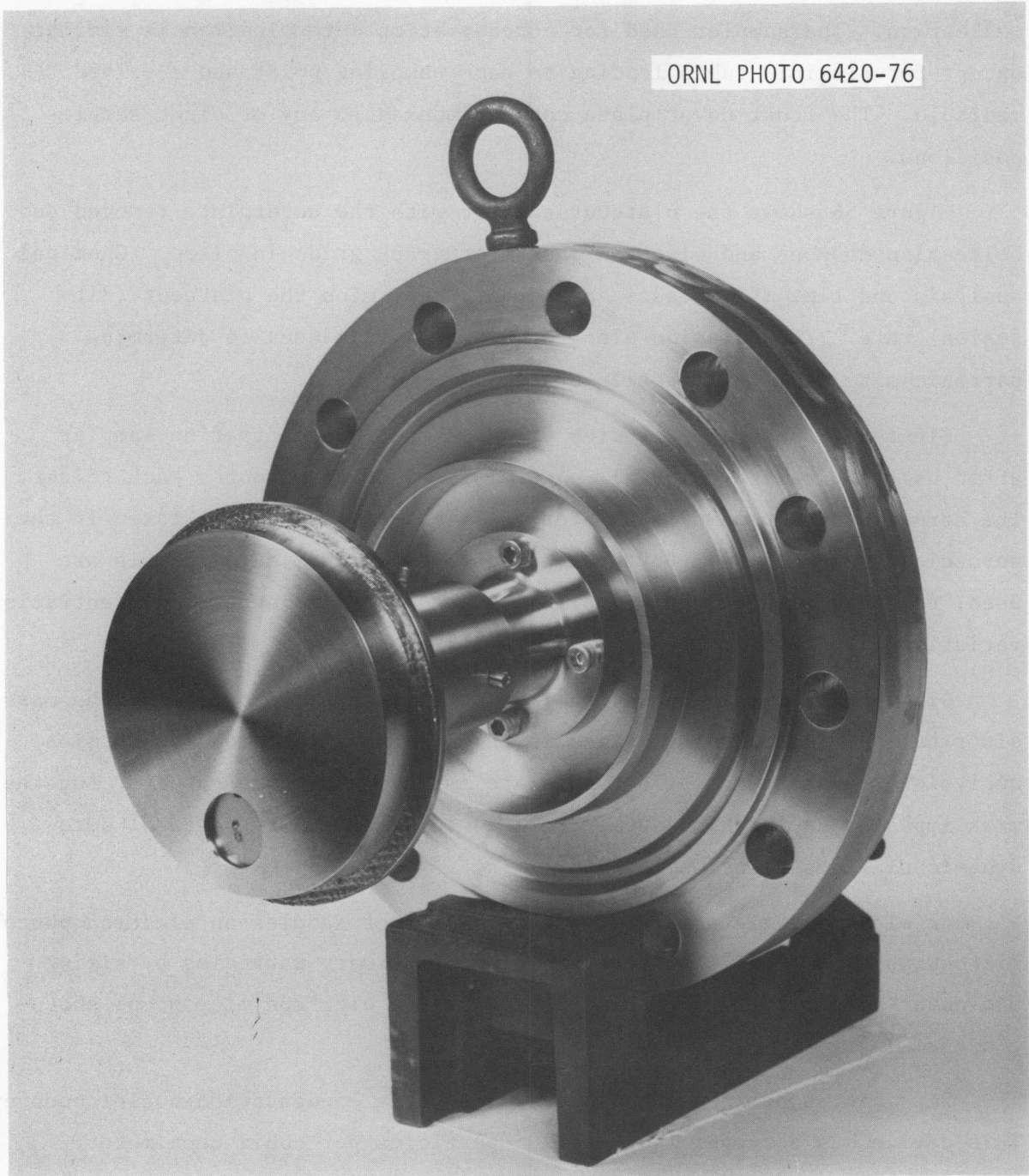


Fig. 35. Rotary plateout sampler.

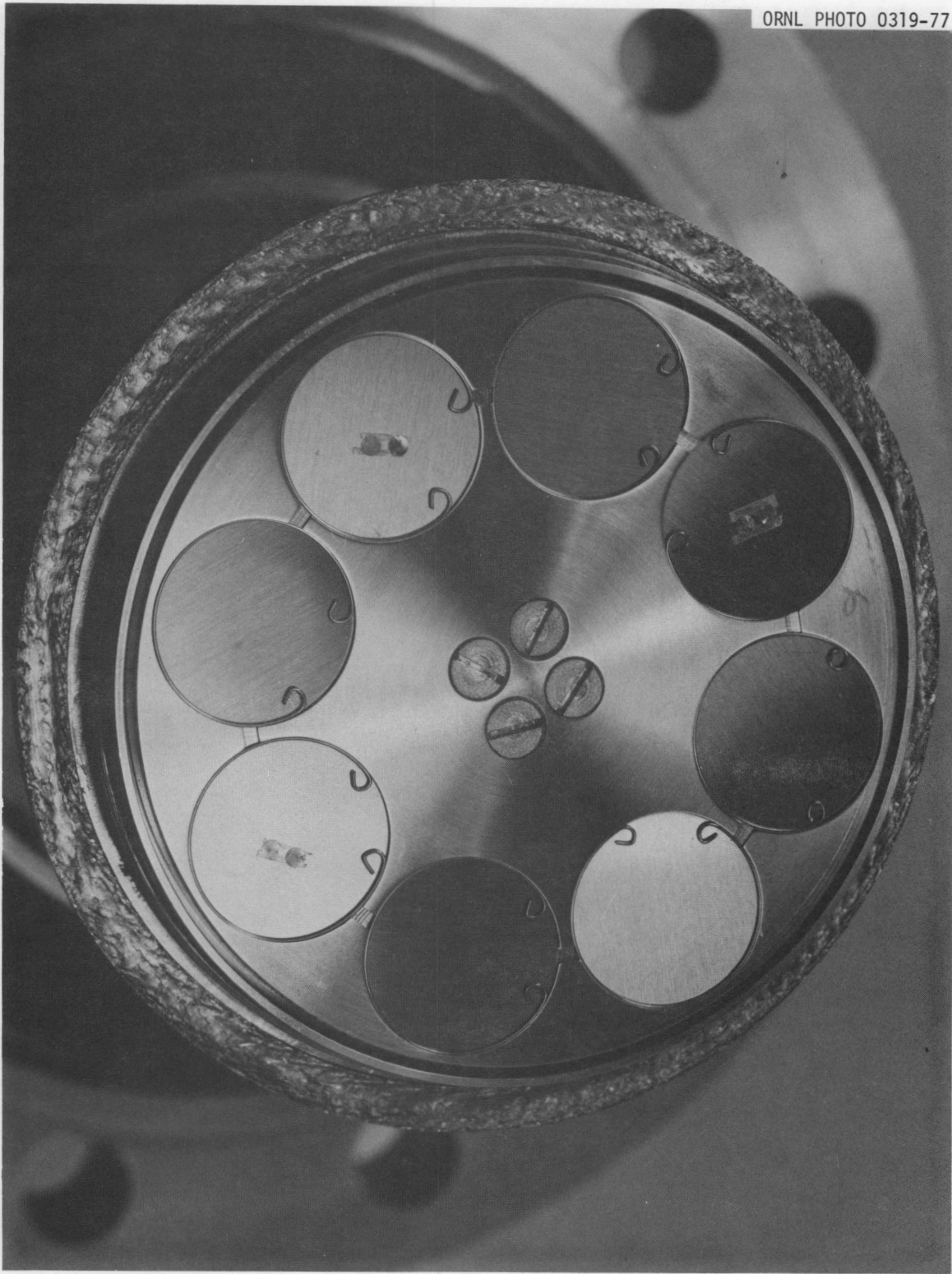


Fig. 36. Plateout sampler with front coverplate removed.

ORNL PHOTO 0318-77

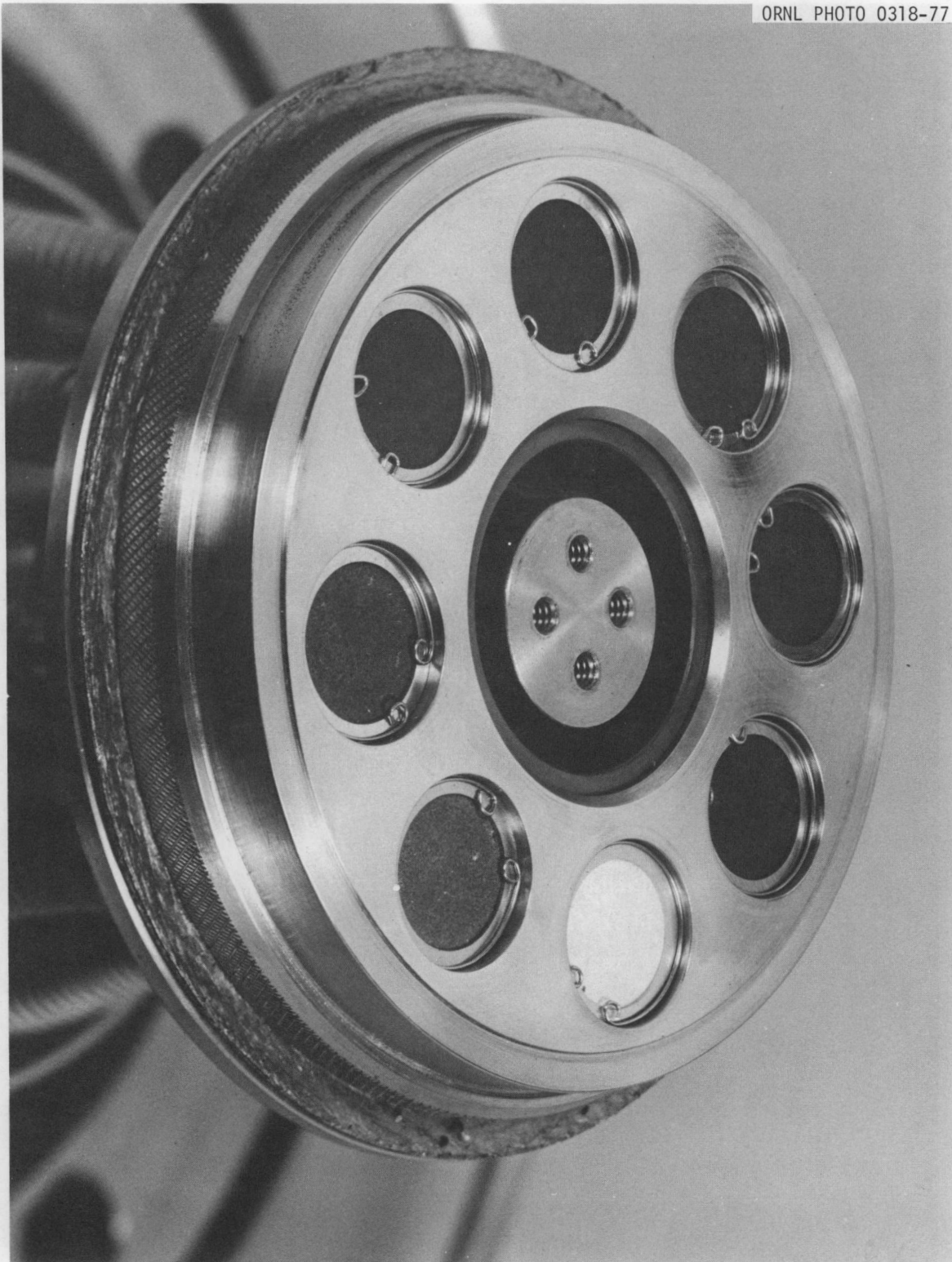


Fig. 37. Aerosol concentration sampler after use with front cover-plate removed.

10.5 Test Articles

During the AEDC development program early tests were plagued with arcing between the center electrode and the outer-current return sheath before significant energy had been deposited in the UO_2 sample. The outer sheath diameter was increased in order to decrease the potential gradient between the electrodes in an effort to eliminate this problem. This technological fix was unsuccessful. However, redesign of the upper lavite insulator to enclose the upper section of the quartz-sample containment tube was an effective solution. Both test-article models, as shown in Figs. 29 and 38, were then used interchangeably for AEDC tests and the first 15 ORNL CDV tests.

Sample assembly produced torsional strains on the sample and containment as the bottom electrode was screwed into place. In addition, the outer sample housing webs appeared to intercept a significant portion of the expanding sample during disassembly. Both of these features were considered to potentially reduce aerosol yield. Consequently, the test article was subsequently modified to the configuration shown in Fig. 39. The torsional strains were completely eliminated since the bottom electrodes could then slide axially into position, with the required spring loading provided by external compression springs as shown. The top and bottom electrodes were lengthened and the web sections replaced by small steel rods to minimize the interception potential.

11. ACKNOWLEDGMENTS

The authors would like to thank Kenneth Rush, A. L. Sutton, Jr., and G. E. Creek of the Oak Ridge National Laboratory for their valuable assistance and participation in the design of electrical systems and for conducting and analyzing the experiments.

ORNL PHOTO 3786-76



Fig. 38. Large-housing-diameter test article.

ORNL PHOTO 3919-77

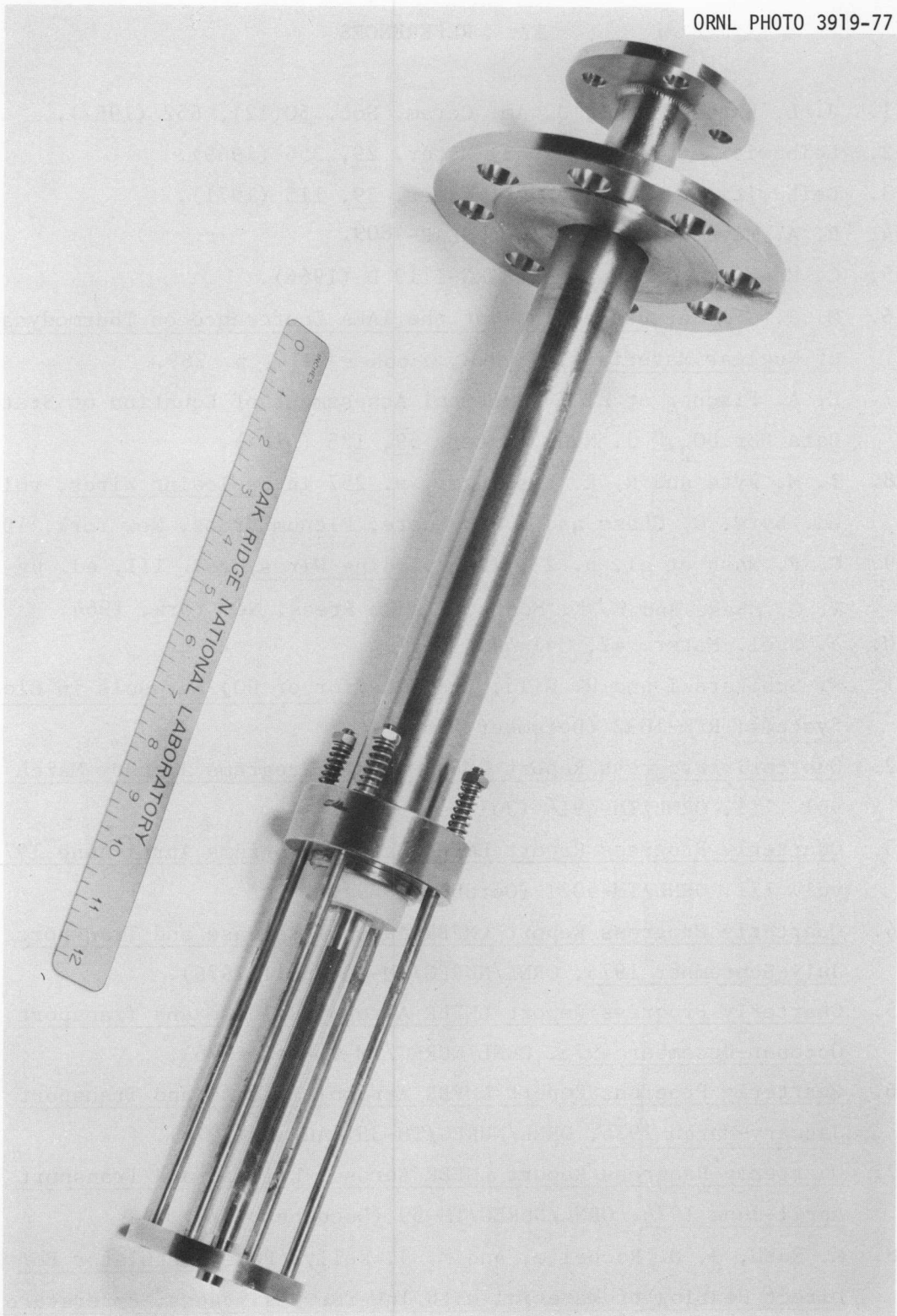


Fig. 39. Present standard ORNL Capacitor Discharge Vaporization test article.

12. REFERENCES

1. J. L. Bates et al., J. Am. Ceram. Soc. 50(12), 652 (1967).
2. Leibowitz et al., J. Nucl. Mater. 29, 356 (1969).
3. Leibowitz et al., J. Nucl. Mater. 39, 115 (1971).
4. R. A. Meyer et al., Report GEAP-4809.
5. C. Menzies, UKADA Report TRG-1119 D (1966).
6. M. J. Gillan, Proceedings of the IAEA Conference on Thermodynamics of Nuclear Materials, Vienna, October 1974, p. 269.
7. E. A. Fischer et al., "Critical Assessment of Equation of State Data For UO_2 ," J. Nucl. Mater. 59, 125 (1975).
8. I. M. Fyfe and R. R. Ensminger, p. 257 in Exploding Wires, vol. III, ed. by W. G. Chase and H. K. Moore, Plenum Press, New York, 1964.
9. C. P. Nash et al. p. 231 in Exploding Wires, vol. III, ed. by W. G. Chase and H. K. Moore, Plenum Press, New York, 1964.
10. J. Nucl. Mater. 42, 341-44 (1972).
11. W. Schikarski and H. Wild, The Behavior of UO_2 Aerosols in Closed Systems, RFK-1032 (December 1969).
12. Quarterly Progress Report LMFBR Safety Programs January-March 1975, vol. III, ORNL/TM-4914 (July 1975)
13. Quarterly Progress Report LMFBR Safety Programs April-June 1975, vol. III, ORNL/TM-5021 (October 1975).
14. Quarterly Progress Report LMFBR Aerosol Release and Transport July-September 1975, ORNL/NUREG/TM-8 (April 1976).
15. Quarterly Progress Report LMFBR Aerosol Release and Transport October-December 1975, ORNL/NUREG/TM-9 (May 1976).
16. Quarterly Progress Report LMFBR Aerosol Release and Transport January-March 1976, ORNL/NUREG/TM-35 (August 1976).
17. Quarterly Progress Report LMFBR Aerosol Release and Transport April-June 1976, ORNL/NUREG/TM-59 (December 1976).
18. K. Rush, J. M. Rochelle, and M. J. Kelly, Power Regulator For Direct Heating of Material with Inverse Resistance Temperature Properties (to be published).
19. J. L. Bates, C. A. Hinman, and T. Kawada, "Electrical Conductivity Uranium Dioxide," J. Am. Ceram. Soc. 50, 652-56 (1967).

20. R. D. Jackson and R. D. Weatherby, "Thyristor Alternating-Voltage Controllers in Closed-Loop System," Proc. Inst. Electr. Eng. 121, 1030-32 (1974).
21. J. P. Sucena-Paiva, R. Hernandez, and L. L. Fريس, "Stability Study of Controlled Rectifiers Using a New Discrete Model," Proc. Inst. Electr. Eng. 119, 1285-93 (1972).
22. P. Q. Hazell and J. O. Flower, "Stability Properties of Certain Thyristor-Bridge Control Systems, Part 1 - The Thyristor Bridge as a Discrete Control System," Proc. Inst. Electr. Eng. 117, 1405-12 (1970).
23. P. A. Hazell and J. O. Flower, "Stability Properties of Certain Thyristor-Bridge Control Systems, Part 2 - The Interrelationships of Discrete - and Continuous - Design Methods," Proc. Inst. Electr. Eng. 117, 1413-20 (1970).
24. F. Fallside, C. J. Goodman, and R. D. Jackson, "Stability of First-order Sampling and Thyristor Systems," Electr. Letters 5, 566-67 (1969).
25. F. Fallside and A. R. Farmer, "Ripple Instability In Closed-loop Control Systems with Thyristor Amplifiers," Proc. Inst. Electr. Eng. 114, 139-52 (1967).
26. N. A. Bjäresten, "The Static Converter as a High Speed Power Amplifier," Direct Current 8, 154-65 (1963).
27. M. Khalifa, M. Obeid, and S. Enamul-Haque, "Effects of Source Impedance on the Steady-state Performance of Thyristor Controlled Circuits," IEEE Trans. Ind. Appl. IA-11, 384-91 (1975).

NUREG/CR-0226
ORNL/NUREG/TM-160
Dist. Category R7

INTERNAL DISTRIBUTION

- | | | | |
|--------|-------------------|--------|-------------------------------|
| 1. | R. E. Adams | 28-31. | J. M. Rochelle |
| 2. | M. Bender | 32. | C. D. Scott |
| 3. | H. W. Bertine | 33. | A. M. Smith |
| 4. | J. R. Buchanan | 34. | A. L. Sutton, Jr. |
| 5. | D. E. Ferguson | 35. | M. L. Tobias |
| 6-8. | M. H. Fontana | 36. | H. W. Trammell |
| 9. | J. T. Han | 37. | D. B. Trauger |
| 10. | H. W. Hoffman | 38. | J. L. Wantland |
| 11-12. | M. J. Kelly | 39. | J. S. White |
| 13-16. | T. S. Kress | 40. | A. L. Wright |
| 17. | Milton Levenson | 41. | R. G. Wymer |
| 18. | R. A. Lorenz | 42-43. | Central Research Library |
| 19. | R. E. MacPherson | 44. | Document Reference Section |
| 20. | A. P. Malinauskas | 45-46. | Laboratory Records Department |
| 21. | F. R. Mynatt | 47. | Laboratory Records (RC) |
| 22-25. | G. W. Parker | 48. | ORNL Patent Section |
| 26. | L. F. Parsly | | |
| 27. | H. Postma | | |

EXTERNAL DISTRIBUTION

49. J. T. Larkins, Experimental Fast Reactor Research Branch,
Reactor Safety Research, Nuclear Regulatory Commission.
50. Director, Research and Technical Support Division, DOE-ORO.
- 51-360. Given distribution as shown for Category R7.